Investigating the Factors Governing the Efficiency and the Electroluminescence Stability in Simplified Phosphorescent Organic Light-Emitting Devices Utilizing One Material for Both Hole Transport and Emitter Host

by

Mina M. A. Abdelmalek

A thesis
presented to the University of Waterloo
in fulfillment of the
thesis requirement for the degree of
Master of Applied Science
in
Electrical and Computer Engineering – Nanotechnology

Waterloo, Ontario, Canada, 2013

AUTHOR'S DECLARATION

I hereby declare that I am the sole author of this thesis. This is a true copy of the thesis, including any required final revisions, as accepted by my examiners.

I understand that my thesis may be made electronically available to the public.

Abstract

Organic Light-Emitting Devices (OLEDs) have reached industrial maturity in display technology, since OLEDs provide salient advantages such as high brightness, fast response, wide viewing angle, mechanical flexibility, and low cost manufacturing. Due to the ability of electroluminescence (EL) from triplet excited states as well as singlet excited states, phosphorescent OLEDs (PHOLEDs) have a potential to achieve 100% internal quantum efficiency. Therefore, PHOLEDs can offer a competitive external quantum efficiency. However, the operational stability of PHOLEDs is relatively poor. Several mechanisms have been proposed to address the chemical and physical phenomena associated with intrinsic degradation of PHOLEDs, nevertheless, the reasons behind voltage rise and luminance loss accompanying PHOLEDs long term operation are not yet well understood. The state of the art *p-i-n* PHOLEDs offer relatively high efficiency and low efficiency roll-off. However, this technology is characterized by structure complexity. Therefore, much of the current research on PHOLEDs focuses on the development of the simplest possible and most easily processed architecture that can deliver the optimal combination of device properties. Simplified PHOLEDs, utilizing one material for both hole transport and emitter host, can be a good candidate for replacement of *p-i-n* technology. Simplified PHOLEDs offer higher efficiency than the *p-i-n* PHOLEDs , yet, their EL stability is found to be poor.

In this thesis, the role of the ITO/organic interface on simplified PHOLEDs efficiency will be investigated. Furthermore, possible degradation mechanisms at the ITO/organic interface will be explored. Moreover, we will correlate degradation at the ITO/organic interface to PHOLEDs operational stability. Eventually, organic layers modifications including but not limited to emissive layer (EML) will be examined.

By studying the indium tin oxide (ITO)/organic interface in simplified PHOLEDs, it was found that this interface is critical to PHOLEDs performance. The study shows that, this interface is critical to the PHOLED overall stability and is considered as one of the limiting factors of the long term operational stability of simplified PHOLEDs. The effect of optical excitation on the ITO/organic interface stability in hole-only devices was investigated. It was found that the ITO/organic interface is susceptible to exciton-induced degradation. This degradation affects the device stability severely compared to current-induced degradation. The exciton-induced degradation can be prevented by doping the hole transport layer (HTL), at the interface with an exciton quencher layer or by blocking the electrons from leaking to the ITO/organic interface that may further recombine with holes to form excitons. Further studies showed that upon combining both electrical stress and optical excitation, the device degradation is even more pronounced which is most likely due to interactions between charges and excitons. By using exciton life-time measurements, a new role of molybdenum trioxide (MoO_3) in the electrical stability of PHOLEDs, as an exciton quencher layer, is introduced.

Delayed EL (DEL) measurements showed that the simplified PHOLEDs are susceptible to triplet-triplet annihilation (TTA) and triplet-polaron quenching (TPQ) which might affect the operational stability of simplified PHOLEDs. Finally, EML modifications showed that the recombination zone of simplified PHOLEDs is located near the HTL/EML interface.

Acknowledgements

First and foremost, I would like to thank God for being on my side throughout my dark times as well as my bright times. I would like to thank Prof. H. Aziz for his supervision while I completed my M.A.Sc. degree. I'm grateful to him for providing me with this great opportunity to study at Waterloo University. Furthermore, I'm grateful to all the group members for their help throughout my degree. Moreover, I would like to thank Prof. K. Karim for his support.

I would like to thank Dr. George Soliman and Sibi Sutty for proofreading my thesis. Furthermore, I would like to thank Prof. Andrei Sazonov and Prof. Dayan Ban for taking their time and review my thesis.

Last but not least, I would like to thank my family and friends for their continuous support, especially Amir Junny.

Table of Contents

List of Figures

List of Abbreviations

OE	Organic Electronics
OFETs	Organic Field-Effect Transistors
OLEDs	Organic Light-Emitting Devices
OSC	Organic Solar Cells
OPD	Organic Photodetectors
EL	Electroluminescence
SiC	Carborundum
AC	Alternating Current
PVK	Polyvinylcarbazole
Alq_3	Tris(8-hydroxyquinoline) Aluminum
HTL	Hole Transport Layer
ETL	Electron Transport Layer
HIL	Hole Injection Layer
EBL	Electron Blocking Layer
HBL	Hole Blocking Layer
EML	Emissive Layer
LUMO	Lowest Unoccupied Molecular Orbital
HOMO	Highest Occupied Molecular Orbital
E_f	Fermi Level
Φ_a	Anode Work Function
Φc	Cathode Work Function
I_E	Ionization Energy
E_A	Electron Affinity
Φ_b	Injection Barrier
DOS	Density of States
SCLC	Space Charge Limited Conduction

ISC	Inter-System Crossing
IC	Internal Conversion
VR	Vibronic Relaxation
SMOLEDs	Small Molecules OLEDs
PLEDs	Polymer OLEDs
TPBi	2,2',2''-(1,3,5-benzinetriyl)-tris(1-phenyl-1-H-benzimidazole)
CBP	4,4'-bis(carbazol-9-yl)biphenyl
R2R	Roll-To-Roll
PHOLEDs	Phosphorescent OLEDs
$Ir(ppy)_3$	Tris(2-phenylpyridine)iridium(III)
ITO	Indium Tin Oxide
DI	Deionized
IPA	Isopropyl Alcohol
RIE	Reactive Ion Etching
ICP	Inductively Coupled Plasma
sccm	Standard Cubic Centimeter per Minute
PVD	Physical Vapor Deposition
LiF	Lithium Fluoride
DC	Direct Current
AC	Alternating Current
CCD	Charge-Coupled Device
PL	Photoluminescence
TCSPC	Time Correlated Single Photon Counting
MoO_3	Molybdenum Oxide
TTA	Triplet-Triplet Annihilation
TPQ	Triplet-Polaron Quenching
PT-ITO	Plasma Treated Indium Tin Oxide

Ar	Argon
IBAD	Ion Beam Assisted Deposition
Cl	Chlorine
DEL	Delayed EL

List of Tables

Chapter 1 Introduction

Recently, a great attention has been paid by industry to organic electronics (OE), since OE will radically change the way society interacts with technology. The OE field initiates a revolution over classical electronics (based on inorganic semiconductors such as silicon or germanium). It creates wide possibilities of industrial technologies including but not limited to disposable electronics, wearable electronics, flexible electronics or printed electronics that were not fully feasible before (Figure1.1). There are salient advantages of OE over classical electronics such as low cost of manufacturing, large area production, eco-friendliness, and mechanical flexibility. Meanwhile, the existence of some drawbacks and challenges such as poor crystalinity, low mobility, possible degradation under environmental influence, and solubility problems are slowing down this technology.

Organic semiconductors are materials based on organic π-conjugated chains that offer semiconducting properties. These materials can be used in various electronic devices, such as organic field-effect transistors (OFETs), organic light-emitting devices (OLEDs), organic solar cells (OSC), organic photodetectors (OPD), and organic memories (Figure1.1). The technology has already reached market maturity and is used efficiently with OLEDs, as OLEDs can be seen in high definition displays. On the other hand, solid-state lighting and flexible displays will be available in the market soon.

OLEDs are light-emitting devices in which the emissive electroluminescent layers and the layers responsible for charge transport are thin films of organic compounds. Electroluminescence (EL) is an optical and electrical phenomenon in which a material emits light under the passage of an electric current or to a strong electric field. This is distinct from black body light emission resulting from heat, or photoluminescence (PL) which is light emission due to the relaxation of excited states that were created due to photons absorption.

In this chapter, the literature review, the structure, the operation mechanism, and materials of the OLEDs, will be introduced. Furthermore, efficiency and degradation mechanisms of PHOLEDs will be discussed. Moreover, a comparison between conventional and simplified PHOLEDs will be established. Eventually, the objectives and approaches of this thesis will be articulated.

Figure 1.1 Examples of organic electronics.

1.1 Overview of OLEDs

The EL Phenomenon dates back to 1907, when H. J. Round discovered yellowish light emitted from carborundum (SiC) crystal upon application of electric field [1]. In 1953, the EL was observed from an organic material by applying a high-voltage alternating current (AC) field to crystalline thin films of acridine orange and quinacrine by Bernanose *et al.* [2]. The direct current (DC) driven EL cell using single crystals of anthracene was first demonstrated by Pope *et al.* in 1963 [3]. In 1975, the first organic EL devices made with a polymer polyvinylecarbazole (PVK) were demonstrated [4].

In early attempts to develop organic EL devices, the driving voltage was on the order of 100V or above in order to achieve a significant light output [5–7]. Vincett *et al.* achieved an operating voltage below 30 V by using a thermally deposited thin film of anthracene [8]. The research focused mainly in the academic field until Dr. C.W. Tang and his coworkers at Eastman Kodak showed, for the first time, efficient organic light-emitting devices in

multilayer configuration with significant performance improvement [9]. The devices were bright green devices based on tris(8-hydroxyquinoline) aluminum (Alq_3), in which the electron-hole pair recombination and light emission occurred. It showed a reduction of operation voltage and an improvement of efficiency, which initiated and led the current research and development of OLEDs.

1.2 Structure of OLEDs

OLED structure gained complexity over time for efficiency and stability enhancement purposes. The structure progressed from a single-layer organic structure [3] to multi-layer organic structure passing through a bi-layer organic structure [9]. The simplest conceivable OLED consists of an organic thin layer sandwiched between two electrodes: a transparent anode with high work function material and a metallic cathode with low work function material. The anode and cathode are used to inject holes and electrons respectively, while the organic layer can act as both charge transport layer and emissive layer.

1.2.1 Single-layer, bi-layer, and multi-layer structure

A single-layer OLED (Figure1.2(a)) was the initial phase of OLED development [3], where the EL was observed using anthracene as the organic material sandwiched between two electrodes. However this kind of single-layer devices suffered poor performance in terms of efficiency and operating voltage. Since the mobility of electrons and holes are different in organic materials, one type of the carriers (electrons or holes) was accumulated at one metal-organic interface where all the recombination happened in the OLED. Thus, the surplus electrons or holes will not recombine, which results in low operation efficiency.

After the single-layer structure, Tang *et al.* [9] proposed the bi-layer structure (Figure1.2(b)), this structure was comparably more efficient. The bi-layer OLED consists of two organic layers: the hole transport layer (HTL) and the electron transport layer (ETL) in addition to the metallic electrodes. This structure allows a balanced charge transport, inside the ETL and the HTL, of electrons and holes respectively. In addition, the ETL may block holes from moving towards the cathode. Similarly, the HTL may block electrons from moving towards the anode. Therefore, the holes and electrons will meet in the middle of two organic layers and recombine, which significantly improves the efficiency of OLEDs.

More typical is an increased complexity OLED structure, the multi-layer structure (Figure1.2(C)) consists of an anode, an anode buffer or hole injection layer (HIL), a hole transport layer (HTL), an emissive layer (EML), an electron transport layer (ETL), a cathode interfacial layer, and a cathode. In some devices, a hole blocking layer (HBL), an electron blocking layer (EBL), and a stabilizer layer are also applied to achieve the desired performance. Although the structure of a typical OLED can contain many layers, not all of these layers are

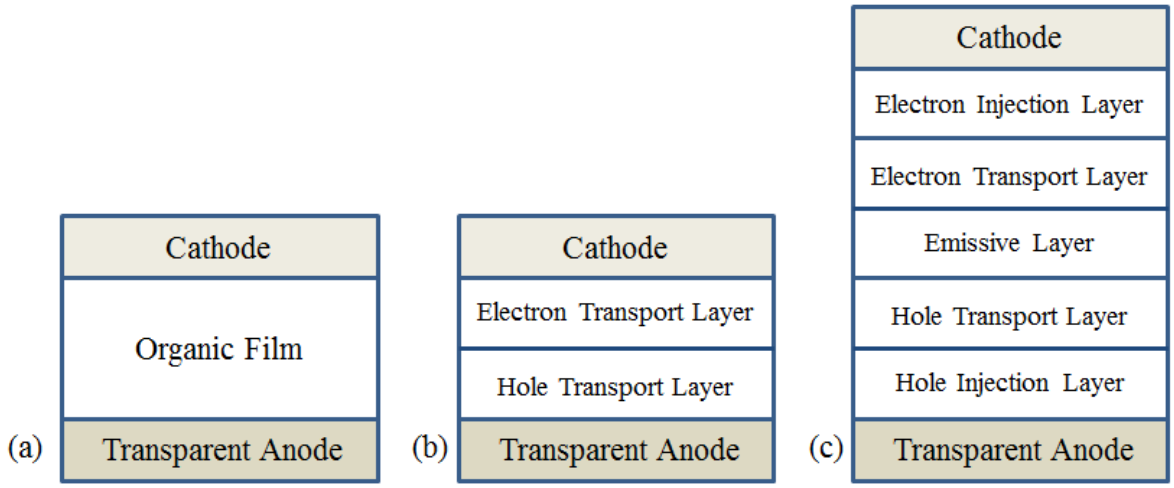

Figure 1.2 Structure of OLEDs: (a) single-layer structure, (b) bi-layer structure and (c) multi-layer structure.

necessarily present in all OLED architectures. Much of the current research on OLEDs focuses on the development of the simplest possible and most easily processed architecture that can deliver the optimal combination of device properties [10-11].

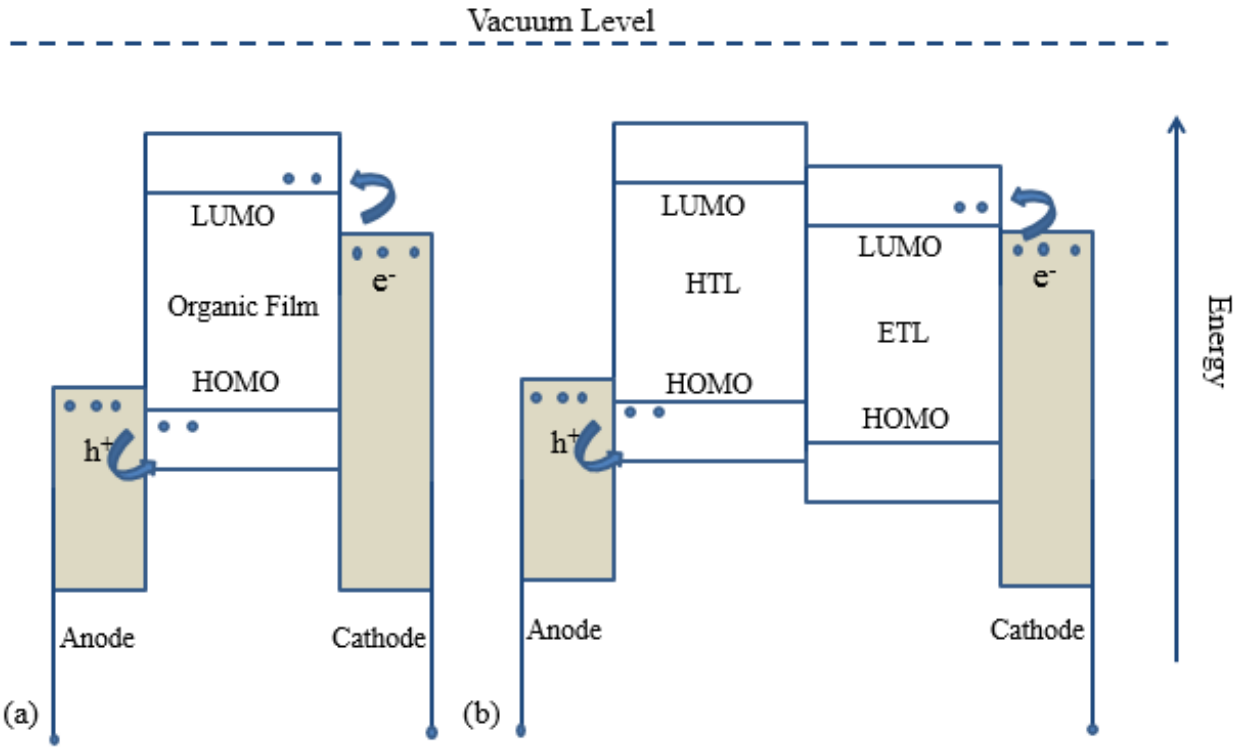

Figure 1.3 The energy band diagram: (a) single-Layer OLED and (b) bi-layer OLED.

The energy band diagram of the single-layer OLED and the bi-layer OLED is shown in Figure1.3. Since the organic materials have a semiconducting properties, there is analogy between organic and inorganic semiconductors. The lowest unoccupied molecular orbital (LUMO) is equivalent to the conduction band of inorganic semiconductors, while the highest occupied molecular orbital (HOMO) is equivalent to the valence band. The HOMO and the LUMO of the organic semiconductor are separated by a forbidden energy gap.

1.3 Operation Mechanism of OLEDs

The operation mechanism of OLEDs can be summarized into four aspects as shown in Figure1.4:

1.Charge carrier injection.
2.Charge carrier transport.
3.Electron-hole pair capture and exciton formation.
4.Radiative decay of excitons.

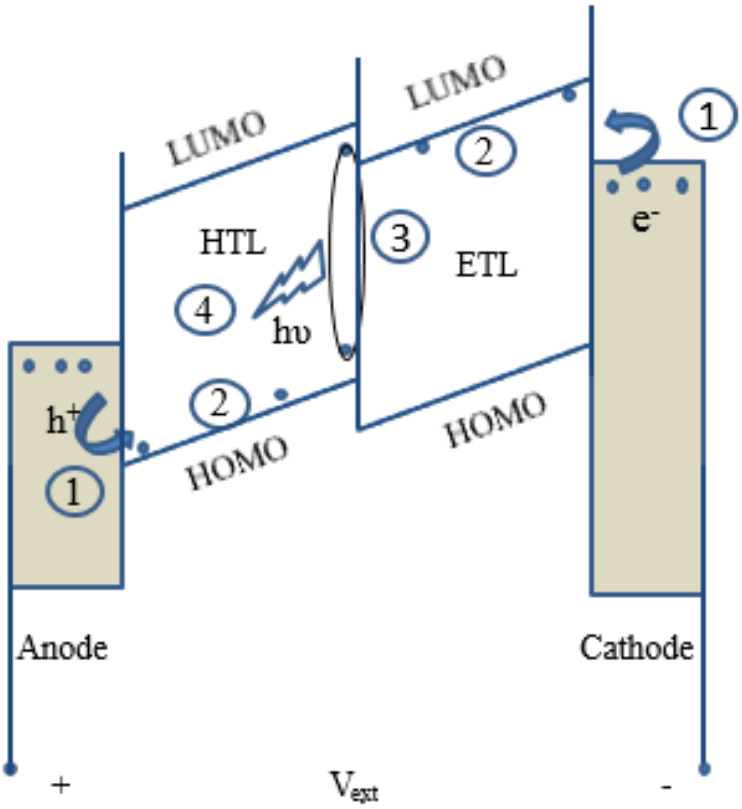

Figure 1.4 Operation mechanism of OLEDs.

1.3.1 Charge Carrier Injection

Charge carrier injection takes place at the electrode-organic interface, electrons and holes are injected from the cathode and the anode, respectively. Upon application of external electric field to organic semiconductors, band tilting occurs, which is closely related to the potential profile across the organic layer in devices. The electric field is often assumed to be constant and the potential is proportional to the position as shown in Figure1.5 [12].

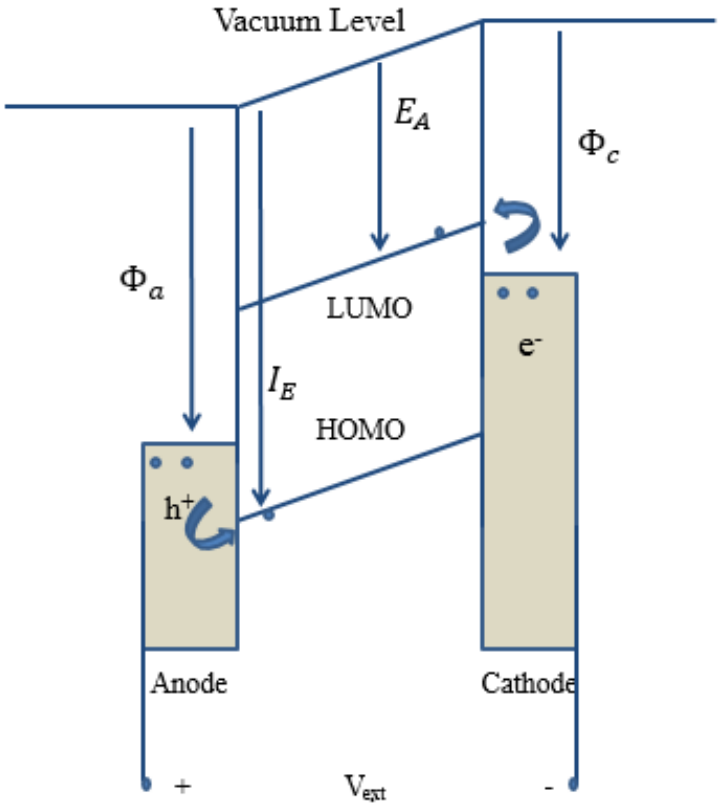

Figure 1.5 The energy band diagram of the OLED under forward bias.

Assuming vacuum level alignment across the interface, the energy barrier of the charge injection can be estimated. The injection barrier is the difference in energy between the electrode Fermi level (E_f) and the organic transport levels at the interface (HOMO or LUMO). The work function of the metal (Φ_m) is the difference in energy between E_f and vacuum level. The ionization energy (I_E) and the electron affinity (E_A) of the organic material are the difference in energy between vacuum level and HOMO and LUMO, respectively. As the organic LUMO level is typically higher than the metal E_f level, electrons at E_f of the cathode are facing a potential barrier $\Phi_b = \Phi_c - E_A$. Similarly, holes at E_f of the anode are facing a potential barrier $\Phi_b = I_E - \Phi_a$.

Two models are often used to describe injection of the carriers from the metal electrode into the semiconductor depending on the applied field strength. The first one is called Richardson-Schottky Model. In this model, charge injection at low applied bias is primarily due to thermal emission of charge carriers over the interface potential barrier when the barrier is not too high for thermal injection (Figure1.6). Field emission is the process whereby carriers tunnel through a barrier in the presence of a high electric field. When the barrier is triangular, the tunneling is called Fowler-Nordheim tunneling (Figure1.7).

$$j_{RS} = A^{*}T^{2}\ \exp\left(-\frac{\varphi_B - \Delta\varphi}{k_B T}\right), \qquad \Delta\varphi = \sqrt{\frac{q^3.F}{4\pi\,.\,\varepsilon_r\,.\,\varepsilon_0}}$$

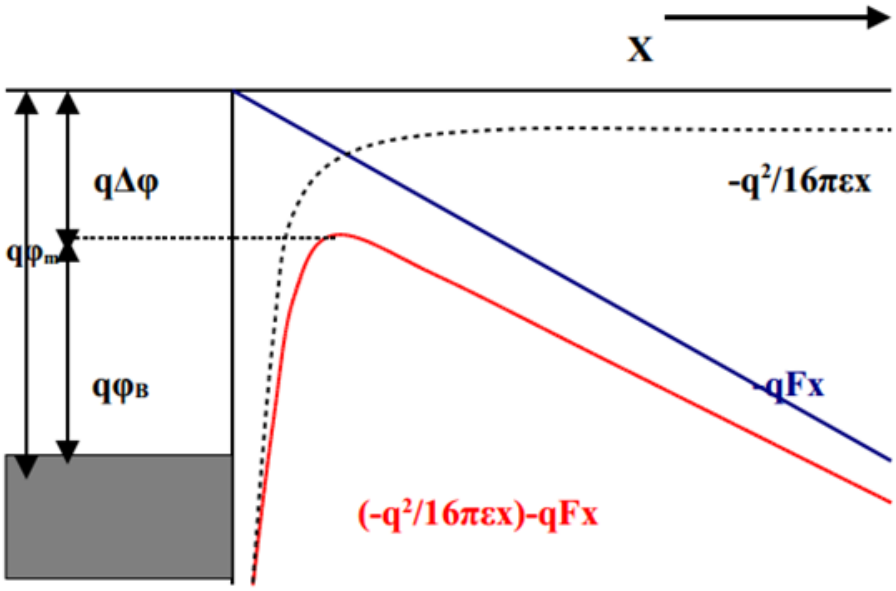

Figure 1.6 Field-assisted thermionic injection over the image force barrier (Richardson-Schottky Model).

$$j_{FN} = \frac{A^*}{\emptyset}\left(\frac{qF}{\propto k_B}\right)^2 \exp\left(-\frac{2\propto \emptyset^{3/2}}{3qF}\right)$$

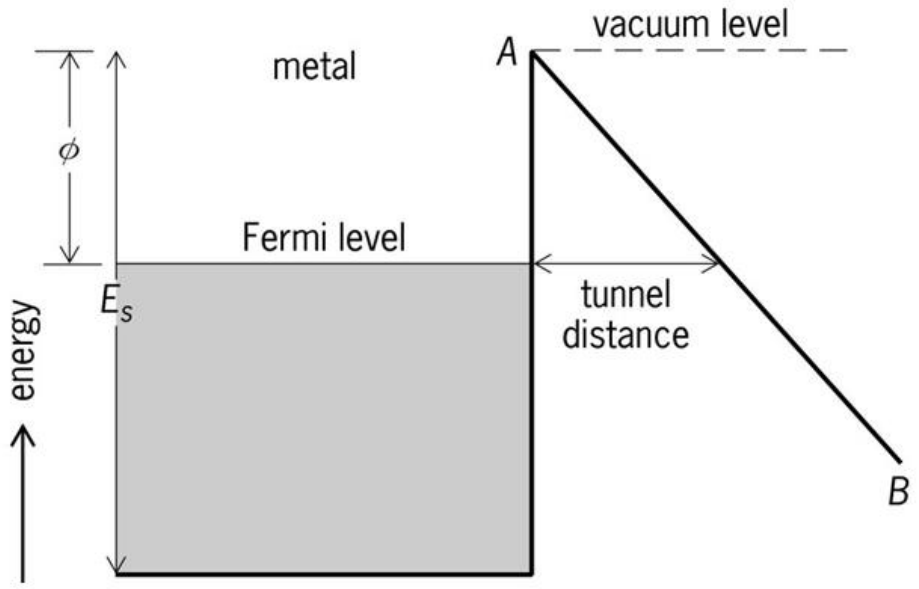

Figure 1.7 Quantum mechanical tunneling of electrons through a triangular energy barrier (Fowler-Nordheim Model).

1.3.2 Charge Carrier Transport

After the charge carrier injection process, the charge carrier transport through the organic thin films takes place. Although the organic materials possess semiconducting properties, the carrier transport process is quite different compared to inorganic semiconductors.

1.3.2.1 Hopping Transport

Due to the weak intermolecular coupling in disordered organic semiconductors, the states of charge carriers are considered localized to individual molecular sites rather than delocalized over the crystal lattice. Charge transport in amorphous organic semiconductor materials occurs by hopping through Gaussian distribution of localized states with superimposed potential disorder (Figure1.8). The relaxation time of carriers between scattering events is lower compared to the carrier residence time on the scattering site - i.e. the carriers are not as mobile as in the case of band transport of inorganic semiconductors [13].

The following equation represents the mobility as a result of hopping transport seen in organic semiconductor materials:

$$\mu \propto \mu_0 \exp\left(-\left(\frac{2\sigma}{3}\right)^2\right) \exp(C(\sigma^2 - \Sigma^2)\sqrt{E})$$

where σ = Density of States (DOS), C = Constant, Σ = Positional disorder and E = Electric field. From this equation, we can see that hopping transport in organic semiconductor materials is dependent on electric field strength.

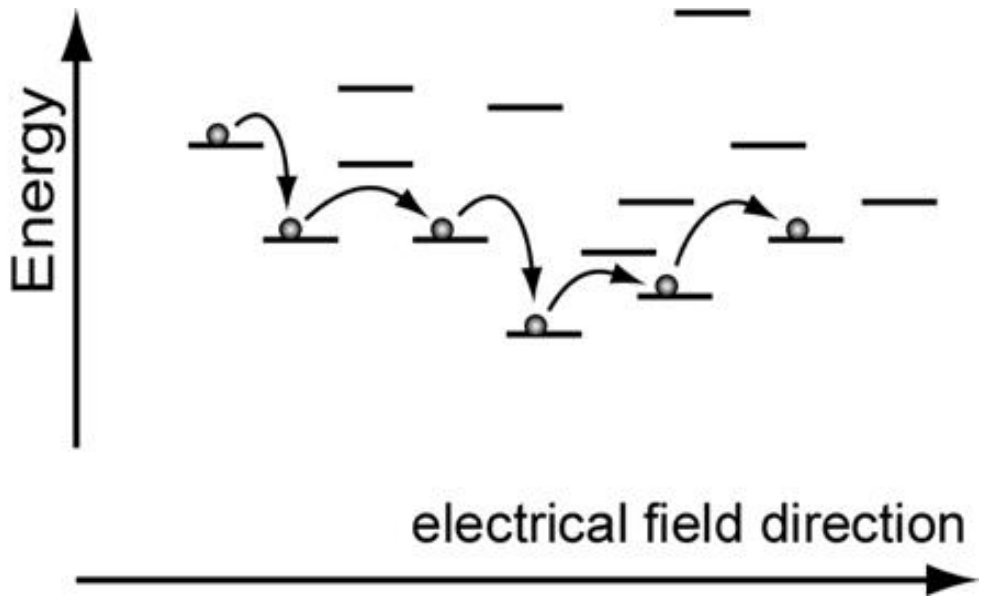

Figure 1.8 The hopping charge transport mechanism in organic semiconductors.

1.3.2.2 Space Charge Limited Conduction (SCLC)

Due to the disordered structure and the chemical or structural defects, organic semiconductors contain many trap states which can capture the injected charge carriers and form a large amount of space charge inside the semiconductor. As all these space charges prevent the transport of the carriers, it is termed as space charge limited conduction [14]. The SCLC-type mechanisms are invariably found to dominate the conduction in organic devices where a strong injection into low-mobility materials takes place.

Starting from ohmic region, as the applied electric field is increased, the trap states are filled gradually. On increasing the applied electric field more, most traps are filled. The traps filled limit V_{TFL} is the condition for the transition from the trapped to the trap-free characteristics (Figure1.9). The current density in each region can be calculated from [15]:

Ohmic:

$J \sim mV$.

Space-Charge Limited Current (SCLC):

$J \sim mV^2$.

Trap-Free Voltage Limit (V_{TFL}):

$V_{TFL} \sim d^2 N_t$, N_t = traps concentration.

Trap-Free SCLC:

$J \sim mV^2$.

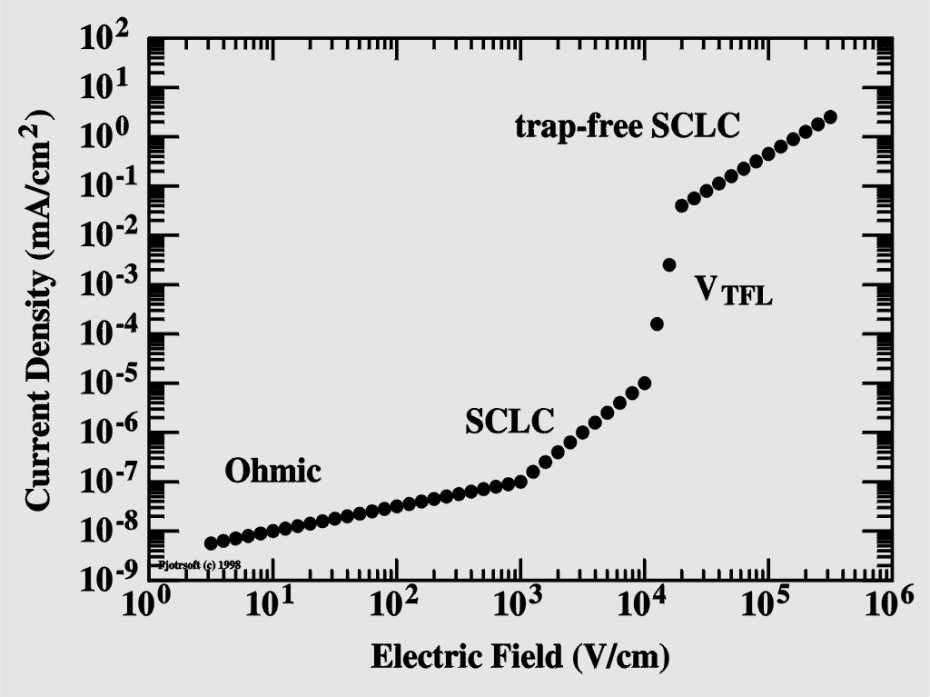

Figure 1.9 Current-density versus electric-field characteristics for organic semiconductors [15].

1.3.3 Electron-hole Capture and Exciton Formation

After the charge injection and the charge transport through the organic material, electron and holes in OLEDs will recombine to form excitons. An exciton is a bound state between an

electron and a hole which are attracted to each other by electrostatic coulomb force. It is electrically neutral quasi-particle that exists in insulators and semiconductors. The exciton is regarded as an elementary excitation of condensed matter that can transport energy without transporting net electric charge [16].

According to the distance and the interaction between the electrons and holes, and the degree of delocalization of the electron around the hole, exciton can be classified into three different types (Figure1.10): (a) Frenkel excitons (highly localized), (b) Wannier-Mott excitons (weakly localized) and (c) Charge-transfer excitons (intermediate degree of localization).

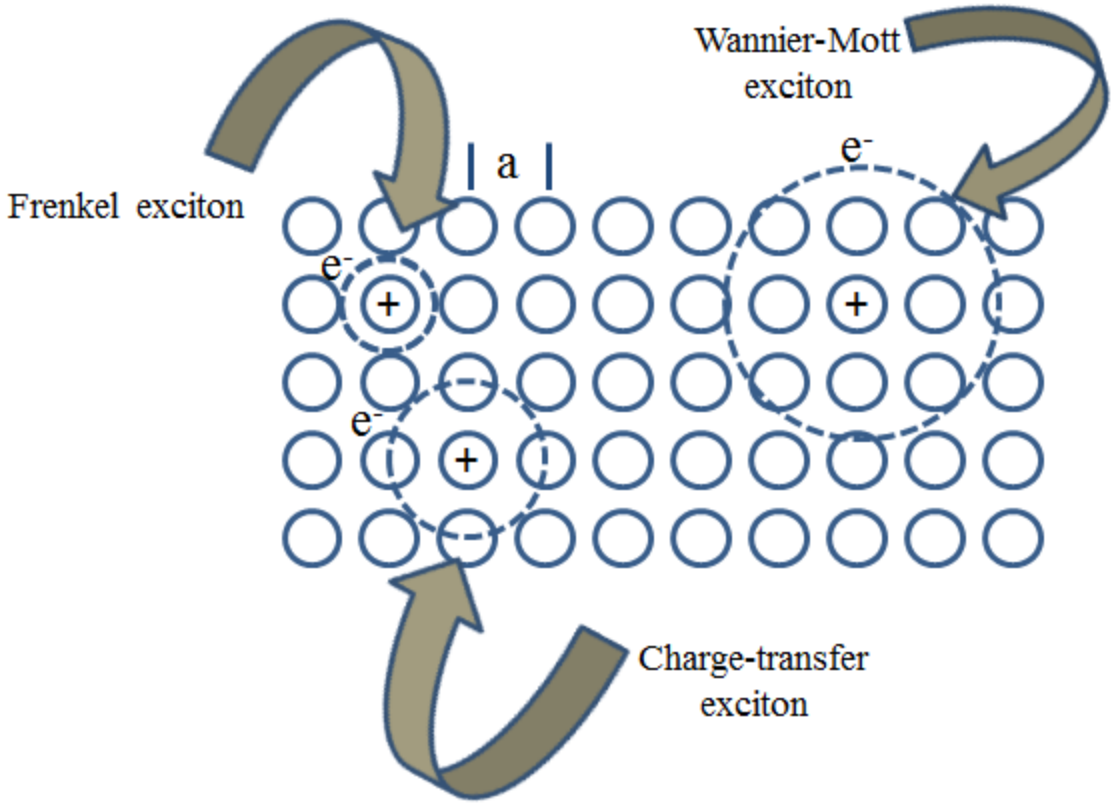

Figure 1.10 Exciton types.

Excitons can also be categorized as being in singlet or triplet state, according to the spin configuration of the electrons in the LUMO and the hole in the HOMO. If the two unpaired particles have the same spin, the exciton can be considered to be in triplet state. However, if the spins of the two unpaired particles are opposite, it is considered a singlet (Figure1.11). In EL phenomenon, electrons and holes are injected with random spin. Therefore, according to quantum mechanics, three out of the four possible spin state configurations lead to the creation of triplets. Therefore, 75% of excitons can be found in the triplet state, while 25% can be found in the singlet state.

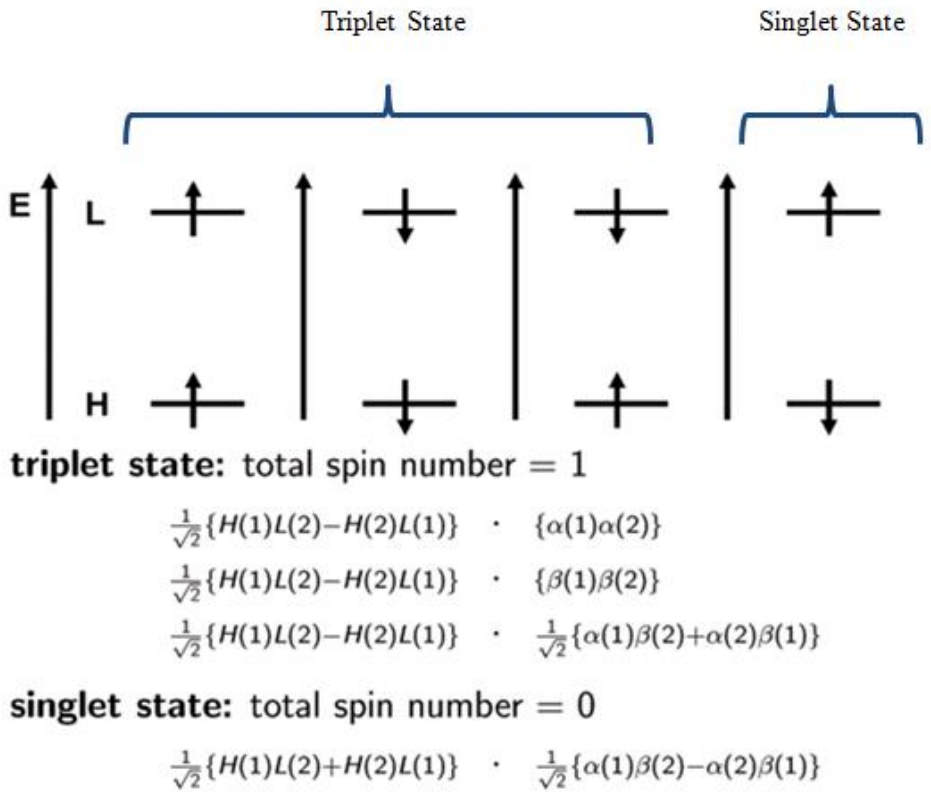

Figure 1.11 Triplet States and Singlet State.

1.3.4 Exciton Relaxation

After exciton formation, exciton relaxation process takes place. Both triplet and singlet states are not long lived (~ns for singlet excited states and ~ms for triplet excited states) [17]. Due to this short life-time, excitons are forced to lose their energy within a period of time induced by quantum fluctuation, collapsing to their ground state. The exciton relaxation process can be in two forms: radiative transition or non-radiative transition. All possible ways of exciton relaxation are shown in the Jablonski diagram (Figure1.12).

A Jablonski diagram is a diagram that illustrates the electronic states of a molecule and the transitions between them. The states are arranged vertically by energy and grouped horizontally by spin multiplicity. Non-radiative transitions are indicated by wavy arrows, while radiative transitions by straight arrows. In the figure, S_0 is the ground state, S_1 is the first singlet excited state, T_1 is the first triplet excited state, ISC is the intersystem crossing and IC is the internal conversion. All the different process can compete with each other over the relaxation of the excited state. (see Figure1.12)

The process of photon absorption can promote an electron from the ground state to an excited state. Such an excited state can release its excess energy via different mechanisms. A

first way is by the emission of a photon, which is called fluorescence or phosphorescence depending on the multiplicity of the excited state. Fluorescence is a rapid radiative process due to singlet excitons, in which the spin multiplicities of the initial and the final states are the same. Phosphorescence, on the other hand, involves the transition from the T_1 excited state to the S_0 ground state, requiring spin-orbit coupling to conserve total momentum. Because this transition is spin-forbidden, its intensity is orders of magnitude smaller than the intensity of fluorescence. For the same reason the lifetime of the triplet state is very long compared to fluorescence. During this long lifetime of the triplet state, the exciton is liable to diffusion towards trap states or to bimolecular reactions with other excitations such as triplet excitons, singlet excitons or charge carriers. These competing processes often prevent the observation of phosphorescence (triplet annihilation), especially at room temperature.

On the other hand, the excited state can also release its excess energy via non-radiative processes. Relaxation of the excited state to its lowest vibrational level is called vibronic relaxation (VR). This process involves the dissipation of energy from the molecule to its surrounding environment and is very fast [18]. The second type of non-radiative transitions is IC, which occurs when a vibrational state of an electronically excited state couples to a vibrational state of a lower electronic state with the same spin multiplicity ($S_{n+1} \rightarrow S_n$ and $T_{n+1} \rightarrow T_n$). A third type is ISC; this is a transition to a state with a different spin multiplicity. In molecules with large spin-orbit coupling, intersystem crossing is much more important than in molecules that exhibit only small spin-orbit coupling. Usually the triplet state is populated via ISC from the optically excited singlet state.

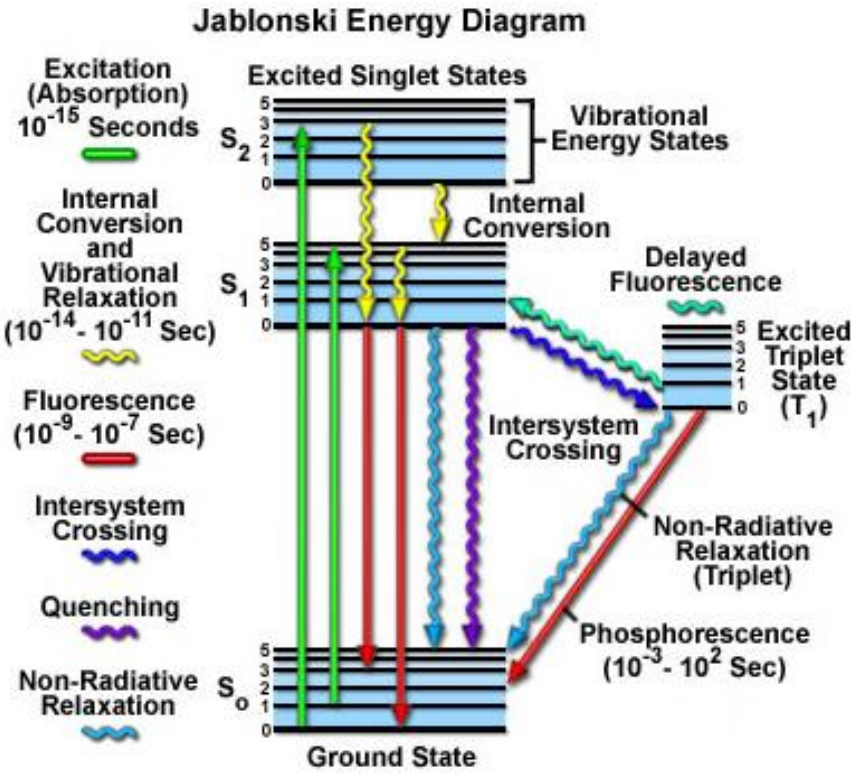

Figure 1.12 Jablonski Energy Diagram.

1.4 Organic Materials

As mentioned briefly in the previous sections, organic materials have semiconducting characteristics. These characteristics are the result of the atomic properties of the carbon atom. The electronic configuration of the ground state of a carbon atom is $1s^2\ 2s^2\ 2p^2$. In this configuration only the two unpaired p electrons in the outer electronic shell are able to form a bond with another atom, leading to e.g. the formation of methylene (CH_2). Mostly, however, the bonding is described by hybridization. Hybridization of the different atomic orbitals leads to more stable molecules and makes it possible to obtain a new set of hybrid orbitals, having an orientation in space matching the actual geometry of the compound much better [19]. Different hybridizations are possible: sp^3, sp^2 and sp hybridization.

For organic semiconducting materials, the sp^2 hybridization (Figure1.13) is the most important one. In this case, the 2s orbital and two of the three 2p orbitals will combine to form three sp^2 hybrid orbitals. These three sp^2 hybrid orbitals are coplanar, having an angle of 120° between them, and will form three covalent σ-bonds with neighboring atoms, which are strongly localized in molecular σ-orbitals. The remaining 2p orbital, which is not used during hybridization, is positioned perpendicular to this plane. If two unhybridized 2p orbitals of neighboring atoms overlap, an additional π-bond is formed via π-orbitals. The overlap region and the electron density of this π-bond is located above and below the plane of the σ-bonds. The combination of a sp^2-sp^2 σ-bond and a 2p-2p π-bond between two neighboring carbon

atoms is referred to as a double bond (C=C). In conjugated systems, the π-orbitals ideally extend over the complete molecule (the π-molecular orbital) and a delocalized electron cloud is created. The delocalized electrons are shared by all atoms of the conjugated molecule and can move freely over the entire molecule.

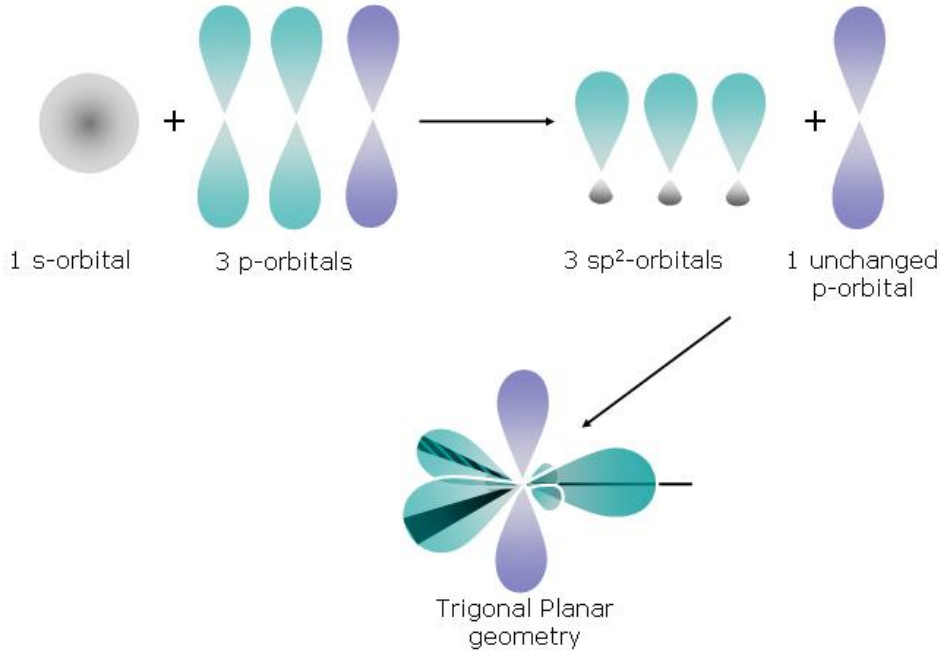

Figure 1.13 SP^2 Hybridization.

The overlap of π-orbitals gives rise to the formation of new, more extended orbitals. This process is denoted by the term 'splitting' (similar to inorganic semiconductors). The energy of these new orbitals with respect to each other and the original orbitals depends on the energy and overlap of the original orbitals: the stronger the overlap, the larger the splitting. In Figure1.14, the 2p orbitals of two carbon atoms in ethene molecule are combined, therefore, splitting occurs into a bonding molecular π-orbital and an anti-bonding molecular π^*-orbital. The bonding molecular π-orbital and the anti-bonding molecular π^*-orbital are, respectively, lower and higher in energy than the original atomic orbitals. Every 2p orbital has only one electron and therefore, according to the Pauli principle, only the bonding molecular π-orbital will be occupied in the ground state. The anti-bonding π^*-orbital is unoccupied. When more atoms are added, more bonding and anti-bonding orbitals with different energies are created. Theoretically, if the number of carbon atoms goes to infinity, the π and π^* energy levels will form quasi-continuous bands. The highest molecular orbital that still contains electrons at 0°K is called the HOMO. The lowest molecular orbital that has no electrons at 0°K is referred to as the LUMO. Typically, the HOMO and LUMO are separated by an energy gap, which induces semiconducting properties in these materials. The larger the molecule, the broader the energy bands and thus the smaller the band gap will be. In general, the energy gap in organic semiconducting materials is relatively large (2 to 5 eV) compared to inorganic semiconductors (1.1 eV for silicon and 1.4 eV for GaAs [20]).

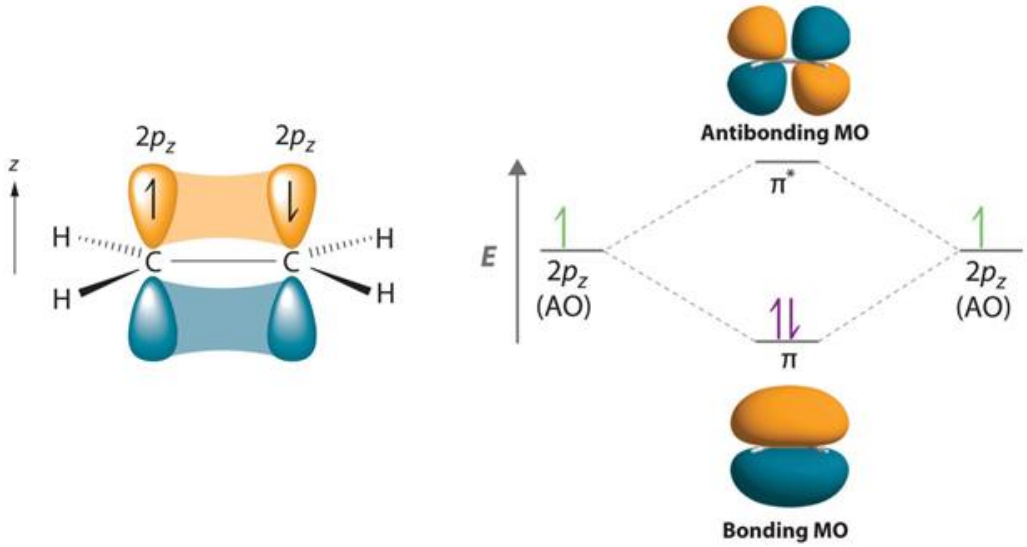

Figure 1.14 Ethene molecule as an example with splitting into bonding and anti-bonding orbitals.

The following classification of OLED materials depends on thin films processing techniques. Small molecules OLEDs (SMOLEDs) are generally prepared by thermal evaporation in vacuum conditions, while polymer OLEDs (PLEDs) are prepared by solution processing in nitrogen atmosphere.

1.4.1 Small Molecules

Small molecule organic materials are low molecular weight organic compounds (<900 Daltons), and are typically deposited from the gas phase by thermal evaporation (physical vapor deposition) under vacuum conditions. SMOLEDs offer higher efficiency compared to PLEDs, because thermal evaporation allows homogeneous organic thin films, better control of thickness and evaporation rate, and complex multi-layer structures without damaging the previously deposited layers. Meanwhile, thermal evaporation uses the organic material inefficiently and requires complicated vacuum system which is expensive to maintain. Current research focus on the solubility of small molecules for solution processing purposes, this solubility can be increased by the synthetic addition of side chains. Recently a SMOLED was fabricated by inkjet printing as an attempt of replacing thermal evaporation with solution processing of small molecules [21]. Figure1.15 shows TPBi (2,2',2''-(1,3,5-benzinetriyl)-tris(1-phenyl-1-H-benzimidazole)) and CBP (4,4'-bis(carbazol-9-yl)biphenyl) as an example of small molecules organic materials, which are used as ETL and HTL, respectively.

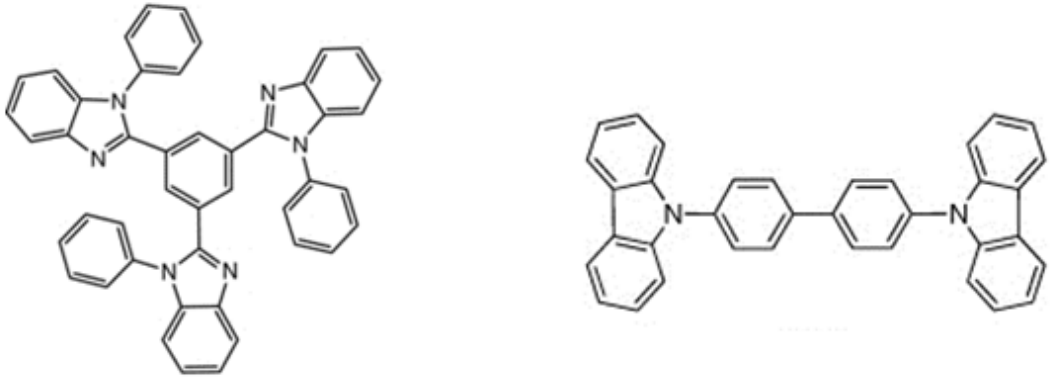

TPBi CBP

Figure 1.15 Examples of small molecules organic materials.

1.4.2 Polymers

Polymer organic materials are large molecular weight organic compounds, and are typically fabricated by solution processing techniques in nitrogen environment. The solution processing is more suitable for larger-area films than thermal evaporation, and it does not require the vacuum environment during the deposition. In addition, the inkjet printing allows large-volume roll-to-roll (R2R) fabrication of organic devices. Thus, the solution processing will reduce the fabrication cost of electronic devices significantly, which is the most attractive feature of organic semiconductor to electronics industry. However, the solution processes have their own disadvantages, such as problems during the deposition of subsequent layers which tends to dissolve those layers already present. Therefore, it is difficult to fabricate complex multi-layer structure. The controlled growth of the highly ordered and homogeneous films by solution processing is currently an ongoing research. Figure1.16 shows some examples of organic polymers used for PLEDs.

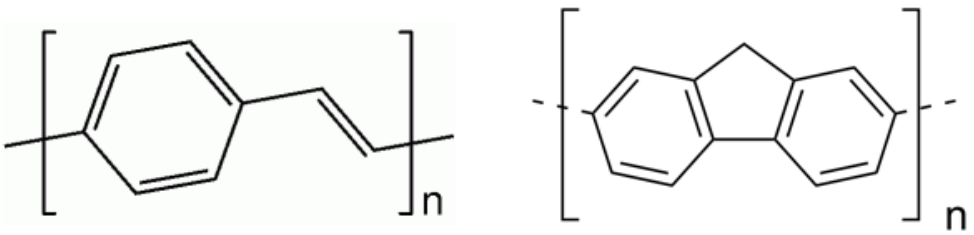

Polyphenylenevinylenes Polyfluorenes

Figure 1.16 Examples of organic polymers.

1.4.3 Phosphorescent Materials

Phosphorescent materials are typically used as dopants in the EML of SMOLEDs, they are known as PHOLEDs. These kind of materials offer a very high internal quantum efficiency. In Figure1.17, all the phosphorescent materials contain a heavy metal atom in their molecules. The heavy metal atom at the center of these molecules exhibits strong spin-orbital coupling, which is able to flip the electrons' spin direction. Consequently, this strong spin-orbital coupling facilitates ISC between singlet excitons and triplet excitons. By doping a phosphorescent materials in the EML of OLEDs, both triplet and singlet can undergo radiative relaxation, and a 100% internal quantum efficiency can be achieved. Such system is called host-guest system, where the guest is the phosphorescent material of smaller band gap than the host material. When a host molecule is excited from the ground state by either absorbing light energy or being driven by electric energy, energy transfer processes will occur form the host molecule to the guest molecule (Figure1.18). This energy transfer occurs through Forster, Dexter, or radiative energy transfer processes [23]. At this point, the radiative relaxation processes will occur eventually from the luminescent guest molecules. It may be noted that the emission spectrum observed is sometimes the emission from only the guest molecules due to complete energy transfer processes, but sometimes it combines the guest and host molecule emission due to incomplete energy transfer. Accordingly, the color of the PHOLED can be tailored according to the emission spectrum of the guest material [22] (Figure1.17).

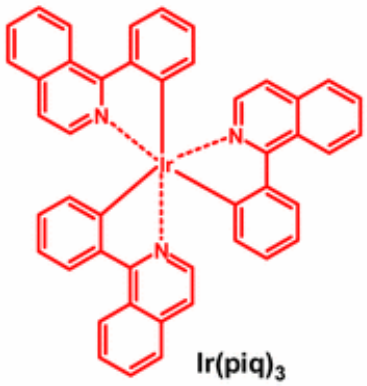

$Ir(piq)_3$

Tris(1-phenylisochinolin) iridium(III)

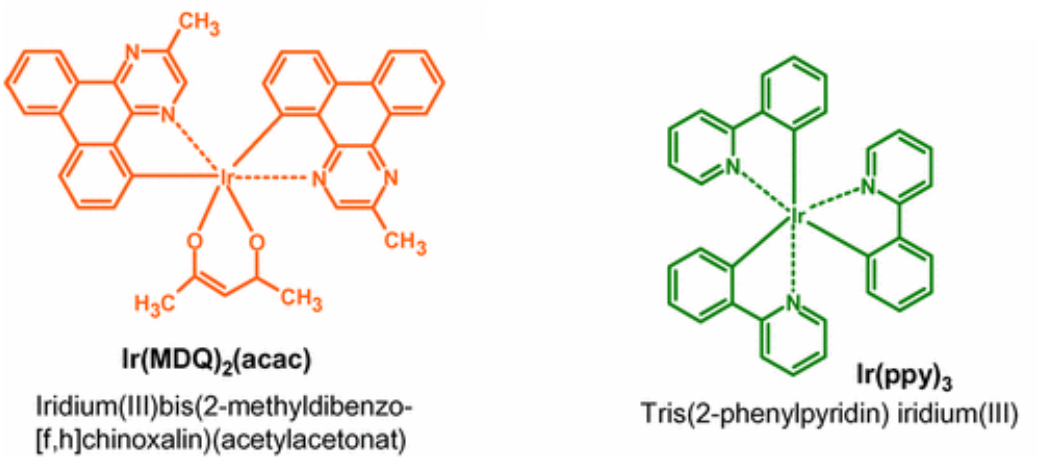

Figure 1.17 Examples of phosphorescent materials [22].

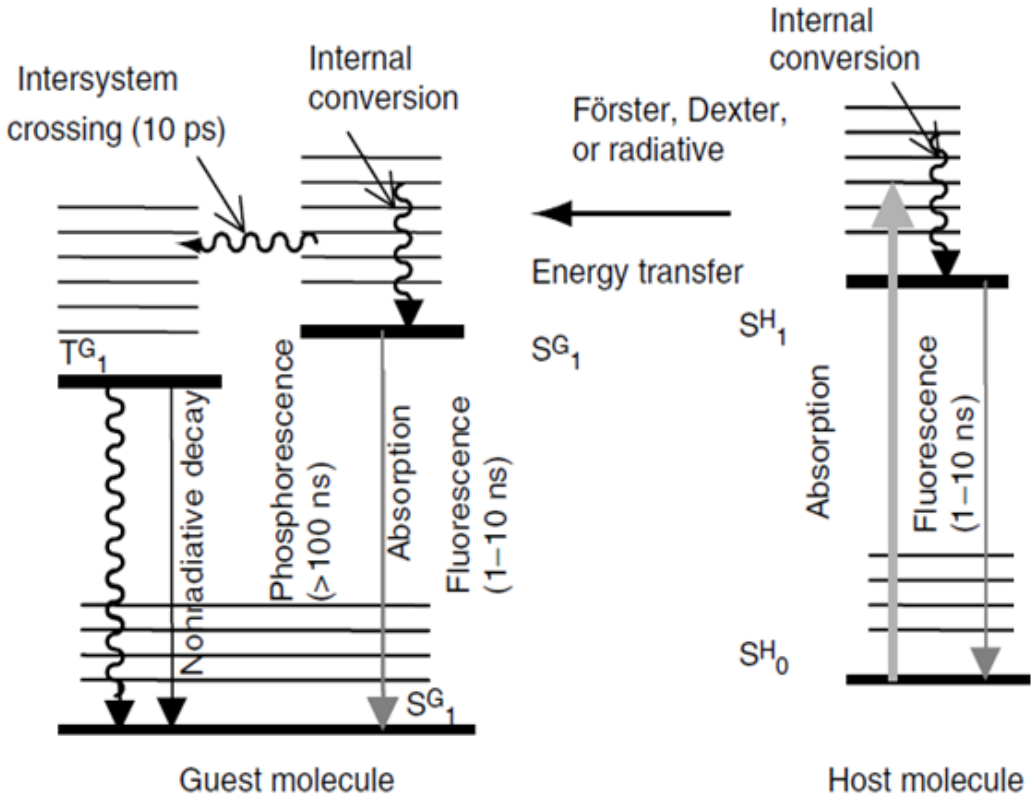

Figure 1.18 Energy transfer mechanism in host-guest system [23].

1.5 Efficiency and Degradation Mechanisms of PHOLEDs

The efficiency and the EL stability of PHOLEDs are important parameters for industrial applications. In this section, the main factors governing the luminescence efficiency of OLEDs will be explained. Also, the degradation mechanisms affecting OLEDs in general will be discussed.

1.5.1 PHOLED Quantum Efficiency

The EL internal quantum efficiency is affected by many factors, which are presented in the following equation:

$$\eta_{EL,\ internal} = \frac{\#\ of\ Photons}{\#\ of\ Electrons} = \eta_{exci} \cdot \eta_{PL} \cdot \eta_{e/h}$$

Where $\eta_{EL,\ internal} \equiv$ EL internal quantum efficiency, $\eta_{exci} \equiv$ Quantum efficiency of exciton formation, $\eta_{PL} \equiv$ Photoluminescence (PL) yield for excitons, and $\eta_{e/h} \equiv$ Charge balance factor.

Since PHOLEDs have the ability of EL from triplet excited states as well as singlet excited states [24], the theoretical limit of η_{exci} is 100%. Hence, $\eta_{EL,\ internal}$ have a potential to achieve 100% [25]. η_{PL} determines the ratio between radiative transitions and non-radiative transitions. Eventually, $\eta_{e/h}$ is the balance factor between both charge carriers (electrons and holes) which recombines to form excitons. In order to achieve high internal quantum efficiency, all the parameters should be maximized. η_{PL} can be maximized by avoiding exciton quenching such as triplet-triplet annihilation (TTA), triplet-polaron quenching (TPQ), concentration quenching. $\eta_{e/h}$ can be maximized by balancing charge injection and transport.

After achieving a high internal quantum efficiency, the external quantum efficiency should be maximized. In order to achieve high external quantum efficiency, an internal or external outcoupling system should be used. This outcoupling should lead to an efficient light extraction and should avoid photons internal reflections as well as photons diffraction.

1.5.2 PHOLEDs Degradation Mechanisms

As mentioned in the previous section, PHOLEDs can offer a competitive external quantum efficiency, however, the operational stability of OLEDs is relatively poor [26]. In general, degradation of OLEDs, can be categorized in two major groups: extrinsic degradation and intrinsic degradation.

Extrinsic degradation is normally caused by ambient conditions, where non-emissive dark spots appear on the device. This type of degradation can be overcome by the use of a proper encapsulation or by keeping the device in an inert environment. Extrinsic degradation studies of PHOLEDs focused on exposure to ambient conditions [27-29], sun stability [30], or photo-oxidation in the presence of ambient oxygen [31].

Intrinsic degradation occurs by reduction in the luminescence intensity in the absence of ambient conditions. Several mechanisms have been proposed to address the chemical and physical phenomena associated with intrinsic degradation, nevertheless, the reasons behind voltage rise and luminance loss accompanying PHOLEDs long term operation are not yet well understood [32].

Recently, Siboni *et al.* studied the intrinsic degradation in PHOLEDs reporting the causes for voltage rise [33] and luminance loss [34,35] independently. They hypothesized that the voltage rise in PHOLEDs with HBL is due to the accumulation of holes at the EML/HBL interface. They showed that, there is a direct correlation between voltage rise trends and the extent of hole confinement in the EML. The more hole confinement in the EML the fastest the voltage rise whereas the least hole confinement the slowest the voltage rise. This voltage rise occurs in order to offset the effect of the positive trapped charges at the EML/HBL interface. By using delayed EL (DEL) studies, they confirmed their hypothesis. Similar findings were reported [34,35] with respect to the luminance loss, since using marginally blocking HBL results in a marginal decrease in device EL stability whereas using strongly blocking HBL results in a significant decrease in EL stability. This decrease in the EL stability occurs as the accumulated holes most likely are acting as exciton quenchers or non-radiative charge recombination centers. They also showed that, the variation in the device stability under test does not arise from a chemical reaction between $Ir(ppy)_3$ and the HBL. On the other hand, the reasons behind the luminance loss in absence of HBL is attributed to the penetration of holes in the ETL leads to its deterioration. This lower electron transport capacity of the degraded ETL alters charge balance, hence causes luminance loss.

Sivasubramaniam *et al.* hypothesized that degradation of the HTL can reduce the operational stability of PHOLEDs [36]. It was found that new reaction products are formed during device operation as a result of HTL dimerization. These new products were characterized by LDI-TOF-MS, and it was hypothesized that they have a lower singlet or triplet energy state which in turn quench the emitter excitons and further reduce the PHOLED operational lifetime.

Giebink *et al.* proposed a model that describes luminescence degradation, voltage rise, EML PL quenching in electrically aged devices [37]. They proposed that defects can act as luminescent quenchers, non-radiative recombination centers, and deep charge traps depending on their energy levels. Both luminescent quenchers and non-radiative recombination centers causes luminance loss, while deep charge traps can cause voltage rise. They identified exciton-polaron annihilation as a main reason of defect formation leading to luminescence degradation. They inferred that energy exchanged by annihilation of guest triplet exciton to the host polaron results in a dissociative process in the host molecule itself. In [38], Giebink *et al.* provided a direct evidence of polaron-induced degradation that limits the operational lifetime of PHOLEDs. Comparing electron-only devices without guest material as a control device to electron-only devices with guest material (device under test), they managed to prove that host anions are unstable and the instability increases upon

excitation. As the control device with no guest material did not show any degradation with current passage or optical excitation, meanwhile the device under test showed degradation due to current passage and the degradation was even more pronounced when the current and the optical excitation are combined. On the other hand, when they attempt to compare hole-only device with or without guest material both were degradable under optical excitation. Therefore, they could not compare the control hole-only device to the hole-only device with the guest material (device under test). Therefore, they hypothesized that the HTL is unexpectedly degradable under sub-energy-gap illumination due to cationic excited states.

Scholz *et al.* studied the chemical degradation of PHOLEDs [39]. They introduced laser deposition/ionization time-of-flight mass spectrometry (LDI-TOF-MS) for analyzing chemical degradation mechanism in DC-driven PHOLEDs. They showed a dependence of PHOLED degradation on the chemical interactions between the Ir based emitter and the HBL. TPBi and BPhen as HBLs showed strong chemical interactions with Ir complex, hence PHOLEDs with these blocking layers demonstrated the least EL stability. Meanwhile, Alq_3 showed minor interactions and BAlq showed no interactions at all. Therefore, they showed that PHOLEDs with BAlq as a HBL tend to become very stable compared to other blocking layer.

Kondakov *et al.* reported that the irreversibility of PHOLED operational degradation is a consequence of irreversible chemical reactions in the EML leading to degradation products [40]. This degradation products accumulates in the form of neutral radical species and their reduced or oxidized form, therefore acting as non-radiative recombination centers and luminescence quenchers.

Lee *et al.* proposed a model for long term degradation of fluorescent OLEDs [41]. According to this model, indium ions diffuses from the ITO electrode into the adjacent organic layers during device operation. This electrical migration of charged indium atoms into organic layers can lead to increase in driving voltage and reduced luminescence efficiency. Since PHOLEDs use ITO as the transparent anode, therefore, this mechanism can cause degradation in PHOLEDs as well.

Other degradation studies showed that in order to achieve a high stable PHOLEDs, a combination of the low current density is needed to reach a certain luminance and also a high stability of the materials against both charge carriers and excitons [42]. In our previous studies of the ITO/organic interface in fluorescent OLEDs [43,44], it was discovered that such an interface is susceptible to photo-degradation, which plays an important role in limiting the operational stability of OLEDs. A gradual charge injection deterioration was observed, upon exposing the OLED to external illumination. Therefore, a correlation between the photo-stability of the ITO/organic interface and the operational stability of the OLED was established. This photo-degradation might also be present in PHOLEDs due to ITO/organics interfaces.

In this work, we will be focusing on the EL stability of simplified PHOLEDs under electrical stress. Therefore, all the stability measurements will be done under nitrogen conditions to exclude any other degradation mechanism and consider only EL stability under electrical stress.

1.6 Conventional versus Simplified PHOLEDs

In this section, the structure of the simplified PHOLEDs is explained. Also, the literature review of the simplified PHOLEDs is presented.

1.6.1 PHOLEDs Structure

The conventional PHOLED structure and the simplified PHOLED structure are presented in Figure1.19. As we can see from the figure, the conventional PHOLED is composed of HTL with a shallower HOMO level in order to facilitate hole injection from the ITO electrode. Followed by a host/guest system for efficient energy transfer with a host of wider band gap and a phosphorescent guest with narrower band gap depending on the required emission spectrum. Since the host material is a wide band gap material, typically it has a deeper HOMO level. After the host/guest system, there is the ETL and eventually the metallic cathode. The simplified PHOLED is composed of one material for both hole transport and emitter host which is typically a deep HOMO level material. After the host/guest system the two structures are identical.

The ITO work function is low (~4.7eV) which adds complexity to the design of organic optoelectronic devices in terms of hole injection due to the large mismatch between the low work function of the ITO and the energy levels of the active organic materials used in devices [45]. Since the HOMO of the HTL in the simplified PHOLED is deeper compared to the conventional one, either ITO surface treatments or the use of HIL is essential for facilitating the process of hole injection into the HOMO of the HTL. Wang *et al.* demonstrated efficient hole injection from the ITO to CBP with deep HOMO (~6.1eV) by using high work function transition metal oxides as a HIL [46]. In the absence of these thin HIL (1nm), the fluorescent OLEDs fabricated demonstrated very high driving voltage and very low efficiency due to the poor injection of holes into the HOMO of the HTL.

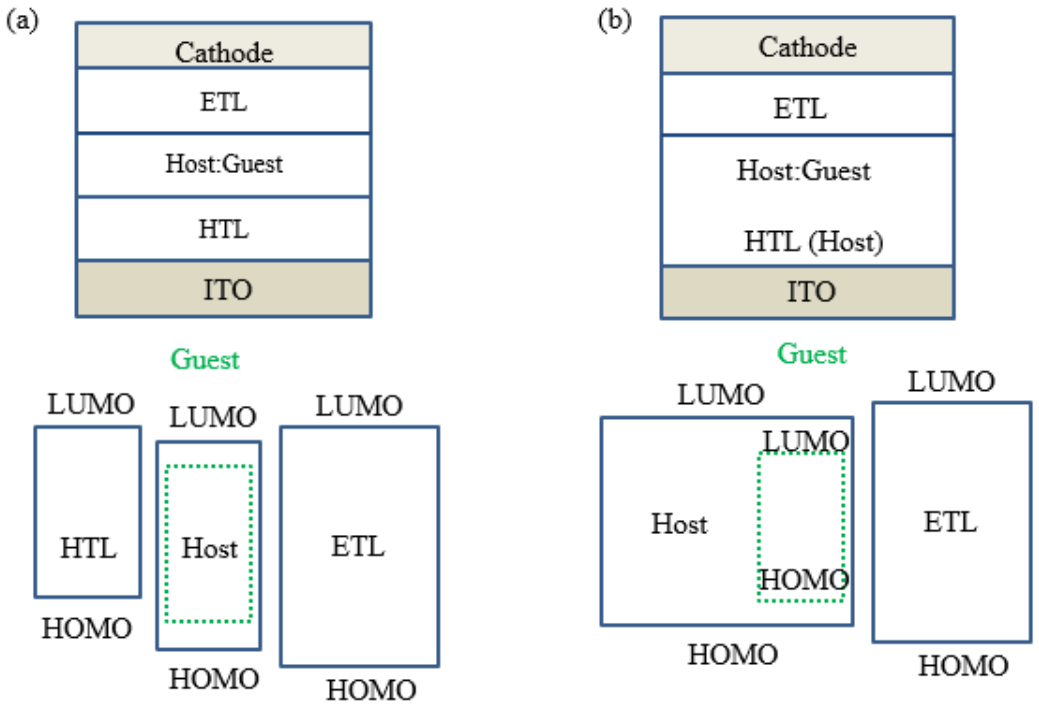

Figure 1.19 Conventional versus Simplified PHOLEDs.

1.6.2 Simplified PHOLEDs

The simplified PHOLEDs were firstly reported in 2011 by Wang *et al.* [10]. The idea behind this simplified structure is to have high efficiency, hence comparable to the state of the art *p-i-n* PHOLEDs, yet with less design complexity and low efficiency roll-off (reduction of efficiency at higher current densities). As mentioned in the previous section, a HIL is necessary for hole injection into the deep HOMO of the HTL of the simplified PHOLED, therefore a 1nm MoO_3 HIL was used for such purpose. They achieved highly efficient green PHOLEDs with low operating voltage, high external quantum efficiency and low efficiency roll-off (>20% external quantum efficiency at >10,000cd/m^2). By studying the EL spectra with increasing current density, they concluded that the triplet excitons are well confined in the EML since there was no change observed in the EL spectra. Eliminating the HTL/EML interfacial energy barrier by using one material in both HTL and emitter host as well as the EML/ETL interfacial energy barrier by selecting transport materials (CBP and TPBi) with almost identical energy-levels, allowed them to suppress triplet excitons quenching processes (such as TPQ) at high luminance, which in turn yielded in lower efficiency roll-off. The high efficiency roll-off in the conventional devices was found to be attributed to the electron-hole imbalance due to the blockage of holes at the HTL/EML interface. On the other hand, they hypothesized that in the simplified PHOLEDs the charge balance is improved hence the roll-off is lower.

Helander *et al.* proposed a surface treatment of the ITO by means of wet chlorination treatment in UV-generated ozone [45]. This treatment allows an anode with a work function greater than ~6.1eV. By incorporating this chlorinated-ITO (Cl-ITO) with the simplified PHOLEDs structure, a more efficient simplified PHOLEDs with low efficiency roll-off (50% external quantum efficiency at 10,000cd/m^2) can be achieved. This efficiency is higher than the state of the art *p-i-n* PHOLEDs which requires more complicated design (more than six organic layers). This enhanced efficiency is attributed to the efficient hole injection process (the PHOLED operating voltage was markedly reduced) and the better electron-hole balance.

Cao *et al.* reported similar work to Helander *et al.* [47]. They treated the ITO with chlorine plasma instead of the wet chlorination, As the developed plasma chlorination process is very effective for surface modification of the ITO meanwhile highly scalable for mass production. Helander *et al.* did not report EL stability data of such simplified PHOLEDs. On the other hand, Cao *et al.* reported very poor simplified PHOLEDs stability. Gao *et al.* also introduced a thermally evaporated $InCl_3$ layer to act as HIL for the simplified PHOLEDs [48]. They also reported very poor EL stability. In both studies [47,48], It has been observed that different treatments on ITO surface lead to different EL stability behavior of such devices.

1.7 This Work

In this section, the work in this thesis will be discussed including the rationale, the main objectives, and the methodology.

1.7.1 Rationale

The literature findings about the simplified PHOLEDs were discussed above. These findings were mainly concerned with the external quantum efficiency and efficiency roll-off. Simplified PHOLEDs showed higher power efficiency to the state of the art *p-i-n* PHOLEDs, yet they are much simpler in terms of design and fabrication. However, the reported EL stability studies are showing very poor EL stability behavior of such simplified PHOLEDs. Being an important aspect for display commercialization, the EL stability of the simplified PHOLEDs should be studied extensively.

It was mentioned in the previous section that the presence of charge blocking layers can alter PHOLEDs EL stability due to TPQ. In simplified PHOLEDs, blocking layers are absent at the HTL/EML interface while it is present at the EML/ETL interface as in the ETL (TPBi) no hole transporting behavior is known [41]. This also reveals the need for EL stability studies of simplified PHOLEDs to confirm the impact of blocking layers on device stability and whether the simplified structure has better EL stability or not.

Furthermore, The reported data regarding the EL stability of the simplified PHOLEDs suggests that different treatments on the ITO surface, leads to different EL stability behavior. This implies that the ITO/organic interface might be hosting an additional degradation mechanism, besides the other degradation mechanisms reported in the previous section. Moreover, it has been assumed, but never been verified, that the difference in the EL stability may be attributed to the joule heating at such interface that can accelerate the crystallization of the organic material which in turn introduces interfacial defects. Another hypothesis was that different treatments on the ITO surface might lead to different rates of indium outdiffusion from the ITO. Therefore, this interfacial degradation at the ITO/organic interface should be considered and identified clearly. Hence, a correlation is needed between such degradation and the EL stability of PHOLEDs. Also, the impact of different ITO treatments on device performance should be outlined

Eventually, more insights on the high efficiency reasons are essential for further enhancing the performance of the simplified PHOLEDs. More insights are needed as well on exciton formation and recombination zone location for further understanding of these devices.

1.7.2 Objectives

This work will focus on the following objectives:

- Study the role of the ITO/organic interface on simplified PHOLEDs performance.
- Understanding the difference in EL stability behavior at different treatments on the ITO surface of the simplified PHOLEDs.
- Study the current efficiency and the efficiency roll-off of the simplified PHOLEDs and have more insights on recombination zone location in simplified PHOLEDs

1.7.3 Methodology

The methodology of this work includes:

- Fabrication: Hole-only devices are fabricated and studied in order to compare the difference in behavior between the conventional and simplified PHOLEDs in terms of charge injection and charge transport using I-V-L measurements. Furthermore, PHOLEDs with conventional and simplified structure are fabricated and the difference in behavior with respect to efficiency, and EL stability, is reported using I-V-L measurements and spectrum analyzer.

- Efficiency studies: Different surface treatments of ITO in addition to the use of different thickness HIL in order to study the impact of the ITO/organic interface on device efficiency. Furthermore, Codeposition experiments of two or three organic materials in the EML, HTL, or the ETL as an attempt to enhance charge balance, operating voltage, and the device efficiency. Moreover, Modified HTL/EML interfaces are studied as an attempt to have multiple active regions in the simplified PHOLEDs for efficiency purposes.

- DEL measurements: are performed in order to have more insights into TTA, TPQ and charge trapping in simplified PHOLEDs.

- EL stability studies: of simplified PHOLEDs with either ITO treatments or HIL is compared under constant DC stress of 20mA/cm^2.

- Optical excitation: experiments for hole-only devices are done using a monochromatic light source in order to study the impact of excitons on the ITO/organic interface.

- Fluorescence lifetime measurements: are done for organic layers of ITO/organic layers in order to study the impact of the surface-treated ITO or HIL on excitons lifetime.

1.8 Thesis Organization

Chapter one is the introduction to OLEDs. It includes an overview, the different structures and operation mechanisms of OLEDs. A brief introduction to organic materials is also included. Moreover, the efficiency the degradation mechanisms of PHOLEDs is discussed. Eventually, a comparison between conventional and simplified PHOLEDs is established.

Chapter two is mainly related to the experimental methods of OLEDs fabrication and characterization. The fabrication section includes substrate structure, substrate handling, thin-film deposition. The testing of OLEDs contains several measurement techniques including IVL, efficiency, EL stability, emission spectrum, DEL, exciton life-time, and Photo-stability measurements.

Chapter three is the main body of the thesis. It includes the results and discussion of the simplified PHOLEDs. It begins with comparing the structure of the conventional PHOLED to the simplified PHOLED. Then, the differences between the conventional PHOLED and the simplified PHOLED with respect to charge injection, charge transport, exciton formation, current efficiency and EL stability, are explained. Then, the role of the ITO/organic interface on simplified PHOLEDs performance is studied. Finally, the effects of codeposition of organic materials or modifying the HTL/EML interface on PHOLEDs efficiency are addressed.

Chapter four is the last chapter of this thesis which includes the conclusion and future work.

Chapter 2 Experimental Methods

Experimental Methods including fabrication of OLEDs, simplified PHOLED structure and testing techniques are presented in this chapter. It worth mentioning that OLED fabrication took place in clean room environment at the Giga-to-Nanoelectronics Center (G2N) at Waterloo University. All the OLEDs were fabricated by thermal evaporation of small molecule organic materials and their testing was done in nitrogen environment under room temperature conditions.

2.1 Fabrication of OLEDs

Device fabrication includes substrate cleaning and thermal evaporation of the organic materials, buffer layers and metallic cathode. Each of these steps substantially determines the quality and performance of the operating OLEDs.

2.1.1 Substrate Structure

A glass substrate with a pre-patterned ITO (15Ω/sq) is used as the transparent anode (150nm). The substrates were purchased from Lumtec corporation. Figure2.1 shows the basic structure of the substrate, ten OLEDs can be made on one substrate with five different device structures.

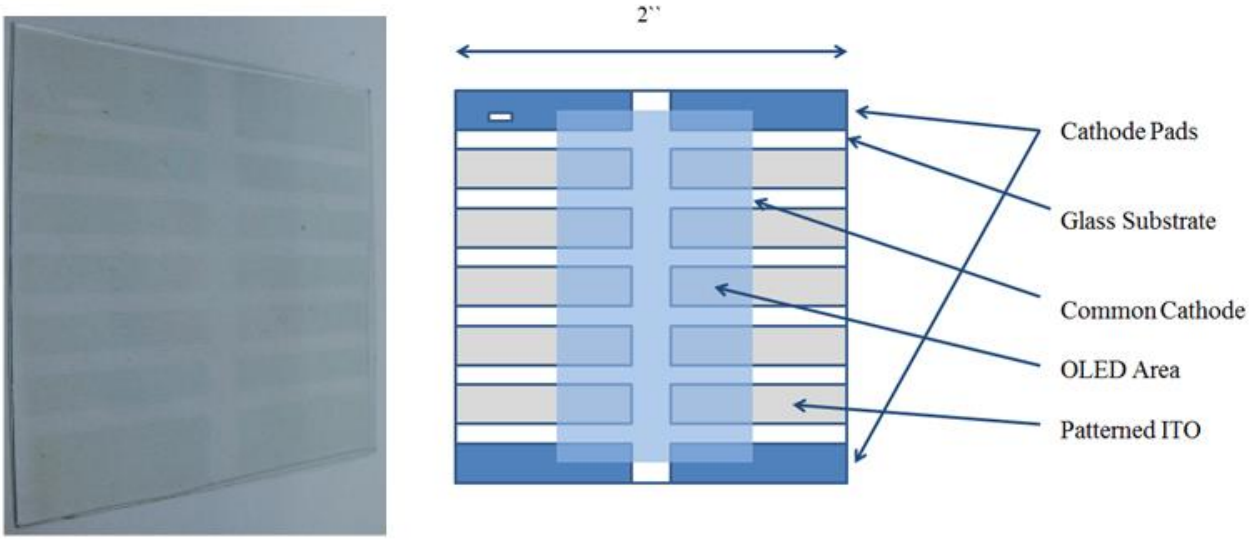

Figure 2.1 Substrate structure.

2.1.2 Substrate Cleaning

Since the device performance is affected greatly by the ITO cleanliness, the cleaning procedure was done carefully. ITO cleaning steps are:

1. ITO substrates are cleaned with deionized (DI) water to get rid of dust particles.
2. ITO substrates are put into 1L beaker filled with Acetone and cleaned with ultrasonic bath for 15 minutes to remove all kinds of organic contaminations on the ITO substrate surface.
3. ITO substrates are cleaned with Q-tips to remove any contaminations sticking on the surface.
4. ITO substrates are put back into 1L beaker filled with Isopropyl alcohol (IPA), and cleaned with ultrasonic bath for another 15 minutes in order to remove acetone residuals.
5. Nitrogen gun is used to dry the ITO substrates and blow away any particles.
6. ITO substrates are baked in the oven at 90° C for 15~20 minutes to remove the moisture and for the complete dryness of the substrates.

2.1.3 Plasma Treatment

Before the OLED fabrication, another cleaning step is added using reactive ion etching (RIE) technology. RIE applies a plasma treatment to the ITO surface in order to improve the work function of ITO, hence, improves the charge balance and the device life-time. The optimal parameters of the RIE for substrate treatment are listed in Table2.1:

Table 2.1 Optimal parameters of RIE for substrate treatment.

Parameter	Value
Pressure	20 mTorr
Inductively Coupled plasma power (ICP)	100 watts
Duration	120 seconds
Gas Proportion	CF_4 (75%) : O_2 (25%)
Gas Rates	CF_4 (15 sccm) : O_2 (5 sccm)

2.1.4 Thin Film Deposition by PVD

Thermal evaporation or physical vapor deposition (PVD) of organic materials and metals was done at a rate of 1-3 Å/s under vacuum conditions at pressure below 5×10^{-6} Torr. Angstrom EVOVAC Deposition system 00903 (Figure2.2 (a)) was used for such purpose. The EVOVAC is capable of combining multiple thin film deposition sources, electron beam evaporation, and four magnetron sputtering target, in the same chamber (Figure2.2 (b)). Since the Angstrom EVOVAC Deposition system has ten thermal evaporation sources which are controlled by 4 outputs and are monitored by 4 crystal sensors, we can mix up to 4 different materials by coevaporation (codeposition). This advantage of the system is critical to investigate the electrical and optical properties of the mixture films.

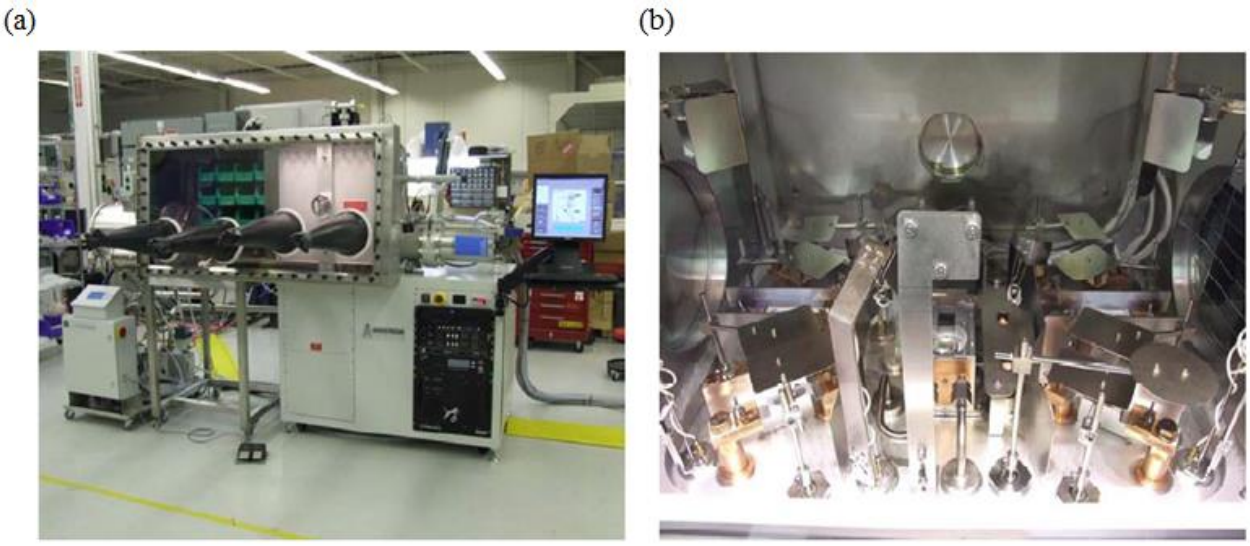

Figure 2.2 (a) The Angstrom EVOVAC Deposition system 00903 (b) The inside look of the chamber.

2.2 Device Structure

The OLED structure depends on the experiment under investigation, the control device structure is shown in Figure2.3. This structure is used as the reference device and any modifications in the design is compared to such structure. ITO is the transparent anode, MoO_3 is the HIL, CBP is used as the HTL and the host material, $Ir(ppy)_3$ is used as the phosphorescent dopant (guest), TPBi is used as the ETL and LiF/Al is used as the cathode. The codeposition of the host-guest system is composed of 8wt. % of $Ir(ppy)_3$. The pristine device structure is ITO/MoO_3 (1nm) /CBP (35nm) /CBP: $Ir(ppy)_3$ (92% : 8%) (15nm) /TPBi (45nm)/LiF (1nm) /Al (100nm).

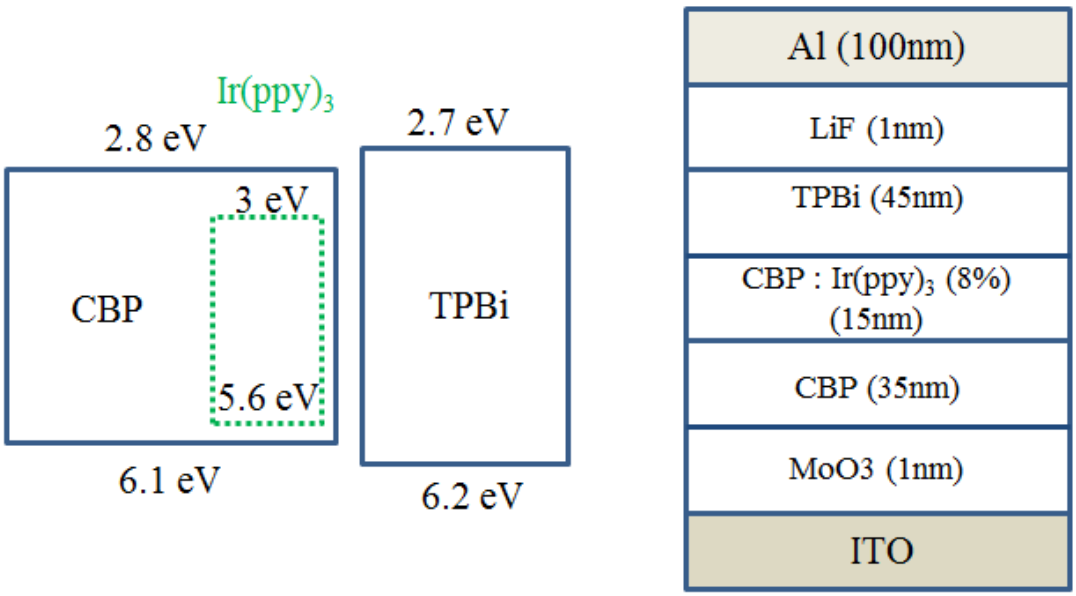

Figure 2.3 Pristine device structure.

2.3 Testing of OLEDs

After the fabrication process, OLEDs go through various testing procedures. The OLED is kept under nitrogen environment and all the measurements are performed at room temperature. In the next few sections, a brief introduction will be given to the different tests and the tools used for such tests.

2.3.1 I-V-L and Efficiency Measurement

The current-voltage-luminescence (I-V-L) measurements is a quick and easy measurement, which is useful in the calculations of turn-on voltage and EL efficiency. A 20 mA/cm^2 is applied using a current source and the voltage is measured using digital multi-meter, while the luminescence and the CIE color are measured using Minolta chromameter CS-100A (Figure2.4(a)). Then, the measurement of I-V-L curves are performed with the aid of Agilent 4155C semiconductor parameter analyzer (Figure2.4(b)) and a photo-diode, by DC (direct current) voltage sweep. Then the current efficiency (in cd/A) is calculated from the data mapping between the measured luminescence at 20 mA/cm^2 and the measured luminescence from the DC sweeps.

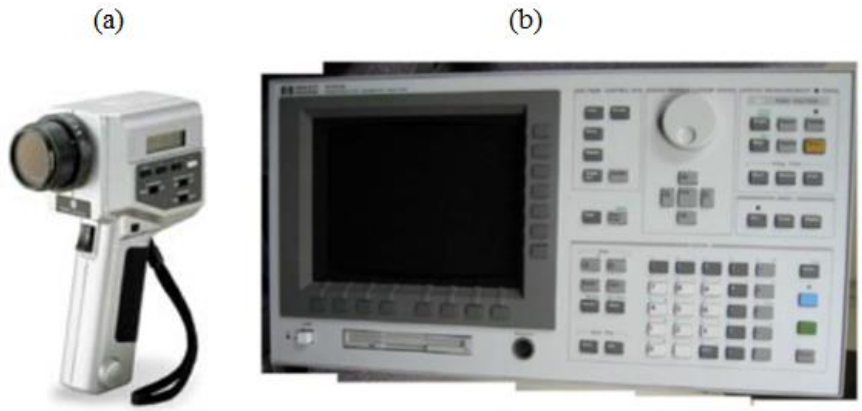

Figure 2.4 (a) Minolta chromameter CS-100A (b) Agilent 4155C semiconductor parameter analyzer.

2.3.2 EL Stability Measurements

In the EL stability measurements, an alternating current (AC) of 20 mA/cm^2 with 50% duty cycle and 100 Hz frequency is used to drive the OLED. The use of AC will help in ruling out the effect of charge accumulation or trapping. With the aid of photodiode and a computer, both the EL intensity and the operating voltage as a function of time are recorded during device ageing. The lifetime of the device is calculated when the device loses 50% of its initial luminescence. The experimental setup is shown in Figure2.5.

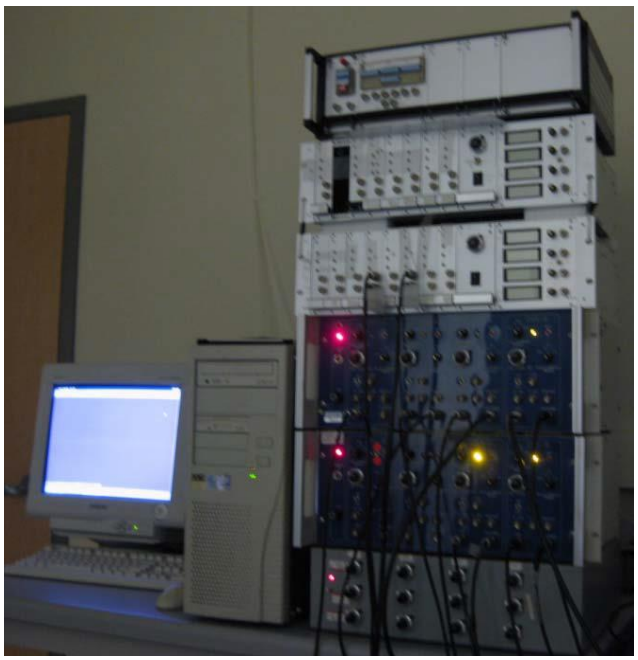

Figure 2.5 Experimental setup for EL stability measurements.

2.3.3 Emission Spectrum

The emission spectrum of the OLED in terms of the wavelength dependence of the EL is determined using an Ocean Optics Model S2000-FL fiberoptic spectrometer with a linear charge-coupled device (CCD) array (Figure2.6). The whole experiment was controlled by a personal computer with the aid of a suitable data acquisition card and general purpose interface bus (GPIB) interface.

Figure 2.6 Ocean Optics Model S2000-FL fiberoptic spectrometer.

2.3.4 Delayed EL

The delayed EL Measurements is performed as explained by Aziz *et al.* [49]. The schematic of the experimental setup is shown in Figure2.7. OLED emission is directed to a photodetector with the aid of an optical fiber bundle with a light chopper sitting in between (Figure2.7(a)). The timing diagram of forward and reverse bias is shown in Figure2.7(b). On applying a forward bias of 10V and a pulse width of 0.5ms, the chopper blade prevents EL from reaching the photodetector which prevents the photodetector saturation. Upon turning off the forward bias, light reaches the photodetector. After a time delay (typically 0.5ms) sufficient enough to ensure the absence of any contributions of the prompt EL in the collected signal, a reverse bias pulse (0.5ms) is applied to the OLED to study the reverse bias effect on the delayed EL intensity while the time evolution of the delayed EL is collected.

For the detection of the time-resolved emission, an R928 photomultiplier tube equipped with a 700nm short-wavelength pass filter is used. This filter was necessary to eliminate the noise signal originating from the light chopper (IRLED-Photodiode combination derived the chopper timing signals). The amplification of the photomultiplier is done by using an Ithaco

Model 1211 current preamplifier, while the time-evolution of the delayed EL is recorded by a Tektronics digital oscilloscope. Variable OLED forward and reverse biases are applied by a homebuilt operational amplifier driven by a Stanford Research System Model DG535 Digital Delay Generator. The wavelength dependence of the delayed EL was determined by the same setup explained in the emission spectrum section. The experimental setup is shown in Figure2.8.

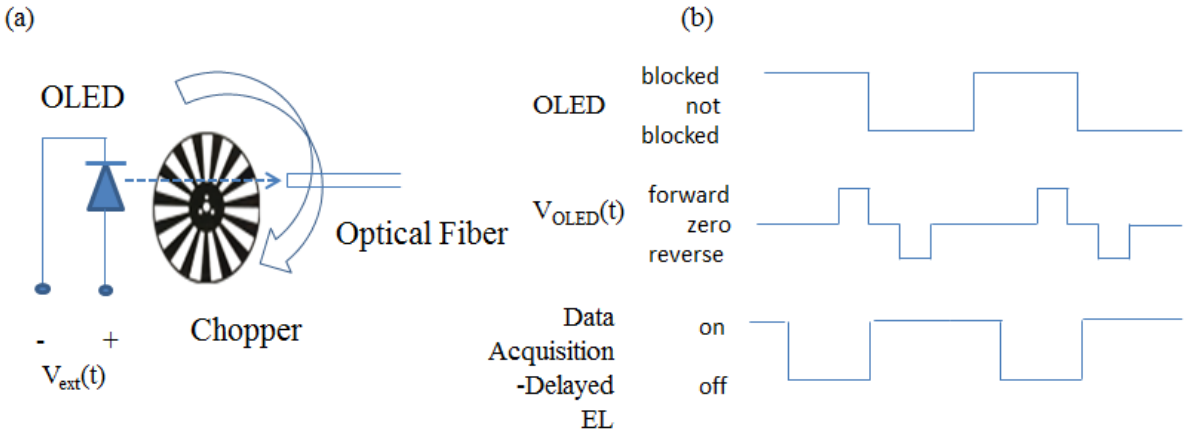

Figure 2.7 Schematic diagram of delayed EL experiment.

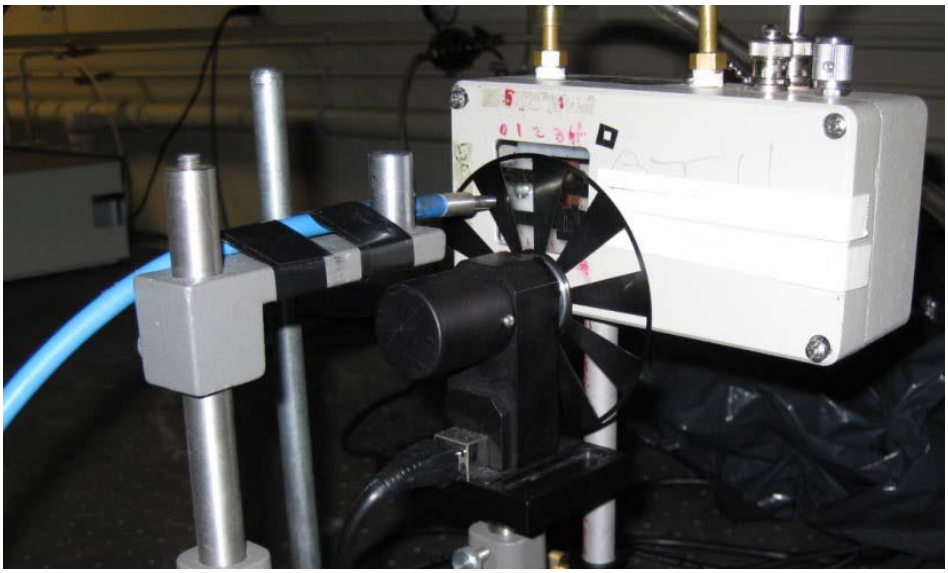

Figure 2.8 Experimental setup for delayed EL measurement.

2.3.5 Exciton Lifetime Measurements

For the exciton lifetime and transient PL measurements, Edinburgh Instruments FL920-t Spectrometer is used (Figure2.9). the excitation source integrated with this system is a 379nm pulsed laser (pulse width < 71ps, average power < 5mW). The FLS920-t is a modular, computer controlled spectrometer for measuring fluorescence life-time spanning the range from picoseconds to microseconds. This technique is based on the measurement principle of Time Correlated Single Photon Counting (TCSPC). In TCSPC, the sample is repetitively excited using a pulsed light source and the measurement builds a probability histogram relating the time between an excitation pulse (START) and the observation of the first fluorescence photon (STOP) [50]. The schematic of the setup is shown in Figure2.9.

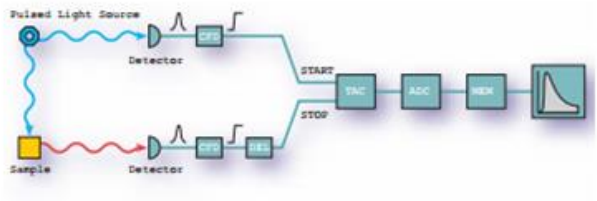

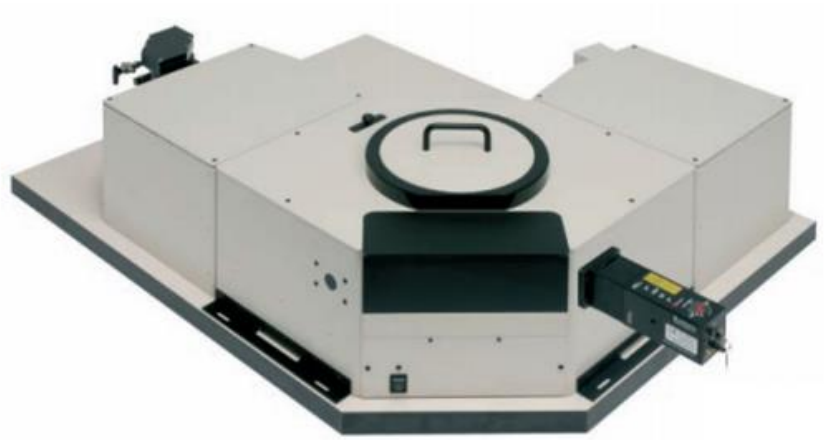

Figure 2.9 Edinburgh Instrument FL920-t Spectrometer [50].

2.3.6 Optical Excitation Tests

The optical excitation test is done using irradiation setup, where the OLEDs are exposed to monochromatic illumination with the possibility of wavelength variation. This setup uses a 200W Hg-Xe lamp equipped with Oriel-77200 monochromator. The power intensity of the illuminated spot is changing at different wavelength, roughly from 0.5mW/cm^2 to 2mW/cm^2. During this experiment, the I-V sweeps take place at different optical excitation duration to trace the degradation due to excitons. In addition to that, a combined optical excitation and electrical stress is monitored. Consequently, the degradation of OLEDs can be studied due to

optical excitation only and due to a combined optical excitation and electrical stress. The experiment is shown in Figure2.10.

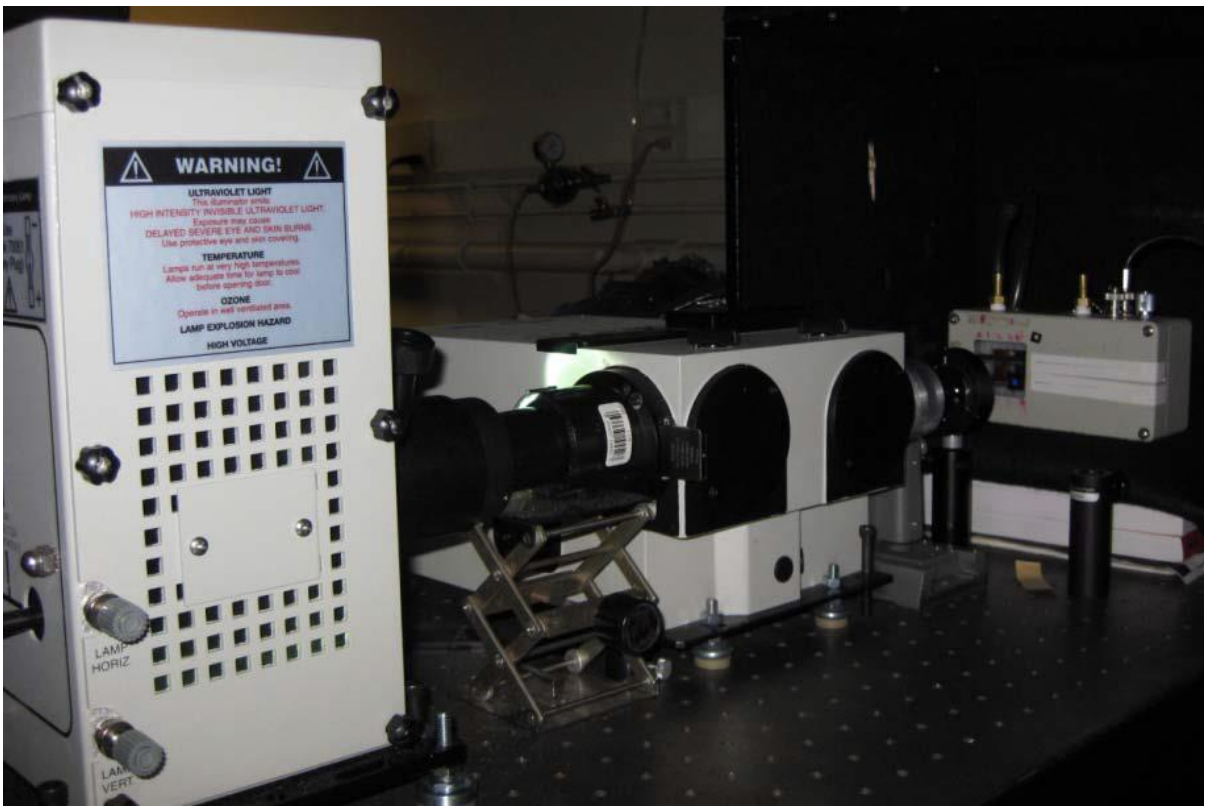

Figure 2.10 Experimental setup for photo-stability measurement.

Chapter 3 Results and Discussion

In this chapter, the results and discussion of the simplified PHOLEDs utilizing one material for both hole transport and emitter host will also be presented. Firstly, we will compare the conventional and simplified PHOLEDs behavior. Therefore, hole-only devices will be investigated for detailed comparison of hole current capabilities of both structures. Then, The efficiency and EL stability of the conventional and simplified PHOLEDs will be investigated. The factors governing the efficiency and EL stability in simplified PHOLEDs will be presented. The main focus of this study is the impact of the ITO/organic interface on efficiency and EL stability of simplified PHOLEDs. Furthermore, the impact of modifying the organic layers on device performance will be studied. Eventually, the influence of modified HTL/EML on PHOLEDs efficiency will be investigated.

3.1 Conventional PHOLED versus Simplified PHOLED

In this section, hole-only devices having both NPB and CBP as the HTL in order to study the hole injection process and the hole transport process. Both ITO/NPB and ITO/CBP interfaces are investigated as a simulation for the conventional and simplified PHOLEDs. These hole-only devices are used as a step for understanding PHOLEDs behavior with the same structure. Eventually, PHOLEDs with the conventional and simplified structures (Figure3.1) will be compared in order to have insights on exciton formation, efficiency, efficiency roll-off, and EL stability.

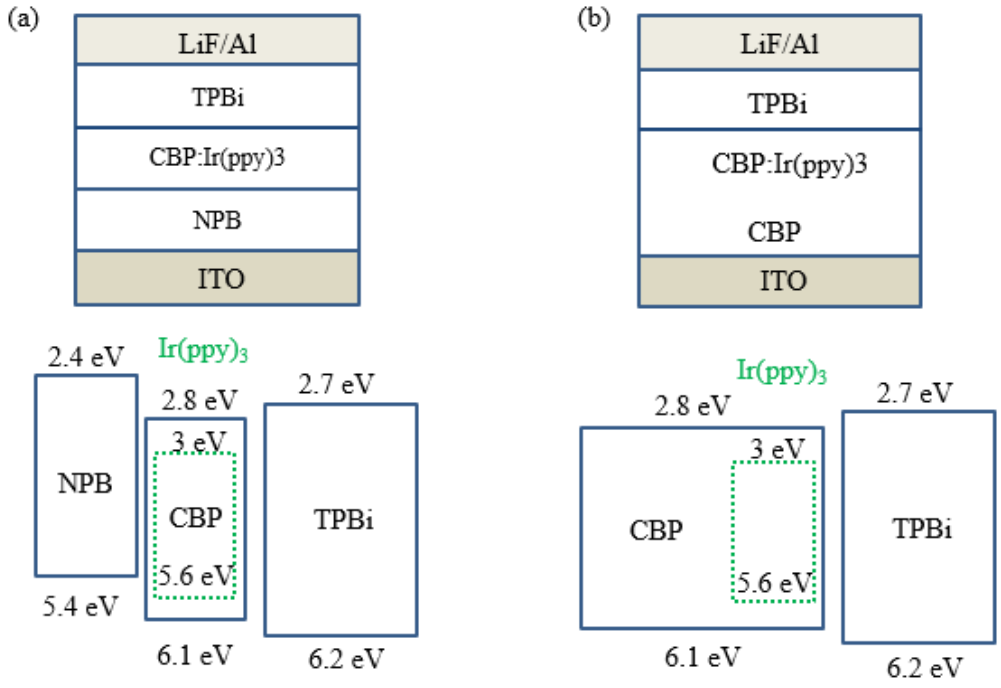

Figure 3.1 Conventional versus Simplified PHOLEDs.

3.1.1 Hole Injection Process

Wang *et al.* studied CBP as HTL in fluorescent OLEDs [46]. The devices demonstrated extremely high driving voltage and very low efficiency due to the poor injection from the ITO (work function ~4.7eV) into the HOMO of CBP (~6.1eV). By using HIL, the devices demonstrated efficient hole injection into the HOMO of CBP, hence low driving voltage and high efficiency were reported. This concept should also apply to the hole injection process in simplified PHOLEDs, since the hole injection barrier is the same with CBP as the HTL. In order to confirm the necessity of the HIL in simplified PHOLEDs and quantitatively compare the current capabilities between both NPB and CBP as HTL, Hole-only device are fabricated and studied having ITO/NPB and ITO/CBP interfaces as shown in Figure3.2. It is worth mentioning that NPB/MoO_3/Al are used on top of these layer as an electron blocking layer since the LUMO of NPB is shallow compared to the work function of aluminum (electron injection barrier ~1.7eV), hence hole-only devices are obtained.

Figure3.3 shows the hole current in both ITO/NPB versus ITO/CBP hole-only devices. As expected, there is a very high hole current in ITO/NPB device while a negligible hole current in ITO/CBP device (hole current in ITO/NPB devices is more than six order of magnitude higher than the hole current in ITO/CBP devices at 5V). Since the hole injection barrier is ~1.4eV in case of ITO/CBP and ~0.7eV in case of ITO/NPB. Therefore, it can be observed from the simplified PHOLEDs either need a HIL or ITO surface treatment for efficient hole injection.

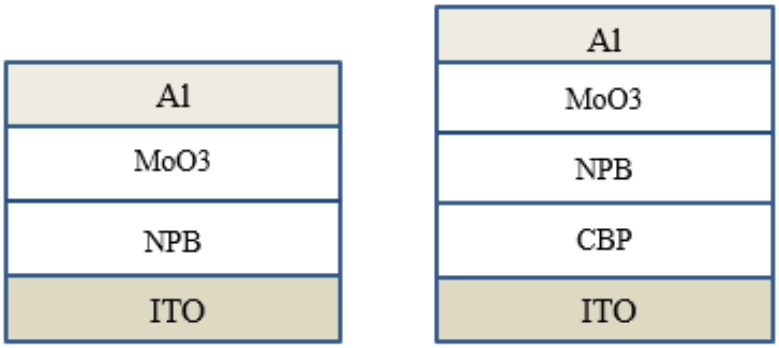

Figure 3.2 Hole-Only Devices with ITO/NPB versus ITO/CBP interfaces.

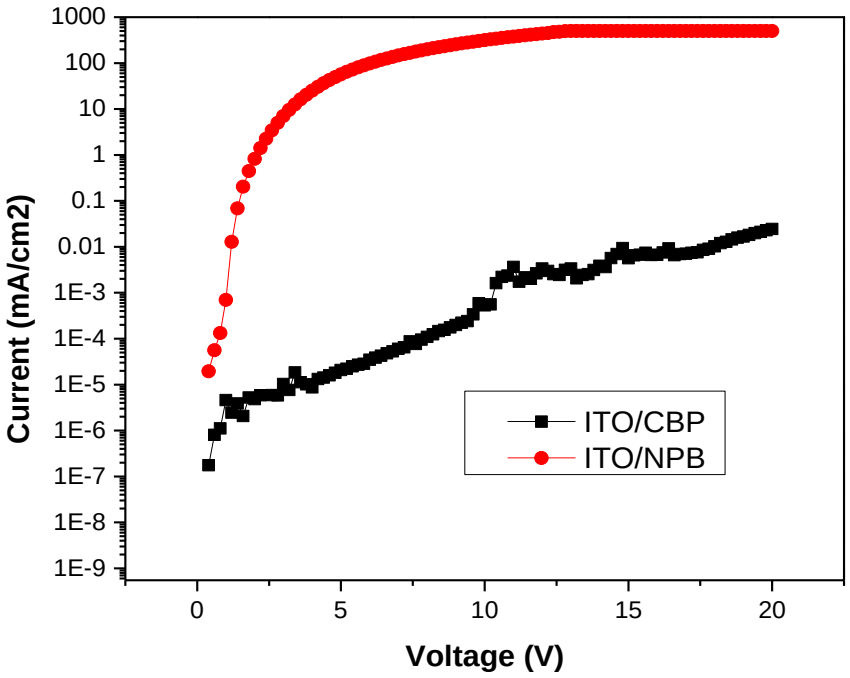

Figure 3.3 Hole Current in ITO/NPB versus ITO/CBP devices.

Figure3.4 shows the hole current in ITO/CBP hole-only devices using 1nm MoO_3 as a HIL or using CF_4:O_2 plasma treated ITO (PT-ITO) as a suggested replacement for the HIL (the plasma parameters and conditions are discussed in chapter 2). As we can see from the figure, plasma treatments leads to a higher hole current than MoO_3, Therefore it can be inferred that PT-ITO might have deeper work function than ITO/MoO_3, hence, less injection barrier and slightly higher hole current capabilities. Furthermore, a higher hole current can be achieved in ITO/CBP devices due to efficient hole injection process, as it shows less turn-on voltage and slightly higher current capabilities than ITO/NPB devices. Therefore, it is convenient to replace NPB by CBP as HTL with respect to charge injection process as explained by Wang *et al.* [46]. Moreover, PT-ITO can be a good replacement for the HIL as it allows a slightly higher hole current for simplified devices.

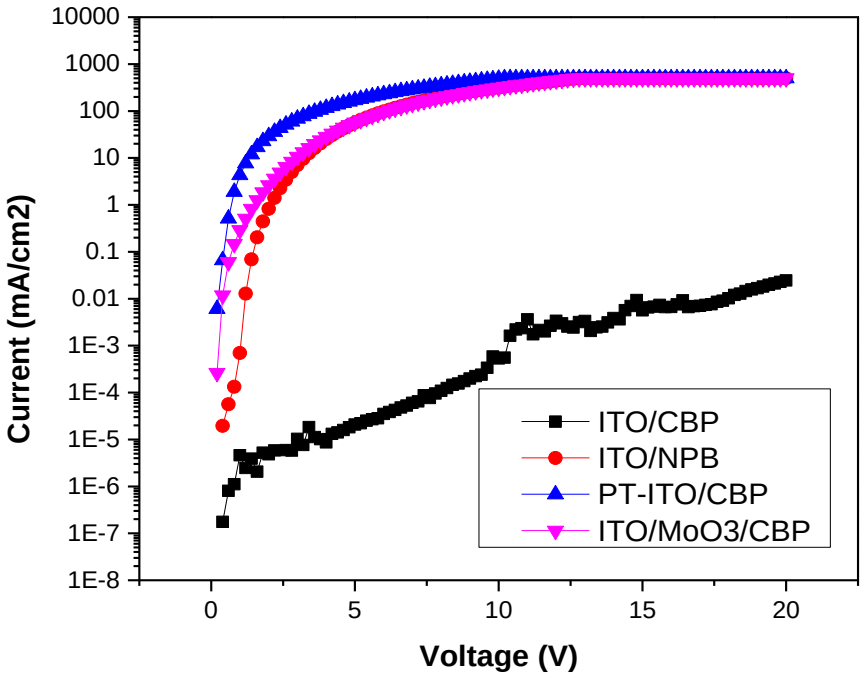

Figure 3.4 Hole Currents using PT-ITO or HIL for ITO/CBP devices compared to ITO/NPB devices.

3.1.2 Hole Transport Process

It can be deducted from the previous section that both NPB and CBP can achieve comparable hole current, upon using either PT-ITO or an HIL in case of CBP. In this section, the hole transport process in both NPB and CBP hole-only devices will be compared. Since the conventional device is having NPB as the HTL followed by CBP as the host material, we will investigate the hole transport properties in devices having an additional CBP layer, since an additional hole injection barrier is present at the NPB/CBP interface (~0.7eV). Figure3.5 shows the schematic of those hole-only devices, while Figure3.6 shows the I-V characteristics of such devices.

As we can see from Figure3.6, hole current in ITO/NPB/CBP devices decreases significantly (~ four orders of magnitude less at 5V) with the additional CBP layer. This decrease is clearly attributed to the accumulation of holes at NPB/CBP interface which might reduce the efficiency of the equivalent conventional PHOLED and possibly increase the efficiency roll-off due to charge imbalance and possible TPQ.

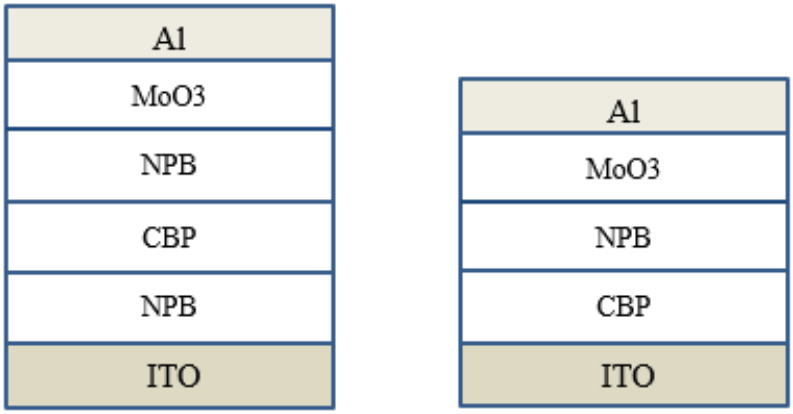

Figure 3.5 Hole-Only Devices with ITO/NPB versus ITO/CBP interfaces.

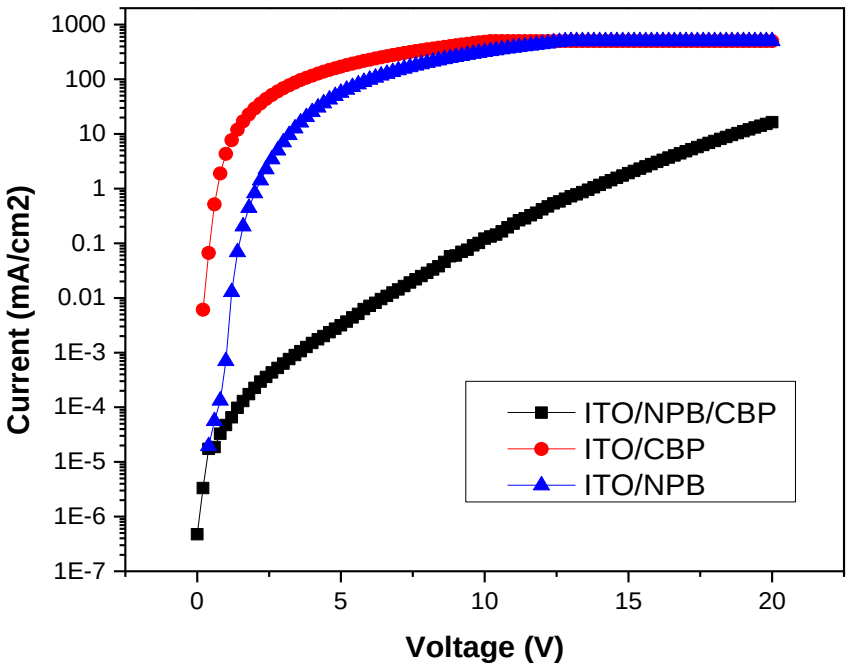

Figure 3.6 Hole Current in ITO/NPB/CBP versus ITO/CBP devices.

3.1.3 Efficiency and EL Stability

In order to have a better understanding of conventional and simplified PHOLEDs performance, the effect of the emitter concentration on device performance will be investigated. Figure3.7 shows the two main structures, the concentration of the emitter

(Guest) will be varied from 2wt. % to 16wt. %. Table3.1 shows PHOLEDs characteristics at different doping concentration of the guest material.

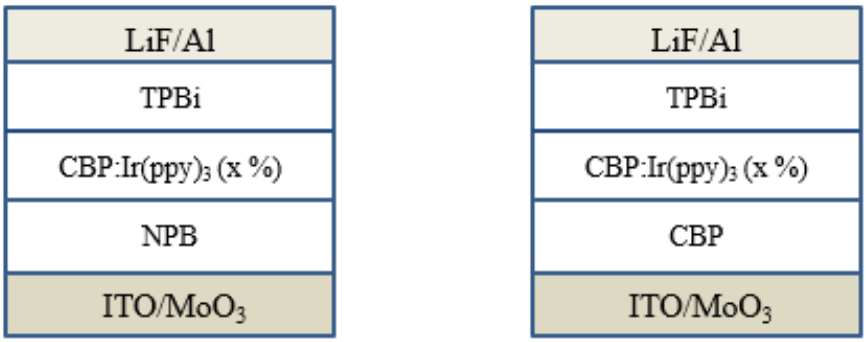

Figure 3.7 Structure of Conventional and simplified PHOLEDs with different Guest Concentrations.

Table 3.1 PHOLEDs characteristics at different guest concentration.

HTL	Emitter Concentration	Voltage (V) at 20mA/cm2	Luminescence cd/m^2 at 20mA/cm2
CBP	2%	6.64	7820
	4%	6.35	7380
	8%	5.87	6860
	12%	5.57	5680
	16%	5.49	5100
NPB	2%	9.41	2100
	4%	8.47	2820
	8%	7.88	4520
	12%	7.94	5110
	16%	7.35	5190

As we can see from the table, the simplified PHOLED can have a lower operating voltage at 20mA/cm^2 as expected which is attributed to better hole injection and transport. Moreover, a clear trend can be observed in both structures. In conventional PHOLEDs, as the emitter concentration increases the luminescence increases and the operation voltage decreases. While an opposite trend in simplified PHOLEDs can be seen, as the emitter concentration decreases the luminescence increases and the operating voltage decreases. This observation in addition to the emission spectrum (Figure3.8) can lead to an insight with

respect to exciton formation process. In simplified PHOLEDs, emission from only the guest is observed which indicates an efficient energy transfer from host to guest as well as the confinement of excitons in the EML. Furthermore, as the guest concentration increases the luminescence decreases which may be attributed to concentration quenching of excitons. In conventional PHOLEDs, at low guest concentration (2% and 4%) NPB fluorescence can be observed which is due to accumulation of holes at the NPB/CBP interface and electrons leakage through the EML [10]. While at higher guest concentrations, exciton can be formed by direct recombination on guest molecules as holes can be injected directly from NPB to $Ir(ppy)_3$ due to lower energy barrier at NPB/$Ir(ppy)_3$ than NPB/CBP interface (0.2eV rather than 0.7eV). Therefore, we can conclude that in simplified PHOLEDs exciton can be formed by energy transfer from host to guest while in conventional PHOLEDs excitons are formed by direct recombination on guest molecule.

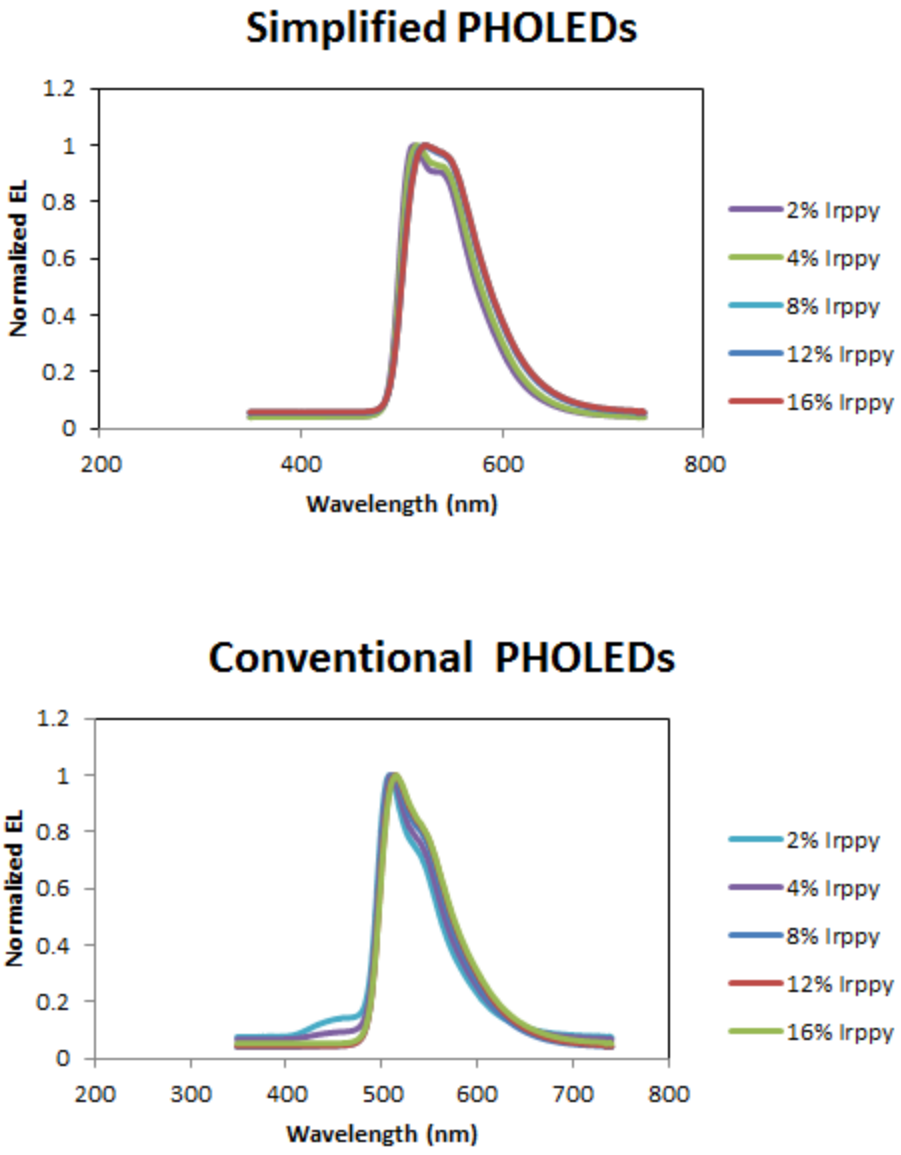

Figure 3.8 EL Spectrum with conventional and simplified PHOLEDs.

The current efficiency and the EL stability differences in both simplified and conventional PHOLEDs will also be presented in this section. Throughout this chapter, we will be using a doping concentration of 8% for the emitter molecule as the control doping concentration.

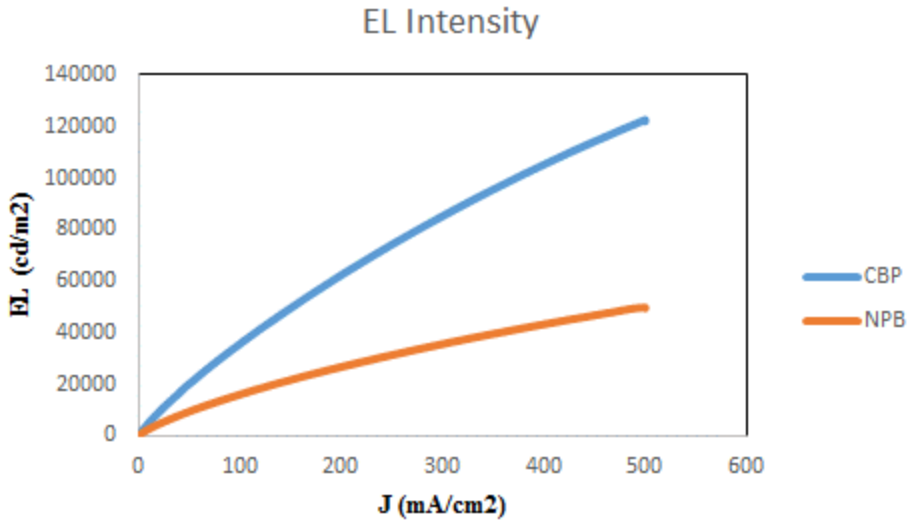

Figure 3.9 EL intensity in Conventional and Simplified PHOLEDs.

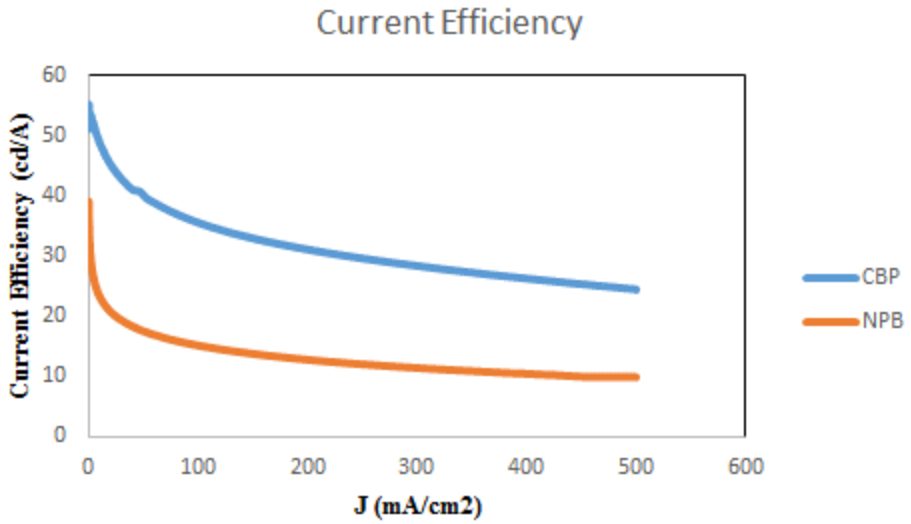

Figure 3.10 Current Efficiency in Conventional and Simplified PHOLEDs.

As shown in Figure3.9, the maximum luminescence for the simplified PHOLED at 500 mA/cm^2 is ~122K cd/m^2. While, the maximum luminescence for the conventional PHOLED at 500 mA/cm^2 is ~50K cd/m^2. Similarly from Figure3.10, the maximum current efficiency for the simplified PHOLED is ~55 cd/A. While, the maximum current efficiency for the conventional PHOLED is ~40 cd/A (summary can be seen at Table3.2). Moreover, it can be clearly observed that the simplified PHOLED showed not only higher current efficiency but also lower efficiency roll-off than the conventional one. The higher efficiency in the simplified PHOLED is attributed to better charge balance due to suppression of charge carrier accumulation. In addition to the efficient energy transfer from host to guest system as explained earlier. While, the lower efficiency and the high efficiency roll-off in the conventional PHOLED can be attributed to the hole accumulation at the NPB/CBP interface which in turn initiates TPQ process and can alter charge balance at higher current density. Therefore, the characteristics of the simplified PHOLEDs under test agree with the reported data in literature [10].

Table 3.2 Summary of Conventional and Simplified PHOLEDs.

HTL	Voltage (V) at 20mA/cm2	Maximum efficiency (cd/A)	Maximum luminescence (cd/m^2)
CBP	5.87	55	122K
NPB	7.88	40	50K

The EL stability of both PHOLEDs under electrical stress can be seen in Figure3.11. Since surface treatment of the ITO is essential for hole injection in case of simplified PHOLEDs, simplified PHOLEDs with PT-ITO will be compared to untreated conventional PHOLEDs. The operating voltage rise and the decay in the normalized EL under constant current of 20mA/cm^2 are shown in Figure3.11. It can be observed that the simplified PHOLEDs are unstable as a rapid decay can be observed in the EL trend and also an abrupt voltage rise occurs at constant current stress. Meanwhile, the conventional NPB PHOLEDs showed a relatively higher stability. Therefore, the stability of simplified PHOLED is limited by an unknown degradation mechanism at the hole-side of the device which is not present in the conventional PHOLED.

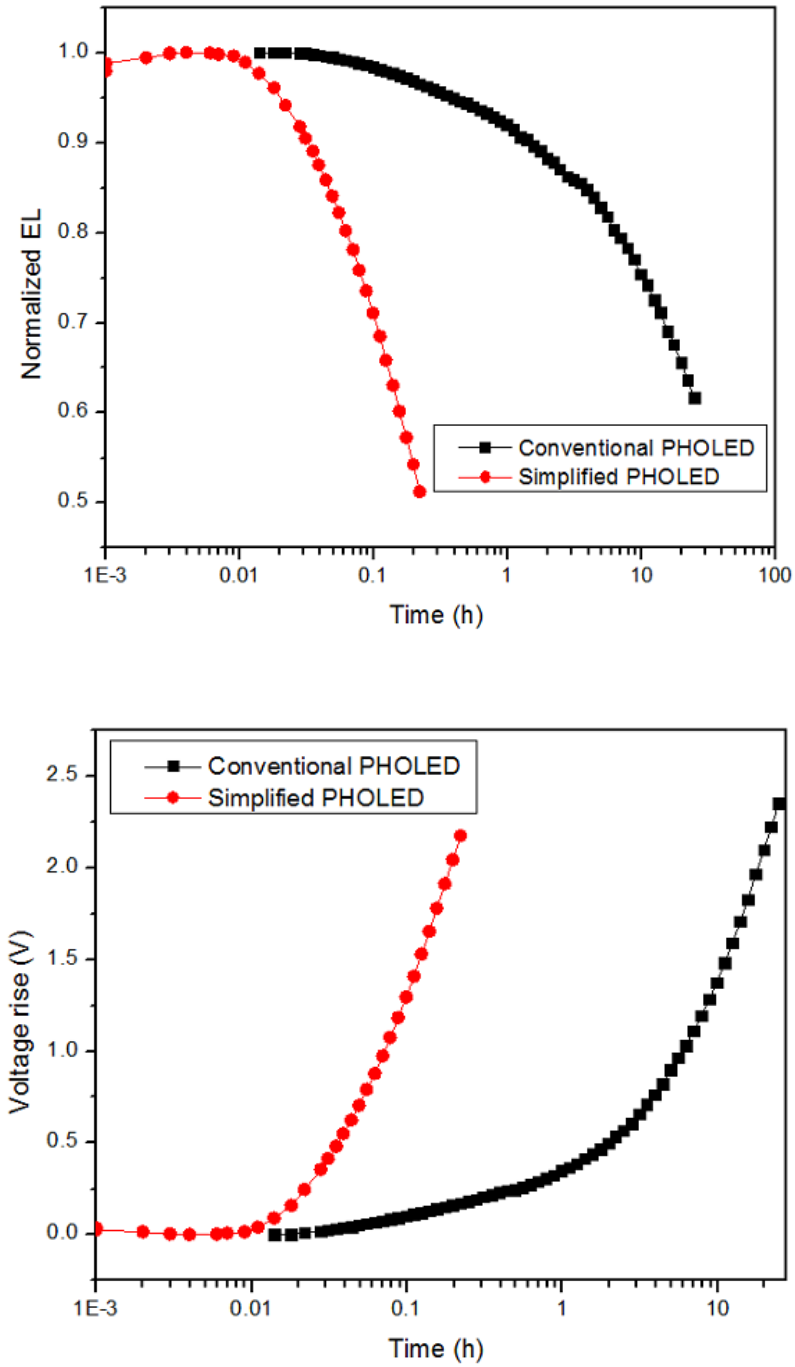

Figure 3.11 EL Stability under electrical stress of Conventional and Simplified PHOLEDs.

3.2 The role of the ITO/organic interface on simplified PHOLEDs efficiency

As mentioned in chapter one, the ITO/organic interface has a critical role with respect to device performance. In this section, different ITO surface treatments are investigated and compared as an attempt to further enhance device performance. Treatments including CF_4:O_2 plasma (as explained in Chapter 2), ion beam assisted deposition (IBAD) of argon ions (Ar), Chorine (Cl) plasma (dry Cl), and wet chlorination (procedure similar to [45]). Also, MoO_3 was used as a HIL with either 1nm or 10nm thickness after ITO surface treatment. Table3.3 shows the summary of the electrical characteristics of the simplified PHOLEDs with different surface treatments.

Table 3.3 Summary of the Electrical Characteristics with different ITO treatments.

MoO_3 (nm)	ITO Treatment	Voltage (V) at 20mA/cm2	Luminescence cd/m^2 at 20mA/cm2
0 nm	CF_4:O_2	6	7190
	Ar^+	N/A	N/A
	Wet Cl^-	6.8	7550
	Dry Cl^-	8.19	6760
1 nm	CF_4:O_2	6.54	7420
	Ar^+	5.4	8180
	Wet Cl^-	6.2	7650
	Dry Cl^-	5.9	7690
10 nm	CF_4:O_2	6.67	6440
	Ar^+	5.78	7340
	Wet Cl^-	6.82	6760
	Dry Cl^-	6.28	6910

From table3.3, it can be concluded that in the absence of HIL, different ITO treatments can facilitate hole injection process, hence modifies the ITO work function except for Ar IBAD which is an inert treatment which helps only with ITO cleanliness. In the presence of 1nm MoO_3 as an HIL, Ar IBAD treatment, which is done inside our thermal evaporator without breaking the vacuum, leads to better ITO cleanliness. Therefore, it leads to the lowest operating voltage and the highest EL. Using 10nm MoO_3 as an HIL leads to higher operating voltage and lower EL. Therefore, either surface treatment of ITO or 1nm of MoO_3 is essential for better device performance. Also, it is recommended to use Ar IBAD with 1nm MoO_3 which leads to a more preferred electrical characteristics.

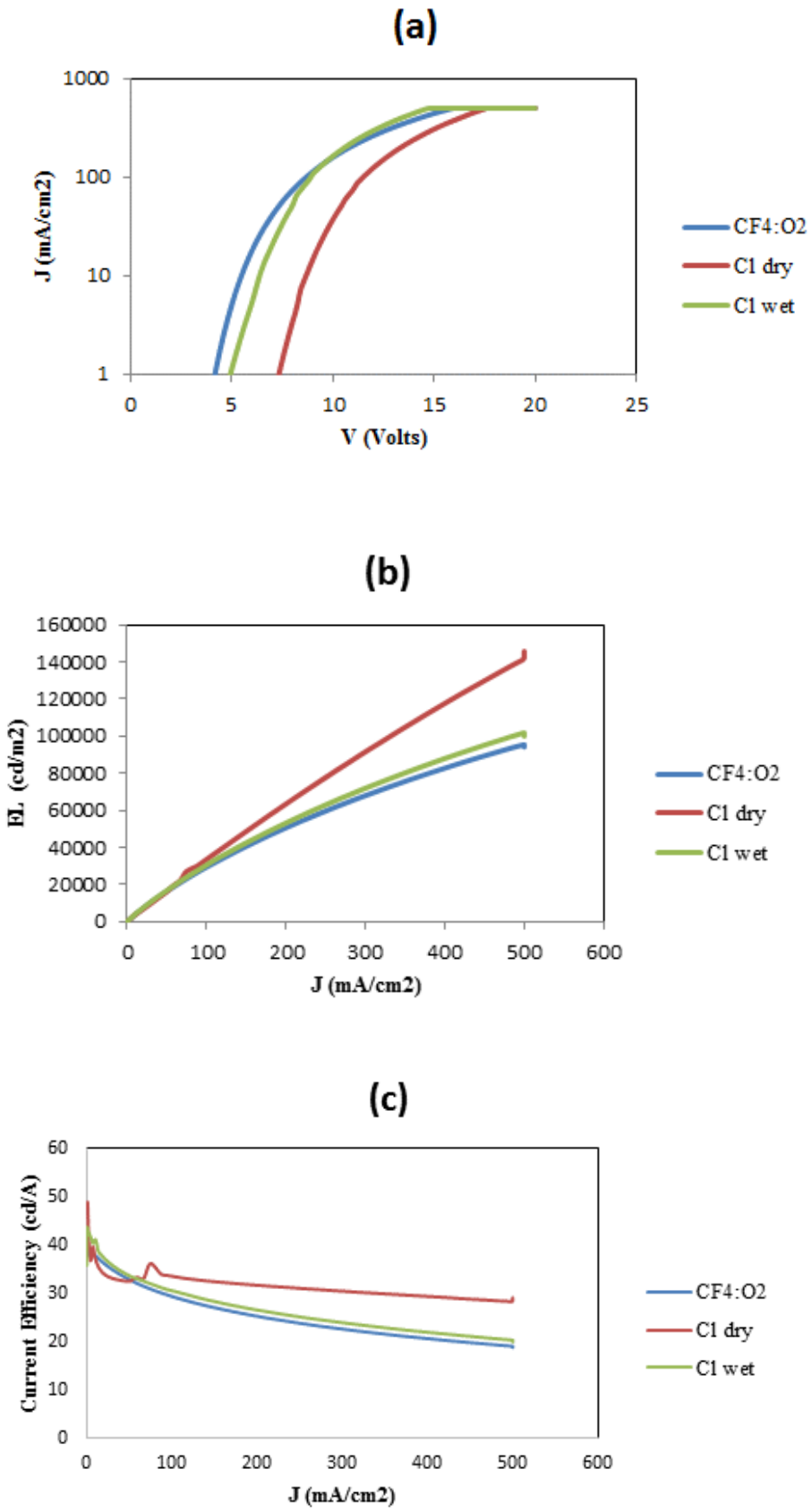

Figure 3.12 The electrical characteristics of PHOLEDs without a MoO_3 HIL, for various ITO treatments.

Figure3.12 shows the electrical characteristics for different treatments in the absence of HIL. Figure3.12(a) shows the J-V characteristics, Figure3.12(b) and (c) shows the EL intensity and the current efficiency, respectively. Since the Cl plasma was done in a different clean room and samples was transferred in air. The behavior of the samples in the absence of MoO_3 is unexpected. Since it tends to have non-uniform luminescence, therefore a higher virtual EL characteristics (Figure3.12(b)) and higher current efficiency (Figure3.12(c)). The sole reason of using Cl plasma was to avoid wet chlorination of the ITO (proposed by Helander *et al.*) since the plasma treatments are compatible with the fabrication of various organic electronics and scalable for mass production. The experiment showed that the Cl plasma can modify the work function of the ITO in principle but it needs further optimization and that the experiment should be done in the same clean room without being exposed to ambient conditions.

Figure3.13 shows the electrical characteristics for different treatments using 1nm MoO_3 as an HIL. Figure3.13(a) shows the J-V characteristics, it can be concluded that the current density is comparable in all devices. Figure3.13(b) and (c) shows the EL intensity and the current efficiency, respectively. It can be seen that using both HIL and ITO surface treatment is not necessary, since 1nm MoO_3 without any ITO treatments leads to the best characteristics.

Figure3.14 shows the electrical characteristics for different treatments using 10nm MoO_3 as an HIL. Figure3.14(a) shows the J-V characteristics, Figure3.14(b) and (c) shows the EL intensity and the current efficiency, respectively. It can be seen that the electrical trends are equivalent to the 1nm MoO_3 as an HIL but with lower current efficiency and higher operating voltage. Therefore, the use of 1nm MoO_3 as an HIL in the absent of ITO surface treatment is recommended.

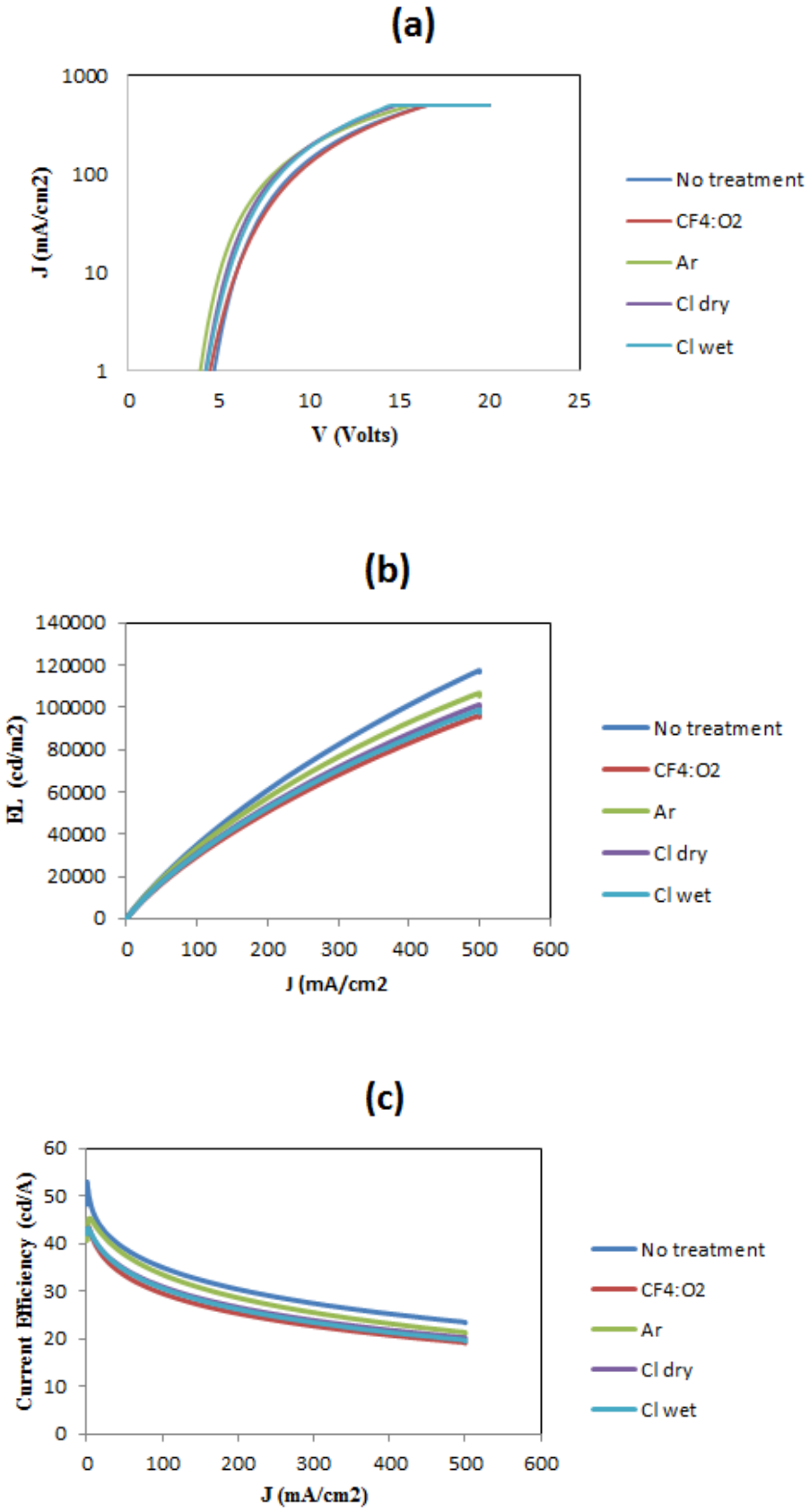

Figure 3.13 The electrical characteristics of PHOLEDs with 1nm MoO3 for various ITO treatments.

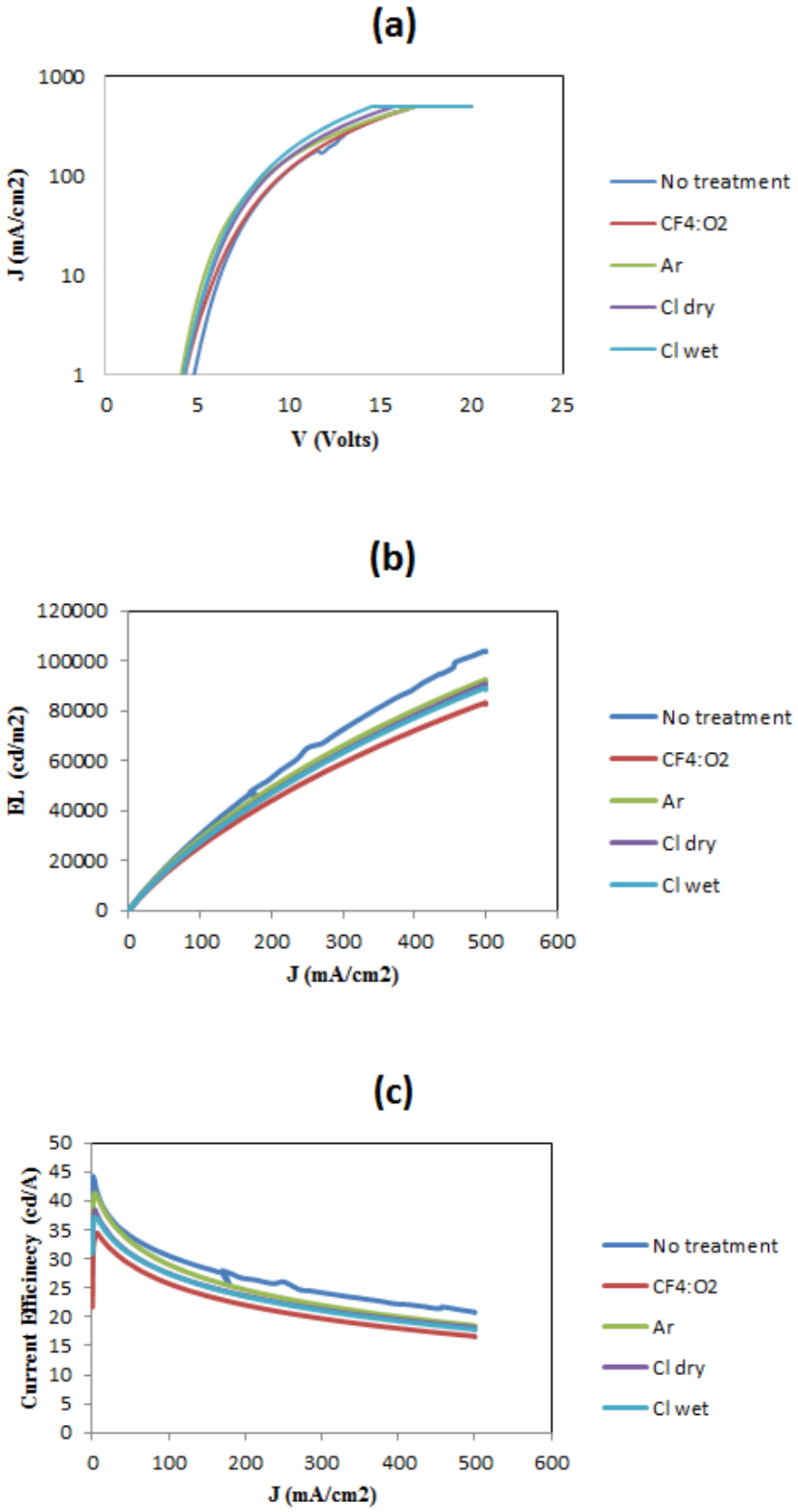

Figure 3.14 The electrical characteristics of PHOLEDs with 10nm MoO_3 for various ITO treatments.

3.3 The role of the ITO/organic interface in limiting the stability of simplified PHOLEDs

In this section, the EL stability of simplified PHOLEDs under electrical stress will be studied. As mentioned in the previous sections, the simplified PHOLEDs offer several enhancements which are related to charge injection, transport, charge balance, current efficiency, and efficiency roll-off. Meanwhile, simplified PHOLEDs demonstrated significantly low EL stability under electrical stress. In this section, a new degradation mechanism, that is occurring at the ITO/organic interface, will be introduced. we discovered that such interface is susceptible to exciton-induced degradation, which plays an important role in limiting the operational stability of PHOLEDs. A gradual charge injection deterioration was observed, upon optical excitation of the devices under test. Therefore, a correlation between the optical excitation of the organic material at the ITO/organic interface and the operational stability of the PHOLED was established. This correlation is due to the presence of excitons, which are created by the recombination of electrons leaked from the EML with holes injected from the ITO. Those excitons can be simulated by using the optical excitation experiment. Furthermore, a new role of MoO_3 as an exciton quencher, will be presented in this section, as it quenches excitons and prevents exciton-induced degradation at the ITO/organic interface which in turn enhances the EL stability of PHOLEDs with such layer.

In order to emphasize the role of the ITO/organic interface in the EL stability of simplified PHOLEDs, three PHOLEDs were fabricated and studied. The only difference in these PHOLEDs is the ITO/organic interface. PHOLEDs with a thin buffer-layer (1nm MoO_3), thick buffer layer (5nm MoO_3), or a PT-ITO, were investigated. The PHOLEDs details are discussed in the experimental methods (chapter 2). It is crucial to mention that there was insignificant difference in the initial current efficiency (~60±5cd/A) at 20mA/cm^2 in these PHOLEDs. Figure3.15 shows the EL stability of PHOLEDs under test under electrical stress of a constant current density of 20mA/cm^2. Figure3.15(a) shows the normalized EL decay versus time (L vs. t) , while Figure3.15(b) shows the increase in the operating voltage versus time (ΔV vs. t) under the previously mentioned electrical stress.

Figure3.15(a) shows that the normalized EL trends of the PHOLEDs are significantly different, although the PHOLEDs structure is exactly the same except for the ITO/CBP contact. The EL trend of the ITO/CBP interface under plasma treatment only, without MoO_3 as a buffer-layer, is decaying fast, since the PHOLED tends to lose its luminescence rapidly. Meanwhile, a tendency can be observed from the PHOLEDs with different thickness of MoO_3, the thicker the buffer-layer the higher the lifetime. This reflects that the ITO/organic interface is critical for the operational stability of the simplified PHOLEDs. From Figure3.15(b) it can be seen that, a rapid voltage rise for the PHOLED with PT-ITO compared to less voltage rise in case of 1nm MoO_3 compared to the least voltage rise for the 5nm MoO_3. Therefore, upon comparing Figure3.15(a) to Figure3.15(b), a direct correlation between the EL trend and the voltage rise trend can be made, as the (ΔV vs. t) trend mirrors

the (L vs. t) trend. In other words, The EL trends are coupled with the voltage rise trends. Therefore, by understanding the reasons behind the voltage rise trends, we can possibly have an insight on the PHOLED operational stability.

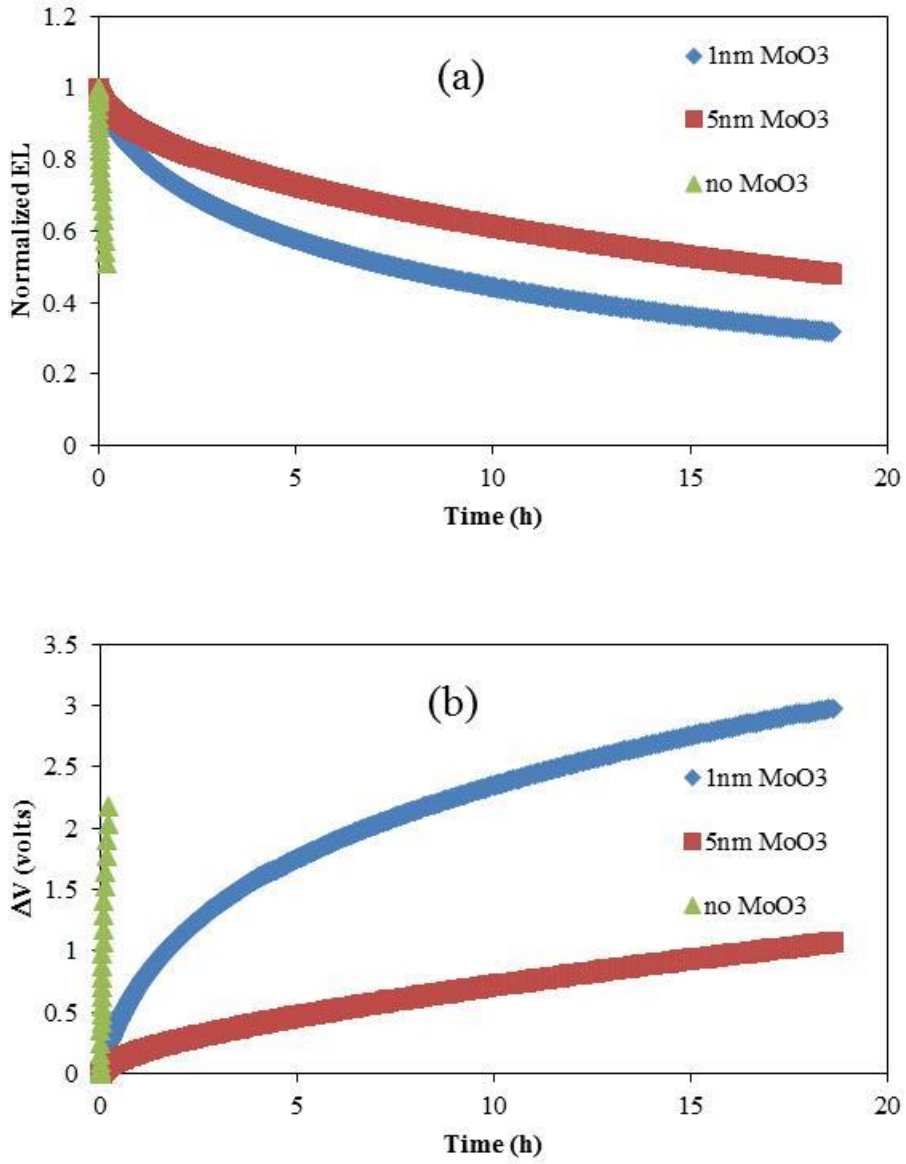

Figure 3.15 The EL Stability under electrical stress in simplified PHOLEDs with different ITO/CBP interface.

In order to focus on the possible reasons behind the different voltage rise trends with different ITO/organic interfaces, the hole injection process from the ITO to the organic material (CBP) will be studied. Therefore, hole-only devices were fabricated and studied. Due to our previous knowledge that the ITO/organic interface is susceptible to photo-stability issues in fluorescent OLEDs [51], a comparison will be made between the stability of the

hole-only devices under electrical stress and photo-stress independently. The electrical stress is done by applying a constant current of 20mA/cm^2 for approximately 20 hours, while the photo-stress is done by exposure of the hole-only devices to a monochromatic light (wave length ~350nm) of power density of ~0.5mW/cm^2 for 70 minutes only. Figure3.16 shows the electrical stability and the photo-stability of the ITO/CBP hole-only devices with either PT-ITO or a thin buffer-layer of MoO_3 (1nm).

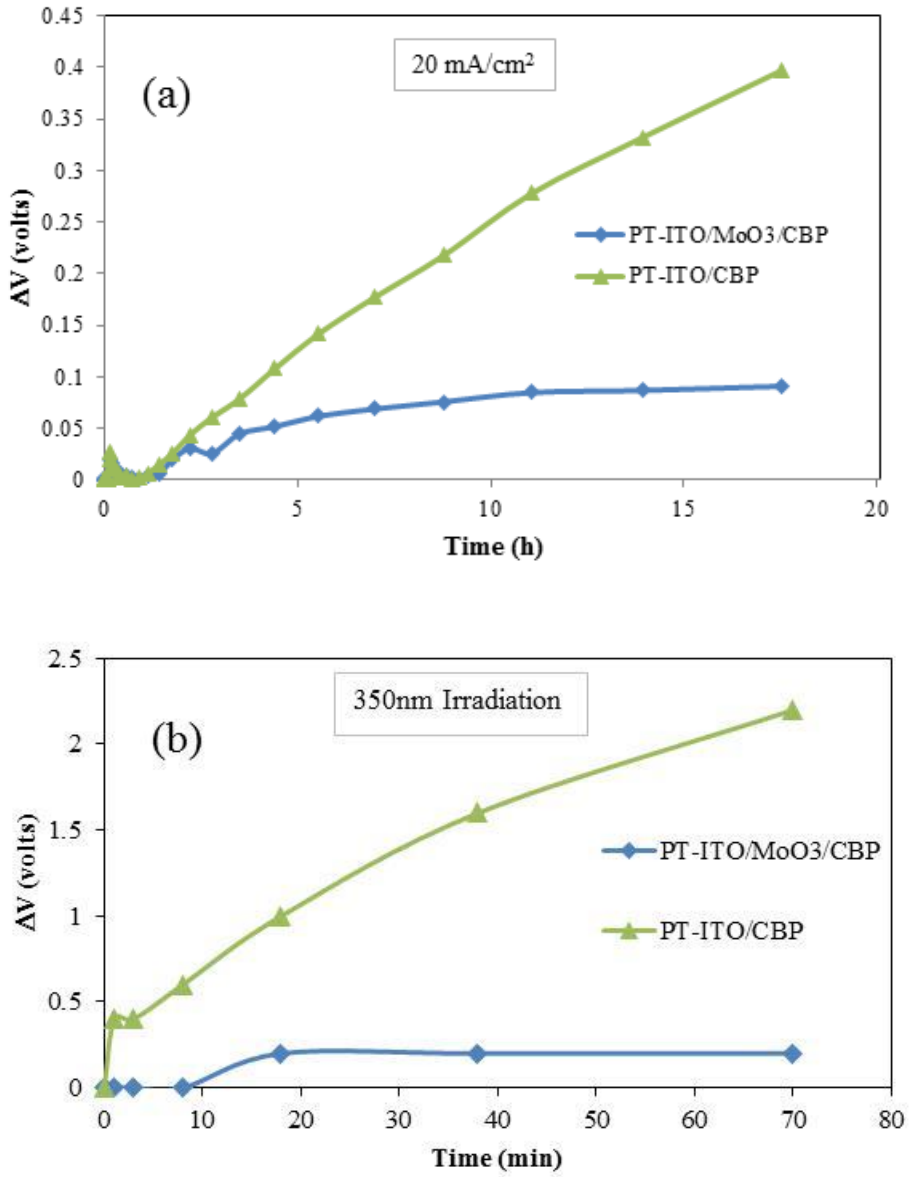

Figure 3.16 Effect of Electrical stress and Photo-stress independently on hole-only devices of ITO/CBP interfaces.

Figure3.16(a) shows the electrical stability of the ITO/CBP devices. As we can observe from the figure, there is insignificant effect of the electrical stress on hole-only devices (PT-ITO/CBP rises ~0.4V and ITO/MoO_3/CBP rises ~0.05V in 20 hours duration). Moreover, it

can be observed that MoO_3 offers more electrical stability than PT-ITO). By comparing the degradation in electrical stability of the hole-only devices to the degradation of the corresponding PHOLEDs under similar electrical stress (Figure3.16(a) to Figure3.15(b)), it can be seen that the electrical stress cannot be the only reason behind the low EL stability of the simplified PHOLEDs. Figure3.16(b) shows the photo-stability of the ITO/CBP devices. Although the experiment was done for only 70 minutes, it is clear that PT-ITO/CBP is photo-unstable compared to ITO/ MoO_3/CBP (PT-ITO/CBP rises ~2.5V while ITO/MoO_3/CBP rises ~0.5V in 70 minutes duration). It can be concluded that there is an underlying degradation mechanism upon exposing the devices to photo-stress, where this degradation is more pronounced compared to the any degradation caused by the electrical stress. Furthermore, it can be noted that a thin layer of MoO_3 is sufficient to slow down such degradation.

In order to analyze the underlying degradation mechanism behind this observed photo-instability for devices without a buffer-layer, we focused on the PT-ITO/CBP hole-only devices which demonstrated an observable degradation under irradiation. In this experiment, we varied the wave length of the monochromatic light used (515nm, 430nm and 350nm) to study the wave length dependence of such degradation, Since our previous studies on the photo-stability of the ITO/organic interface in fluorescent OLEDs showed wavelength dependence [44]. It was found that this photo-degradation is wave length dependent as the degradation takes place only at a wavelength enough to excite the organic material at the ITO interface (350nm in case of ITO/CBP). In order to exclude any degradation due to possible heat effects that may arise from illumination at 350nm which in turn can accelerate crystallization of the organic material that can introduce interfacial defects [47,48], we further studied the heat stability under illumination of 350nm while the device is covered by a black scotch tape. It was found that the device is relatively stable under heat-only stress. Eventually, it was hypothesized that this degradation is due to excitons at the ITO/CBP interface that is created upon optical excitation using the monochromatic illumination.

In order to confirm that excitons is the reason for this degradation, a thin exciton-quencher layer (5nm) of CBP doped with DCJTB (1wt. %) was used as shown in Figure3.17(b). It was found that the device becomes photo-stable at 350nm illumination upon excitons quenching at the ITO/organic interface. Figure3.17(a) shows the degradation of the hole-current density of the ITO/CBP devices due to different illumination wavelength, heat effect, and using the exciton-quencher layer (CBP doped with DCJTB). As we can see from Figure3.17(a) that heat related degradations and optical excitation at irrelevant wavelength is negligible. Moreover, it is important to highlight that upon using DCJTB to quench excitons, the devices tend to be photo-stable at 350nm of optical excitation. Therefore, it can be confirmed that the ITO/organic interface is susceptible to exciton-induced degradation.

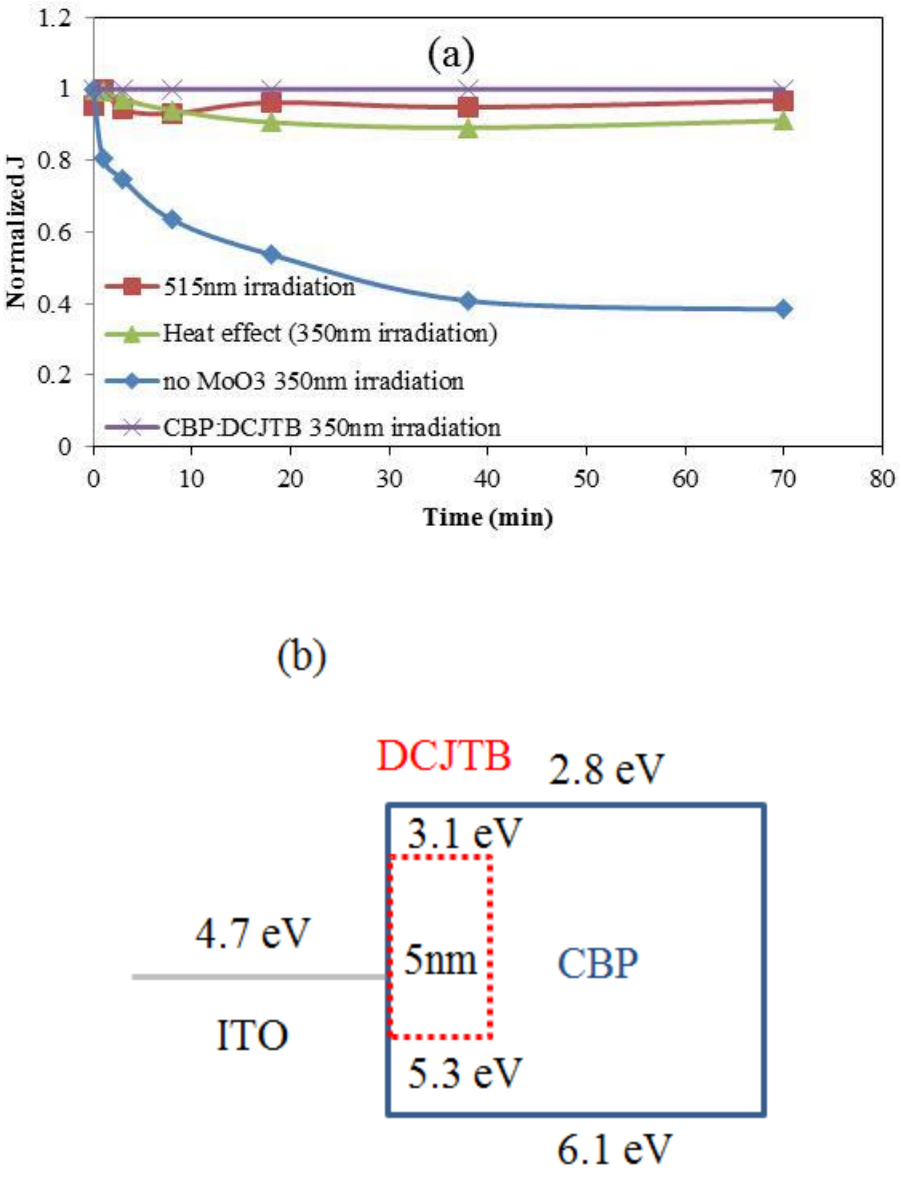

Figure 3.17 (a) The normalized current density versus time upon exposure to photo-stress, (b) The structure of the exciton-quencher layer.

Since it was concluded that excitons can cause exciton-induced degradation to the ITO/organic in hole-only devices, it is important to create a correlation between exciton-induced degradation in hole-only devices to the EL stability of simplified PHOLEDs. Therefore, PHOLEDs were fabricated with the same exciton-quencher layer (CPB doped with DCJTB) without using any buffer-layer (only PT-ITO). Figure3.18 shows the EL stability of PHOLEDs under electrical stress with the added exciton-quencher layer. It can be seen that the devices tend to be electrically stable which was not the case previously. Therefore, it can be confirmed that exciton-induced degradation is a mechanism that can take place in PHOLEDs.

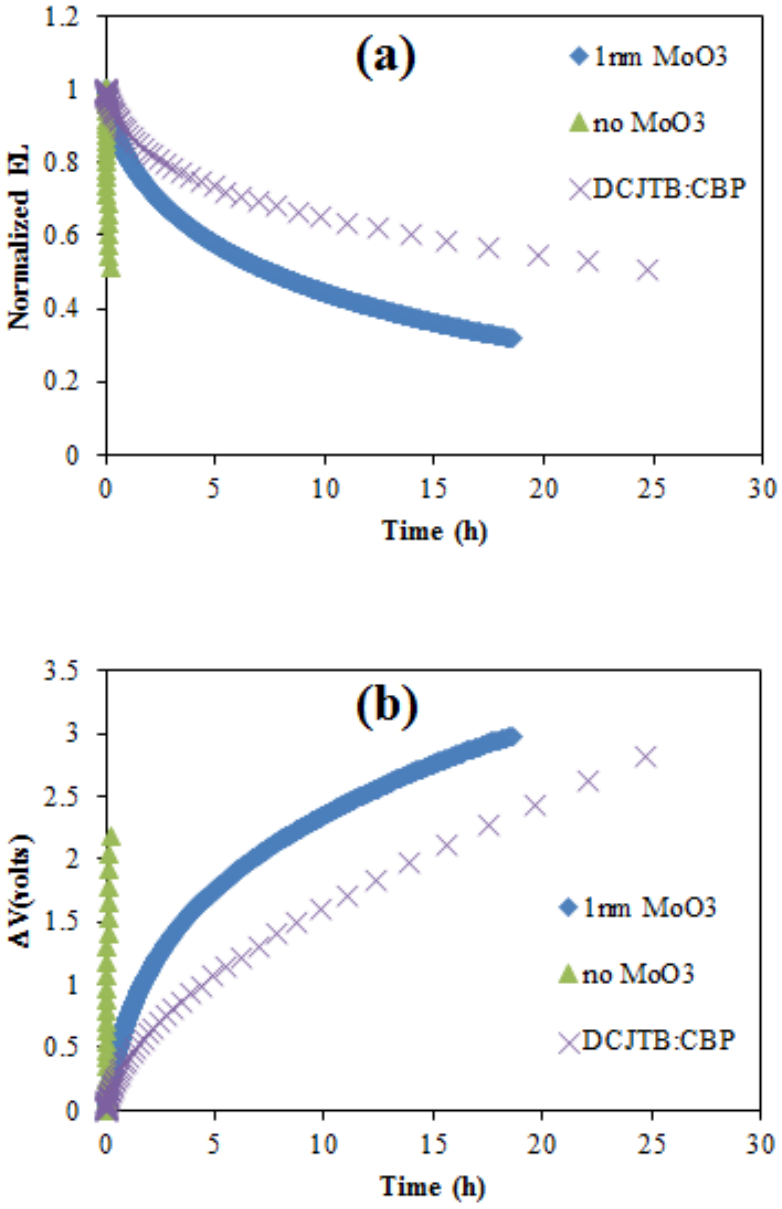

Figure 3.18 The EL stability of simplified PHOLEDs with exciton-quencher layer.

Since a thin buffer-layer of MoO_3 leads to a relatively stable devices (Figure3.18(b)), it is important to understand the role of MoO_3 with respect to the EL stability of simplified PHOLEDs. In order to investigate the role of MoO_3 in preventing exciton-induced degradation (Figure3.16(b)), exciton lifetime measurements will be studied. Figure3.19 shows CBP exciton lifetime measurements for untreated ITO, PT-ITO and ITO/ MoO_3/CBP. It can be observed that, there is a clear reduction in exciton lifetime in case of using MoO_3 compared to PT-ITO, which clearly confirms the negligible exciton-induced degradation in case of MoO_3 compared to PT-ITO. Hence, a new role of MoO_3 in the EL stability of

PHOLEDs as an exciton-quencher layer that protects the ITO/organic interface from exciton-induced degradation.

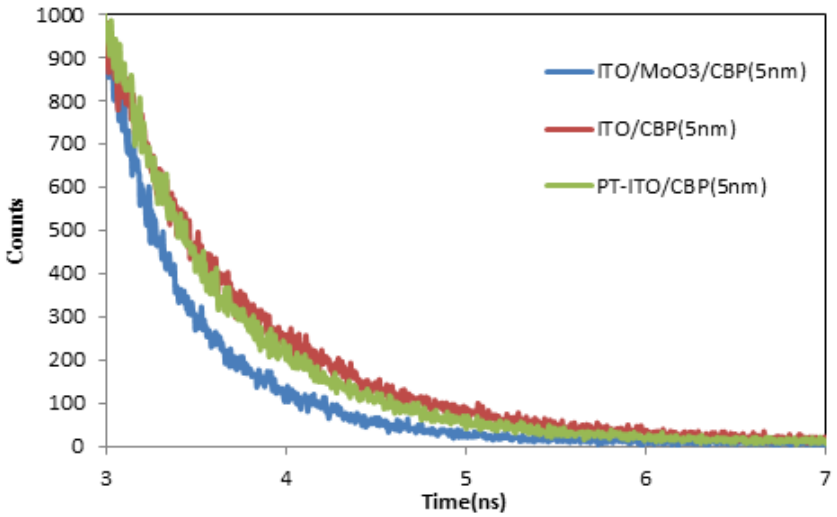

Figure 3.19 Exciton Lifetime measurements for ITO/CBP layers.

Giebink *et al.* provided a direct evidence of polaron-induced degradation at the EML that limits the operational lifetime of PHOLEDs. Comparing electron-only devices without guest material as a control device to electron-only devices with guest material (device under test), they managed to prove that host anions are unstable and the instability increases upon excitation. As the control device with no guest material didn't show any degradation with current passage or optical excitation, meanwhile the device under test showed degradation due to current passage and the degradation was even more pronounced when the current and the optical excitation are combined due to interactions with excitons [38]. By the same concept, it is important to investigate whether exciton-induced degradation at the ITO/organic interface becomes more severe due to interactions between excitons and holes injected from the ITO electrode or it is unaffected. The effect of combining both electrical and optical excitation on hole-only devices with different ITO/organic contacts, is further investigated. Firstly, an electrical stress was applied to the devices for two hours which was performed to assure that the devices are electrically stable with current-only conditions. Then, the devices were irradiated with the 350 nm source for 70 minutes without removing the electrical stress. Figure3.20 shows the electrical stability trend (ΔV vs. t) for such experiment. By comparing Figure3.16(b) and Figure3.20, it is clear that the degradation effect is accelerated and the rising slope of (ΔV vs. t) tends to be sharper. Two important remarks were observed: firstly, using thicker MoO_3 leads to less combined degradation mechanism which explains the reason that 5nm of MoO_3 leads to more stable PHOLEDs compared to 1nm MoO_3 as shown in Figure3.15. Secondly, this combined degradation mechanism is hypothesized to be due to the interactions between excitons and holes at ITO/organic interfaces which is similar to the hypothesis by Giebink *et al.* Moreover, by studying the irreversibility of the exciton-induced

degradation, it was found that this effect is irreversible upon the removal of the optical excitation.

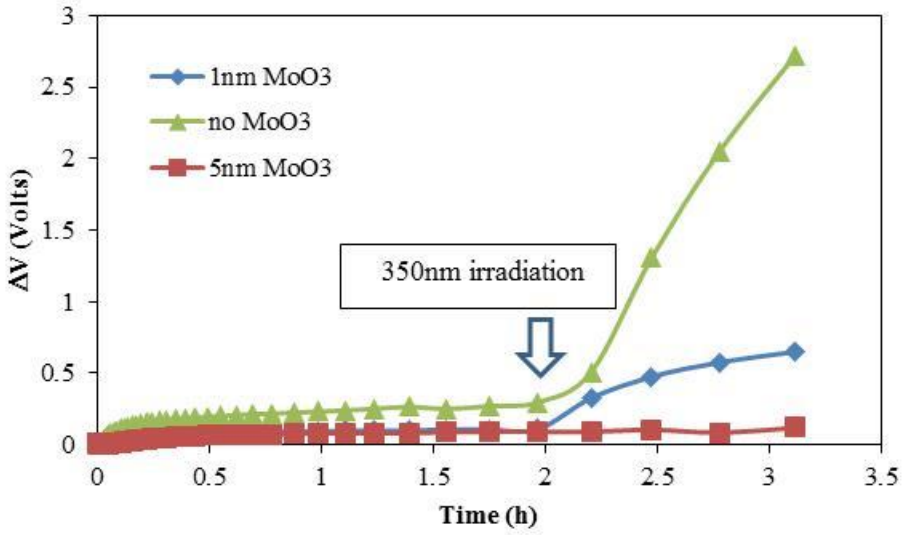

Figure 3.20 Effect of combining current induced-degradation and exciton-induced degradation.

As an attempt to further enhance the EL stability, the simplified PHOLEDs structure was modified by adding mCP layers (Figure3.21) to act as an exciton-blocking layer as well as electron-blocking layer at the ITO/CBP interface and at the CBP/EML interface. Therefore, preventing excitons from degrading the ITO/organic interface and blocking electrons from leaking through the HTL which can form excitons that can possibly lead to exciton-induced degradation at the ITO/organic interface. The electrical characteristics of these devices are compared in table3.4.

Since mCP has a higher triplet energy than CBP (3eV rather than 2.67eV) it can act as an exciton-blocking layer. Also mCP can act as an electron blocking layer since it has shallower LUMO compared to CBP (2.4eV rather than 2.8eV). Therefore, adding mCP layer will help both exciton and electron blocking. From table3.3, it can be seen that adding mCP layer as shown in Figure3.21(a) will slow down hole injection, therefore higher operating voltage and lower EL can be observed. Also, adding mCP layer before the EML (Figure3.21(b)) can confine excitons as well as block electrons which leads to higher operating voltage and higher EL. On the other hand, adding two mCP layers as shown in Figure3.21(c) can lead to intermediate EL intensity as it slows down hole injection which can lead to lower EL meanwhile confine excitons and block electrons which can lead to higher EL. In those devices excitons as well as electrons are blocked, therefore the ITO/organic

interface is protected against exciton-induced degradation. It is expected that these devices will offer higher EL stability under electrical stress.

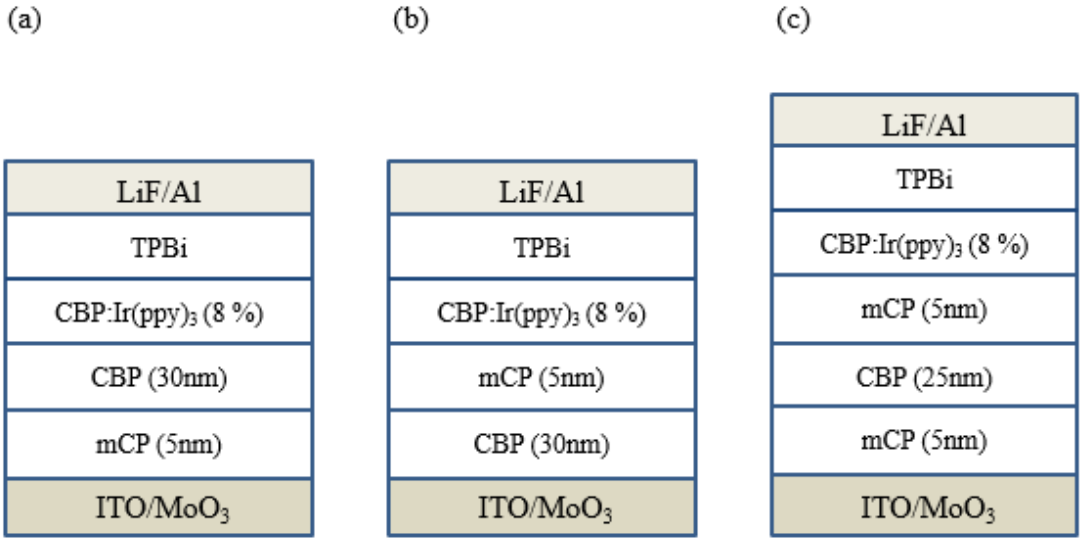

Figure 3.21 Using mCP as a Blocking Layer.

Table 3.4 Electrical Characteristics of PHOLEDs with mCP as a Blocking Layer.

Device	Voltage (V) at 20mA/cm2	Luminescence cd/m^2 at 20mA/cm2
(a)	9.2	5040
(b)	9.2	8000
(c)	8.1	7650

Figure3.22 shows the EL stability under electrical stress for mCP devices and is compared to the control device (with 1nm MoO_3 as HIL). It can be seen that, using mCP enhances the EL stability by a factor of ~3. And it is better to have both mCP layers for optimized EL stability and EL intensity.

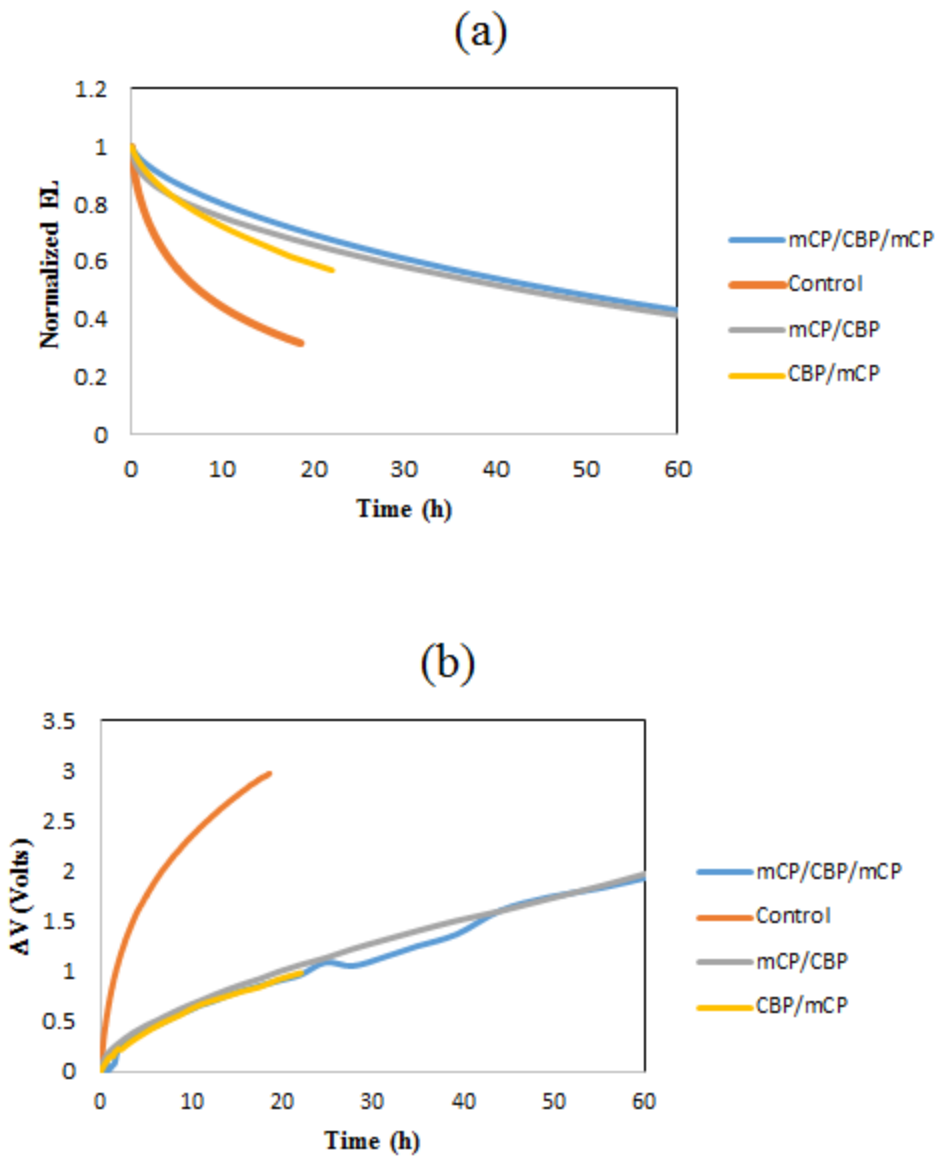

Figure 3.22 The EL stability with mCP Layers.

In our recent studies, It was found that excitons, causing exciton-induced degradation at the ITO/organic interface, are formed by the recombination of excess electrons leaking through the EML and the HTL with injected holes at such interface [52].

3.3 The effect of modifications of the organic layers on simplified PHOLEDs performance

In this section, we will be using codeposition of organic materials in different layers of the device including the EML, ETL, and the HTL. The main purpose of codeposition of the transport layers is to enhance charge transport as well as charge balance for efficient exciton formation and higher overall internal quantum efficiency. On the other hand, codeposition of the EML is done for better energy transfer from host to guest (ISC) by having higher spin orbit coupling and better charge balance by having an ambipolar host. It worth mentioning that these experiments did not contribute to the EL stability of the simplified PHOLEDs under electrical stress. Therefore, the EL stability results will not be included in the corresponding section.

3.3.1 Modifications of the EML

The codeposition of the EML with cohost which is composed of CBP and TPBi, in addition of $Ir(ppy)_3$ (8wt. %) as the guest. This was done in order to obtain an ambipolar host for better charge balance in the EML and in order to have unlimited interfaces between both hosts therefore higher probability of creating host excitons. In these experiments, the variable is either the codeposition percentages of the cohost or the ETL thickness as shown in Figure3.23. The summary of the electrical characteristic of those devices are shown in table3.5.

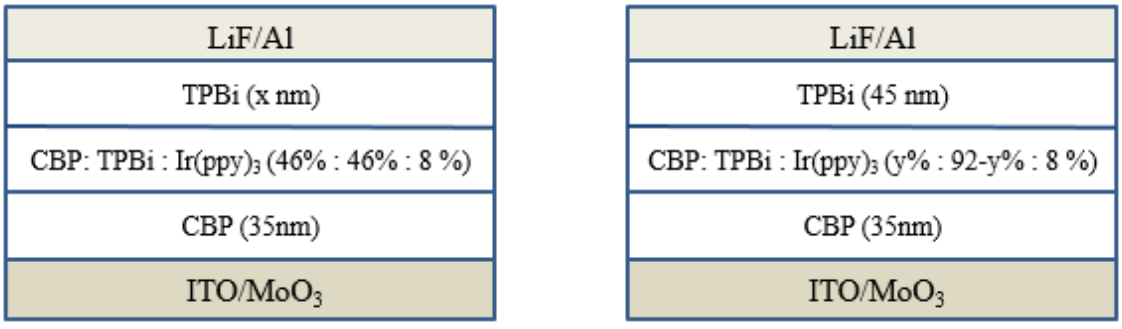

Figure 3.23 Cohost system with TPBi and CBP.

Table 3.5 Electrical Characteristics of Cohost PHOLEDs.

Parameter	Value	Voltage (V) at 20mA/cm2	Luminescence cd/m^2 at 20mA/cm2
	25	4.54	6700
	35	4.79	8010
x	45	5.08	8250
(nm)	55	5.06	8340
	65	5.05	8220
	46	5.39	8170
	42	5.34	8220
y	25	5.48	8240
(wt. %)	50	5.13	7630
	67	6.14	8120

From table3.5, it can be seen that codeposition of the EML helps reducing the operating voltage by ~1V (driving voltage at 20mA/cm^2 ~6V for single host system and ~5V for cohost system), while demonstrating similar luminescence. This lower driving voltage is attributed to better electron transport properties in the EML.

In order to have more insights on the exciton quenching techniques in this system, the delayed EL for these devices is studied. In this technique, a device is driven using a square pulse driving scheme, with a forward bias of 10V and a pulse width of 0.5 ms (the pulse is sufficiently long for prompt EL to reach its steady-state intensity). An optical shutter opens to collect delayed EL around 0.3 ms after the end of the forward bias pulse, which is significantly longer than the lifetime of $Ir(ppy)_3$ triplet state lifetime (<1 μs), hence ensuring the absence of any contributions from prompt EL in the collected signal. As such, any collected signal will arise from the radiative decay of excitons that are formed after the end of the forward bias pulse. In general, this delayed EL can be the product of: (a) recombination of trapped charges that get released after the end of the forward bias pulse; (b) various bimolecular interactions such as TTA, which in this case will be primarily due to the fusion of host triplet excitons (i.e., host-host TTA). This is because any contributions from guest-guest TTA to delayed EL in the milliseconds time frame due to the much shorter lifetime of phosphorescent guest triplet excitons are insignificant. In order to differentiate between these processes, a 0.5 ms reverse bias pulse (with variable magnitude) is applied on the devices during the delayed EL signal collection, and subsequent changes in delayed EL characteristics are monitored [33].

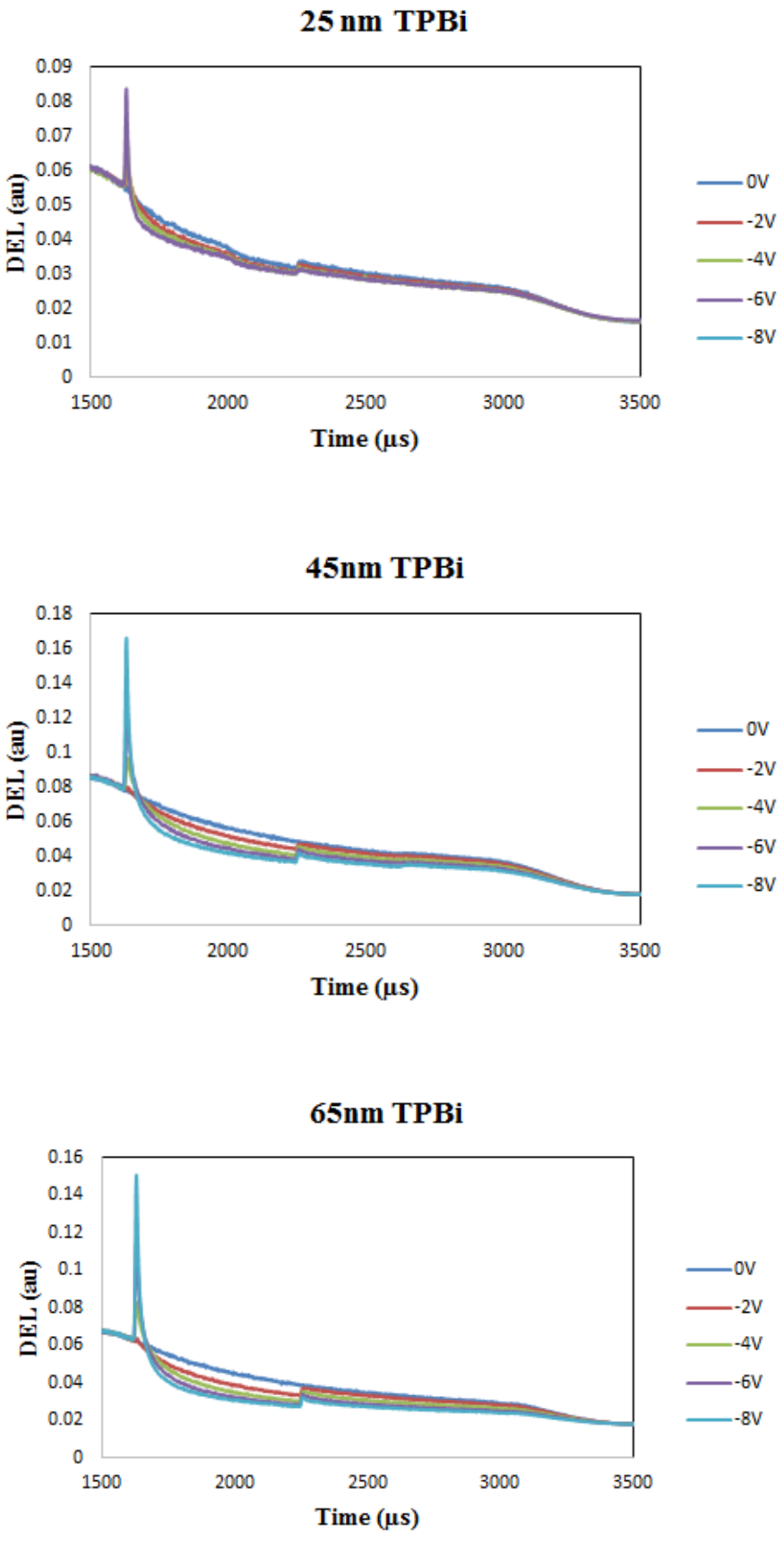

Figure 3.24 Delayed EL of PHOLEDs with Different TPBi thickness.

From Figure3.24, a spike can be seen in the DEL signal upon applying a reverse bias pulse which indicates charge accumulation in such devices and that the accumulation increases as the thickness of TPBi increases. This implies that although the energy levels of CBP and TPBi are almost aligned yet TPBi helps blocking holes in the EML and as the thickness of TPBi increases the blocking and charge accumulation increases. This agrees with literature as K. Leo *et al*. mentioned that TPBi can be used as HBL which offers no hole transporting behavior [39]. This indication of accumulated charges implies that TPQ can also be present in such devices which in turn can affect the long term operational stability of such devices. The full recovery of the DEL signal at the end of the applied reverse bias, indicates TTA which is higher in case of 45nm TPBi device and even more higher in the 65nm TPBi device.

In order to enhance the energy transfer from host to guest especially the ISC by offering higher spin orbit coupling (due to the presence of both Ir complexes) which is mainly to obtain higher quantum efficiency without any concentration quenching, FIrpic was used as a coguest system in addition to $Ir(ppy)_3$ as shown in Figure3.25. Table3.6 shows the electrical characteristics of the coguest system PHOLEDs. It can be seen from the table that there is an increase in the operating voltage and a decrease in the EL, which was not expected. Therefore, we studied the delayed EL of such coguest system in order to understand the reason behind the unexpected EL decrease.

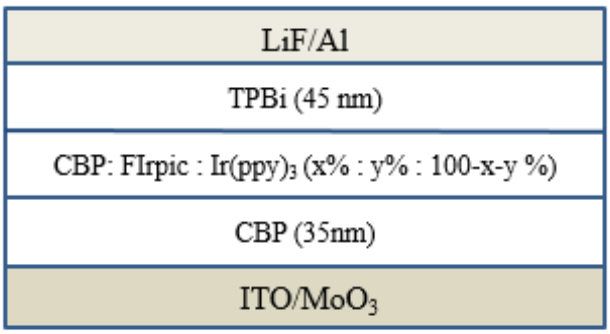

Figure 3.25 Coguest system with FIrpic.

Table 3.6 Electrical Characteristics of FIrpic Coguest System.

Parameter	Value	Voltage (V) at 20mA/cm2	Luminescence cd/m^2 at 20mA/cm2
	92:0	6.65	8720
	88:4	7.23	7880
x:y	84:8	7.17	8010
(wt. %)	80:12	7.06	8150
	80:8	7.19	7620

Charge accumulation can be seen from the delayed EL (Figure3.26),which implies TPQ, also TTA can be observed at the end of the applied reverse pulse. In addition, there is another quenching mechanism of simplified PHOLEDs excitons that can be observed in this coguest system which is electric-field induced quenching (EFIQ) of triplet states. At lower reverse field -2V, a full recovery of the DEL signal at the end of the applied reverse bias. Moreover, as the bias is higher than -2V it can be seen that there is partial recovery only which might be due to EFIQ as the applied electric field quenches FIrpic excitons. This EFIQ is hypothesized to be because of FIrpic being a wide band gap guest that electric field can dissociate excitons which might be one of the possible reasons of the lower stability of blue PHOLEDs. This was not observed neither in the cohost devices nor in the single host simplified PHOLEDs, hence it is not accompanied with green PHOLEDs. This EFIQ may also be the reason of the lowered EL in such devices than $Ir(ppy)_3$ devices. Therefore, this coguest system not only demonstrated TTA and TPQ but also EFIQ as can be seen from Figure3.26. This EFIQ in FIrpic excitons is not well understood and needs further investigation which is outside the scope of this thesis.

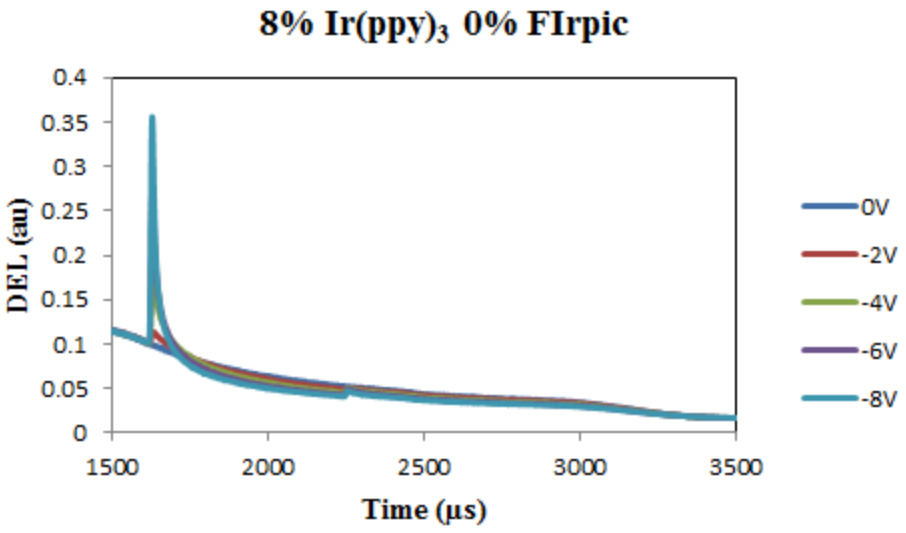

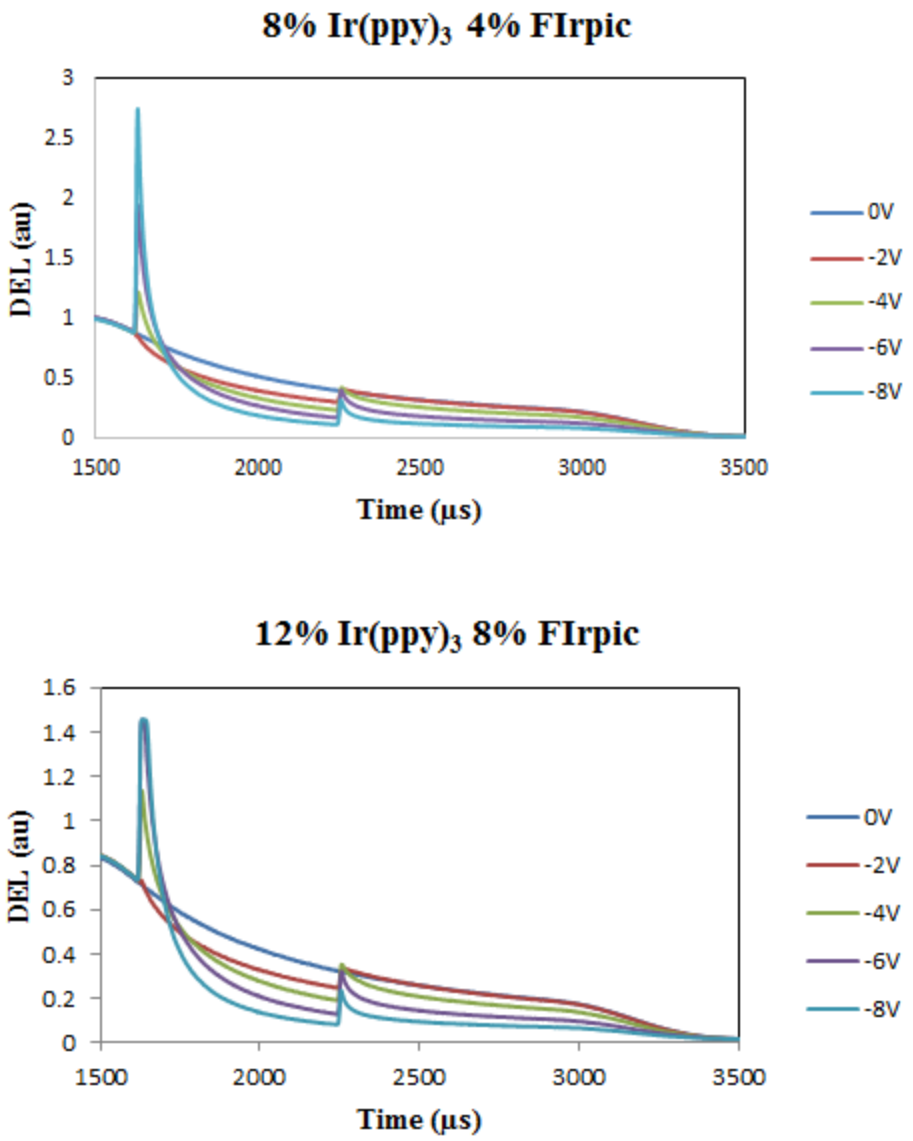

Figure 3.26 Delayed EL of FIrpic Coguest System.

3.3.2 Modifications of the HTL and the ETL

Upon studying different codeposition systems for both the HTL and the ETL, It was clear that the efficiency limiting factor in those devices is mainly the HTL (results are not shown). By codeposition of the ETL, the electrical characteristics of the simplified PHOLEDs did not show a significant change. Meanwhile by codeposition of the HTL, the device demonstrated an observable rise in the operating voltage and drop in the EL. In this section, only one of those experiments is reported. Figure3.27 shows the structure of the PHOLEDs under test in such experiment. A 5nm test-layer of NPB codeposited with CBP (50wt. %) is inserted in different device regions, at the beginning (region 1), middle (region

2), or end of the HTL (region 3), or at the end of the EML (region 4). The summary of the electrical characteristics is shown in Table3.7.

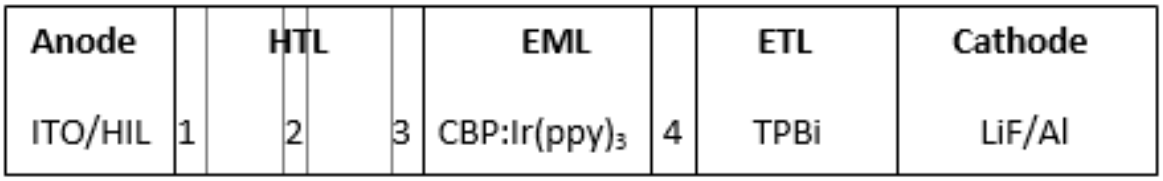

Figure 3.27 The structure of the Codeposition Experiment.

Table 3.7 Electrical Characteristic using Test Layer.

Region	Test Layer	Voltage (V) at 20mA/cm2	Luminescence cd/m^2 at 20mA/cm2
Control	No	6.19	7830
R1	Beg. HTL	9.47	2610
R2	Mid. HTL	8.1	3180
R3	End HTL	6.65	5110
R4	End EML	7.05	6380

Figure3.28 shows the electrical characteristics for the test-layer in different regions within the PHOLED. Figure3.28(a) shows the J-V characteristics, Figure3.28(b) and (c) shows the EL intensity and the current efficiency, respectively. It can be seen that the presence of the test layer at the beginning of the HTL slows down charge injection, hence the voltage rises and the EL drops significantly. Furthermore, the presence of the test layer in the middle of the HTL, affects the hole transport, therefore, a high voltage rise and lower luminescence can be observed. Having the test layer at the HTL/EML (end of HTL) interface does not show a large voltage rise and shows similar J-V characteristics to the control device, hence it does not affect either the charge injection or the charge transport, meanwhile it noticeably affects the EL characteristics. Meanwhile, having the test layer at the end of the EML does not show a large change in terms of either the J-V or the EL-J characteristics. Therefore, we can conclude from this that the recombination of excitons in the simplified PHOLEDs might be interfacial, which mainly occurs at the HTL/EML interface which agrees with [33]. The reason behind this is the hole trapping nature of $Ir(ppy)_3$, also the ambipolarity of CBP which allows electrons to reach the HTL/EML interface which agrees with [10].

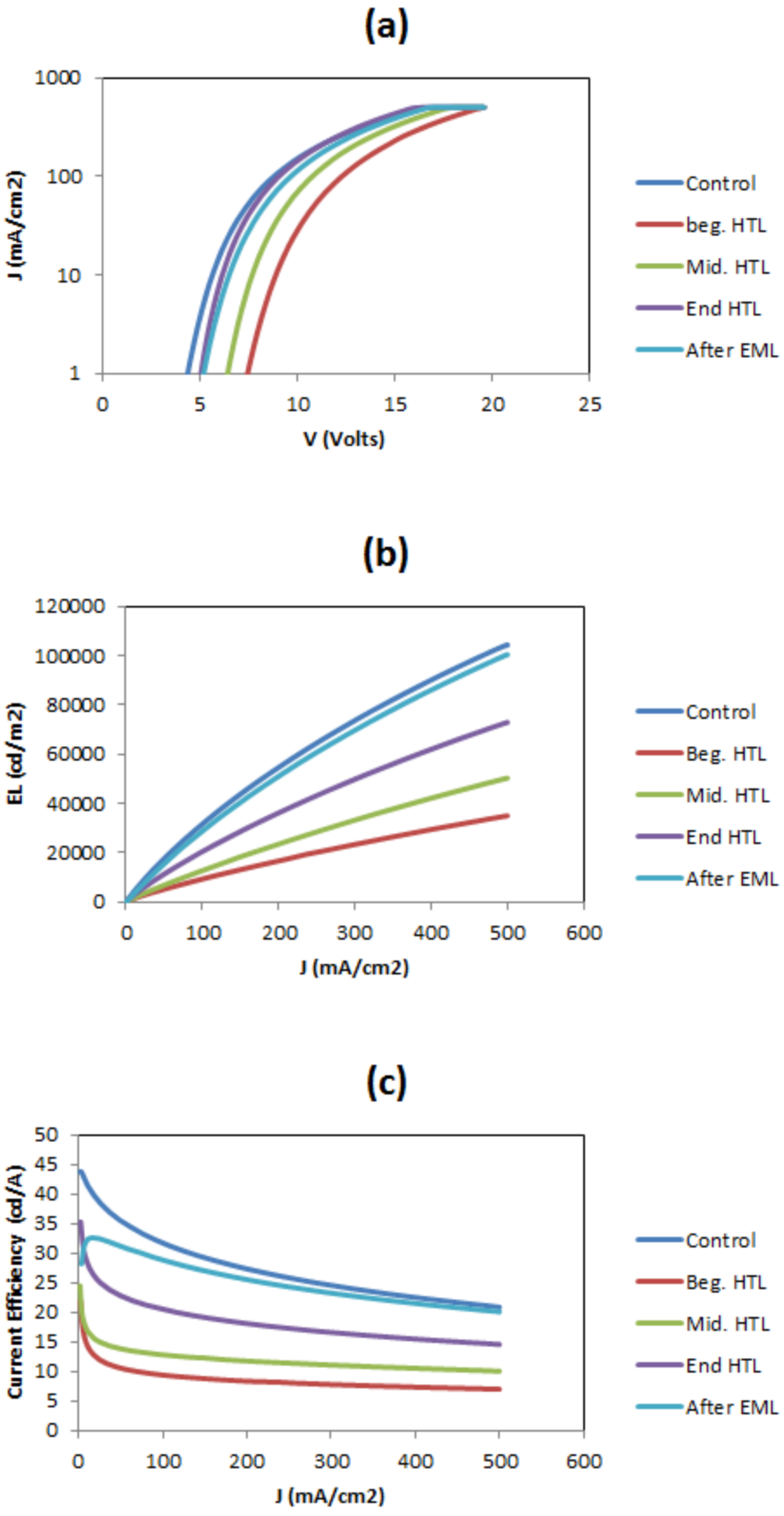

Figure 3.28 The Electrical Characteristics of the PHOLEDs with a Test Layer.

3.4 The effect of modified HTL/EML interface on simplified PHOLEDs efficiency

Since it was hypothesized in the previous section that the CBP/CBP:Ir(ppy)$_3$ interface is the recombination zone responsible for light emission, this interface will be modified for higher current efficiency purposes. In this section, multiple CBP/CBP:Ir(ppy)$_3$ interfaces will be used as shown in Figure3.29. Table3.8 shows the summary of the electrical characteristics of such PHOLED.

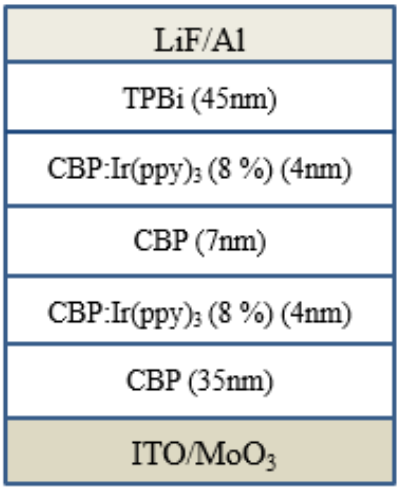

Figure 3.29 Multiple HTL/EML Interfaces.

Table 3.8 Summary of Electrical Characteristics of PHOLED with Multiple HTL/EML Interfaces.

Device	Voltage (V) at 20mA/cm2	Luminescence cd/m^2 at 20mA/cm2
Control	7.98	6260
Multiple	8	6320

It can be seen that the resulting operating voltage and EL is comparable, which is might be due to the ambipolarity of CBP which can transport electrons to the HTL/EML interface and the hole trapping properties of Ir(ppy)$_3$ which traps holes at the same interface leading light emission.

Chapter 4 Conclusions

4.1 Conclusions

Although simplified PHOLEDs offer higher efficiency compared to conventional PHOLEDs, their EL stability is found to be very poor. Furthermore, it was found that either PT-ITO or 1nm of MoO_3 as a HIL can be used to facilitate hole injection process into the deep HOMO of the HTL which in turn will lead to highly efficient simplified PHOLEDs. On the other hand, results of this thesis shed light on a new degradation mechanism occurring at the ITO/organic interface. This interface is susceptible to exciton-induced degradation that results in poor EL stability of simplified PHOLEDs. This exciton-induced degradation is even more pronounced due to interactions between charges (holes) and excitons at such interface as the degradation is accelerated. MoO_3 as a HIL is found to have a new role in the EL stability of simplified PHOLEDs as it acts as an exciton quencher layer that in turn reduces exciton-induced degradation. Furthermore, it was found that thicker MoO_3 (5nm) can lead to higher EL stability of simplified PHOLEDs as it stops the accelerated degradation (due to interactions between excitons and charge carriers (holes)). Moreover, by adding exciton and electron blocking layers at the HTL/EML interface the EL stability of PHOLEDs can be enhanced.

Furthermore, DEL measurements showed that simplified PHOLEDs suffer TTA and TPQ which might affect the operational stability of PHOLEDs. Eventually, codeposition experiments showed that the recombination zone is interfacial and possibly located near the HTL/EML interface.

As a summary, the conclusions are as follows:

- Simplified PHOLEDs need either surface treatment or thin layer of MoO_3 for efficiency purposes.
- Simplified PHOLEDs EL stability is poor and changes with the ITO surface treatments.
- The ITO/organic interface is susceptible to exciton-induced degradation that result in poor EL stability of simplified PHOLEDs.
- The exciton-induced degradation is even more pronounced due to interactions between charges (holes) and excitons at such interface as the degradation is accelerated.

- MoO_3 as a HIL is identified to have an additional role in the EL stability of simplified PHOLEDs as it acts as an exciton quencher layer that in turn reduces exciton-induced degradation.

- Thicker MoO_3 (5nm) can lead to higher EL stability of simplified PHOLEDs as it stops the accelerated degradation.

- By adding exciton and electron blocking layers at the HTL/EML interface the EL stability of PHOLEDs can be enhanced.

- DEL measurements showed that simplified PHOLEDs suffer TTA and TPQ which might affect the operational stability of PHOLEDs.

- Modifications of organic layers experiments showed that the recombination zone is interfacial and possibly located near the HTL/EML interface.

4.2 Recommendations for Future Work

The proposed future work can be summarized as follows:

Simplified PHOLEDs structure:

- Investigate the possibility of simplifying the PHOLEDs to one layer of mixed organic materials with concentration gradient since the codeposition experiments of the EML (cohost) and the ETL did not lower the current efficiency yet lowered the operational voltage.

- Examine different material sets while maintaining the simplified PHOLEDs structure. In this thesis, CBP and TPBi where investigated as the HTL and the ETL respectively. Therefore, it is recommended that the simplified PHOLEDs concept is examined with different organic materials. Moreover, the impact of using different organic material on current efficiency and EL stability should be identified.

Simplified PHOLEDs efficiency:

- Understand the role of Ar IBAD in lowering the operating voltage and enhancing the current efficiency of simplified PHOLEDs since using both Ar IBAD as a surface treatment for ITO in addition to MoO_3 as a HIL led to more preferred electrical characteristics in terms of operating voltage and EL.

Simplified PHOLEDs El stability:

- Exploring exciton-induced degradation at organic/organic interface since this degradation mechanism affected the ITO/organic interface. Therefore, it is hypothesized that the exciton-induced degradation can also degrade organic/organic interface especially interfaces close to the EML.

- Investigate the chemical interactions between TPBi and Ir complex and possible degradations due to such interactions since TPBi was the ETL used in the simplified PHOLEDs under test.

- Measuring the EL stability of simplified PHOLEDs at constant EL instead of the measurement under constant current density since simplified PHOLEDs offer a high current efficiency (one order of magnitude higher than fluorescent OLEDs).

Blue PHOLEDs stability:

- Explore the EFIQ in blue emitters such as FIRPIC and its impact on operational stability of blue PHOLEDs since this exciton quenching mechanism was only observed in green PHOLEDs while having a FIRPIC as a coguest.

Bibliography

[1] H. J. Round, *Electrical World,* 19:309-310, 1907.

[2] A. Bernanose, M. Comte, P. Vouaux, *J. Chim. Phys.*, 50:64-68, 1953.

[3] M. Pope, H. Kallman, P. Magnante, *J. Chem. Phys.*, 38:2042-2043, 1963.

[4] RH Partridge, Radiation Sources, U.S. Patent 3,995,299, 1976.

[5] W. Helfrich, WG Schneider, *Phys. Rev. Lett.*, 14:229–231, 1965.

[6] J. Dresner, *RCA Rev.*, 30:322–334, 1969.

[7] DF Williams, M. Schadt, *J. Chem. Phys.*, 53:3480–3487, 1970.

[8] PS Vincett, WA Barlow, RA Hann, GG Roberts, *Thin Solid Films*, 94:171–183, 1982.

[9] CW Tang, SA VanSlyke, *Appl. Phys. Lett.*, 51:913–915, 1987.

[10] Z.B. Wang, M.G. Helander, J. Qiu, D.P. Puzzo, M.T. Greiner, Z.W. Liu, Z.H. Lu, *Appl. Phys. Lett.*, 98, 073310, 2011.

[11] Z.W. Liu, M. G. Helander, Z.B. Wang, Z.H. Lu, *Org. Electron.*, 14, 852, 2013.

[12] *Physics of Organic Semiconductors*, edited by W. Brutting, WILEY-VCH Verlag GmbH & Co. KGaA, Weinheim, 2005.

[13] University of Waterloo, ECE730 Class Tutorial, Prof. H. Aziz.

[14] M.A. Lampert, P. Mark, *New York: Academic Press Inc.*, 1970.

[15] *Theory of electrical characterization of (organic) semiconductors*, Peter Stallinga, adopted from: http://www.stallinga.org/.

[16] W. Y. Liang, *Physics Education,* 5: 226, 1970.

[17] J.A. Barltrop, J.D. Coyle, *Excited States in Organic Chemistry* (Wiley-VCH, New York, 1975).

[18] M.V. der Auweraer, *Photophysics and photochemistry of molecular materials*, B-KULG0I12A.

[19] J.C. Kotz, P. Treichel, *Chemistry and Chemical Reactivity* (Saunders College Publishing, Philadelphia, 1999.

[20] C. Kittel, *Introduction to Solid State Physics*, 6th edn. (Wiley, New York), 1986.

[21] H. Gorter, M.J.J. Coenen, M.W.L. Slaats, M. Ren, W. Lu, C.J. Kuijpers, W.A. Groen, Thin Solid Films, Volume 532, Pages 11-15, 2013.

[22] R. Meerheim, B. Lussem, K. Leo, *Proceedings of the IEE,* V97, n9, p1606-26, 2009.

[23] Z. Li, H. Meng, *Organic Light-Emitting materials and Devices,* Taylor and Francis Group, 2010.

[24] Satoshi Hoshino and Hiroyuki Suzuki, *Appl. Phys. Lett*. 69, 224 (1996).

[25] M. A. Baldo, S. Lamansky, P. E. Burrows, M. E. Thompson, and S. R. Forrest, *Appl. Phys. Lett*. 75, 4 (1999).

[26] Hany Aziz, Zoran D. Popovic, Nan-Xing Hu,Ah-MeeHor, and GuXu. *Science*, 283 (5409), 1900-1902.

[27] Hany Aziz, ZoranPopovic, Carl P. Tripp, Nan-Xing Hu, Ah-MeeHor, and GuXu, *Appl. Phys. Lett*. 72, 2642 (1998).

[28] Hany Aziz, ZoranPopovic, ShuangXie, Ah-MeeHor, Nan-Xing Hu, Carl Tripp, and GuXu, *Appl. Phys. Lett*. 72, 756 (1998).

[29] Yoon-FeiLiew, Hany Aziz, Nan-Xing Hu, Hardy Sze-On Chan, GuXu, and ZoranPopovic, *Appl. Phys. Lett*. 77, 2650 (2000).

[30] H. Heil, G. Andress, R. Schmechel, H. von Seggern, J. Steiger, K. Bonrad, and R. Sprengard, *J. Appl. Phys*. 97, 124501 (2005).

[31] S. Scholz, C. Corten, K. Walzer, D. Kuckling, and K. Leo, *Org. Electron*. 8, 709 (2007).

[32] Giebink, N. C. and D'Andrade, B. W. and Weaver, M. S. and Mackenzie, P. B. and Brown, J. J. and Thompson, M. E. and Forrest, S. R., *Journal of Applied Physics*, 103, 044509 (2008).

[33] Siboni, Hossein Zamani and Aziz, Hany, *Applied Physics Letters*, 101, 173502 (2012).

[34] Zamani Siboni, Hossein and Luo, Yichun and Aziz, Hany, *Journal of Applied Physics*, 109, 044501-044501-6 (2011).

[35] Hossein Zamani Siboni, Hany Aziz, , *Organic Electronics*, Volume 12, Issue 12, December 2011, Pages 2056-2060, ISSN 1566-1199.

[36] Varatharajan Sivasubramaniam, Florian Brodkorb, Stephanie Hanning, Oliver Buttler, Hans Peter Loebl, Volker van Elsbergen, Herbert Boerner, Ullrich Scherf, Martin Kreyenschmidt, *Solid State Sciences*, Volume 11, Issue 11, November 2009, Pages 1933-1940, ISSN 1293-2558.

[37] Giebink, N. C. and D'Andrade, B. W. and Weaver, M. S. and Mackenzie, P. B. and Brown, J. J. and Thompson, M. E. and Forrest, S. R., *Journal of Applied Physics*, 103, 044509 (2008).

[38] Giebink, N. C. and D'Andrade, B. W. and Weaver, M. S. and Brown, J. J. and Forrest, S. R., *Journal of Applied Physics*, 105, 124514 (2009).

[39] Sebastian Scholz, Rico Meerheim, Karsten Walzer, Karl Leo, *Proc. SPIE 6999, Organic Optoelectronics and Photonics III*, 69991B (April 16, 2008).

[40] Kondakov, D. Y. and Lenhart, W. C. and Nichols, W. F., *Journal of Applied Physics*, 101, 024512 (2007).

[41] Lee, S. T. and Gao, Z. Q. and Hung, L. S., *Applied Physics Letters*, 75, 1404-1406 (1999).

[42] Rico Meerheim, Karsten Walzer, Martin Pfeiffer, and Karl Leo, *Appl. Phys. Lett*. 89, 061111 (2006).

[43] Qi Wang, YichunLuo, and Hany Aziz, *Appl. Phys. Lett*. 97, 063309 (2010).

[44] Qi Wang, Graeme Williams, Ting Tsui, and Hany Aziz, *J. Appl. Phys*. 112, 064502 (2012).

[45] M. G. Helander, Z. B. Wang, J. Qiu, M. T. Greiner, D. P. Puzzo, Z. W. Liu, and Z. H. Lu. *Science* 20 May 2011: 332 (6032), 944-947.

[46] Wang, Z. B. and Helander, M. G. and Qiu, J. and Liu, Z. W. and Greiner, M. T. and Lu, Z. H., *Journal of Applied Physics*, 108, 024510 (2010).

[47] Cao, X. A. and Zhang, Y. Q., *Applied Physics Letters*, 100, 183304 (2012).

[48] Chun-Hong Gao, Shi-Duan Cai, Wei Gu, Dong-Ying Zhou, Zhao-Kui Wang, and Liang-Sheng Liao. *ACS Applied Materials & Interfaces* 2012 4 (10), 5211-5216.

[49] Z. D. Popovic, H. Aziz, *J. Appl. Phys*. 98, 013510, 2005.

[50] *Edinburgh Instrument FL920-t Spectrometer brochure*, adopted from: http://www.edinburghphotonics.com/.

[51] Qi Wang, Graeme Williams, Hany Aziz, *Organic Electronics*, Volume 13, Issue 10, October 2012, Pages 2075-2082.

[52] Yingjie Zhang, Mina M. A. Abdelmalek, Qi Wang, and Hany Aziz, *Appl. Phys. Lett*. 103, 063307 (2013).